8-27-2015 12:00 AM

Morphological response of sand bed streams to unsteady flow events: an experimental study

Etta Haley Gunsolus
The University of Western Ontario

Supervisor
Dr. Andrew D. Binns
The University of Western Ontario

Graduate Program in Civil and Environmental Engineering
A thesis submitted in partial fulfillment of the requirements for the degree in Master of Engineering Science

MORPHOLOGICAL RESPONSE OF SAND BED STREAMS TO UNSTEADY FLOW EVENTS: AN EXPERIMENTAL STUDY

(Thesis format: Integrated Article)

by

Etta Haley Gunsolus

Graduate Program in Civil and Environmental Engineering

A thesis submitted in partial fulfillment
of the requirements for the degree of
Master of Engineering Science

The School of Graduate and Postdoctoral Studies
The University of Western Ontario
London, Ontario, Canada

Abstract

Changes in riverine discharge, such as those due to reservoir flushing, seasonal variation or extreme precipitation, can alter sediment transport rates and morphology of the stream bed. Experimental laboratory research investigated the effect of unsteady flow event hydrographs on stream bed morphological response. Laboratory experiments were conducted in a 5.0 m-long sediment transport flume with a bed comprised of a medium sand. Experimental hydrographs were composed of antecedent (base-flow), unsteady event (flood) and post-flood (return to base-flow) stages. Three distinct series of experimental laboratory runs were conducted to systematically investigate the effect of three characteristics of unsteady flow event hydrographs. Series A investigated the effect of the magnitude of the unsteady flow event hydrograph; Series B investigated the effect of the duration of the event; and Series C investigated the effect of the hydrograph shape (i.e., time-to-peak flow). Bed morphological adjustments, sediment transport rates and the composition of the sediment in transport were measured throughout all stages of the experimental runs. Measured values were compared to predicted values calculated using traditional sediment transport and bed form geometry equations assuming steady flow conditions. In general, predicted values greatly underestimated both measured values of sediment transport and bed form geometry. Results show that systematic changes in the magnitude, duration and time-to-peak flow of the unsteady hydrograph cause varying types of hysteresis (clockwise or counter-clockwise) of the sediment transport rates which has a considerable effect on the subsequent bed morphological adjustments. Shorter duration and symmetrical hydrographs exhibit counter-clockwise hysteresis while longer duration and asymmetrical hydrographs exhibit clockwise hysteresis. Results from this thesis have made considerable contributions towards evaluating the effects of unsteady flow event hydrograph characteristics to improve numerical modelling capabilities and accuracies, as well as river and dam management, engineering and restoration.

Keywords

Rivers and streams; laboratory experiments; unsteady flow; flooding; bed morphology; sediment transport

Co-Authorship Statement

The work of this thesis is a collaborative effort by the present author and Dr. Andrew D. Binns. Chapter 3 will be submitted for publication in the near future with the present author as primary author and Dr. Binns as second author as he provided valuable feedback on the manuscript. A version of Chapters 4 and 5 will also be submitted in the near future for publication with the present author as primary author and Dr. Binns as second author, as Dr. Binns assisted in the development and design of the experiments as well as with the analysis of results and editing of the manuscripts.

Chapter 3 will be submitted for publication as:

Gunsolus, EH and Binns, AD. Morphological response of stream beds to unsteady flow events: a review of recent laboratory experiments. To be submitted.

Chapter 4 will be submitted for publication as:

Gunsolus, EH and Binns, AD. Quantification of stream bed morphological response to unsteady flow event hydrographs of varying peak flow magnitude and duration. To be submitted.

Chapter 5 will be submitted for publication as:

Gunsolus, EH and Binns, AD. Quantification of stream bed morphological response to variation in hydrograph shape. To be submitted.

Acknowledgments

I would like to express my extreme gratitude towards my supervisor, Dr. Andrew D. Binns, for the patient guidance, unwavering encouragement, thoughtful advice, and financial support that you have provided me throughout my degree. Thank-you for introducing me to the world of river mechanics, a subject I that have grown to love. The belief and dedication that you have in your students is exceptional and a gift that I will carry with me for the duration of my life. I am grateful and humbled to be one of your first students and look forward to working with you for the next four years.

I would like to acknowledge to the rest of the Binns Group for the support they have offered me. I would especially like to thank Jack McKee, who has been my right hand man for the last two years. The re-assurance and friendship you provided me with is invaluable. Also, I would like to thank Chris Howlett for his hard work, dedication and exceptional assistance over the last two summers. Appreciation is also extended to Wilbert Logan for his trouble-shooting assistance in the laboratory on a number of occasions.

A very special thanks to my parents, Ann and Drew, who succeeded wildly at making my academic life easier in countless ways. Mom and Dad, thank-you for your monumental and unequivocal belief in me. Thank-you to my sister, Claire, who patiently listened and provided valuable feedback to a multitude of presentations throughout my degree. The commitment, acceptance and unconditional love you have offered me throughout my life is a blessing. I greatly valued the long phone calls over the course of my degree with my sweet, yet sassy, 95 year old Nana Banana who showered me with applause, encouragement and joyful laughter at times when I needed it the most. I would like thank my girlfriends: Mariah, Alecia, Crystal, Emily, Victoria, Sarah, and Elaine, who are an inspiring collection of independent and strong women. Finally, thank-you to Sara and Jake for allowing me to love their children, Emily, Josh and JoJo, whose happiness is contagious.

Table of Contents

List of Tables

List of Figures

List of Notation

A	parameter for specific volumetric bed load formula of Yalin
a	antecedent stage
B	flow width
(b)	flood stage b, the first flood stage of three in Series C
BF	base-flow
B_s	roughness function
c	resistance factor
c_f	pure friction component of c
c_Δ	bed form component of c
(c)	flood stage c, the second flood stage of three in Series C
$(c_f)_{av}$	channel-averaged Chézy resistance coefficient
(d)	flood stage d, the third flood stage of three in Series C
D_{50}	average grain size
Fr	Froude number
f	flood stage
g	acceleration due to gravity
h	flow depth
h_{av}	average flow depth

$h_{\max}$	maximum flow depth
i	initial experimental stage
K	von Karman constant (= 0.4)
k_s	height of the granular roughness
ℓ	length of flume
m_δ	exponent in δ_D equation
m_Λ	exponent from Λ_D equation
p	porosity of the granular material
pf	post-flood stage
Q	flow rate
q_{sb}	specific volumetric bed load rate
$q_{sb,\exp}$	experimental specific volumetric bed load transport rate
$q_{sb,calc}$	calculated specific volumetric bed load transport rate
$\left(q_{sb,\exp}\right)_{avg}$	average experimental specific volumetric bed load transport rate
R	Reynolds number
R_*	roughness Reynolds number
S	longitudinal bed slope
s	parameter for specific volumetric bed load formula of Yalin
t	time

t_r	hydrograph time-to-peak
t_s	sediment time-to-peak
t_{lag}	lag in time between t_r and t_s
u_{av}	mean velocity
W	density ratio
X	grain size Reynolds number
Y	mobility number
Y_{cr}	critical mobility number
Y_{Δ}	undulated bed corrected sediment mobility number
Z	ratio between the flow depth and D_{50}
z_b	bed elevation measured with respect to z_o
z_0	datum, bottom of flume floor
β	dimensionless coefficient dependent on properties of fluid and bed material
γ_s	specific weight of grains in fluid (= 16186.5 N/m^3 for the present sediment material and fluid)
Δ	bed form height
Δ_D	dune height
Δ_R	ripple height

Δq_{sb}	change in specific volumetric bed load rate
Δt	change in time
Δ_x	change in longitudinal distance
Δz_b	change in bed elevation
$\Delta_{avg,\exp}$	experimental average bed form height
$\Delta_{avg,calc}$	calculated average bed form height
δ	bed form steepness
δ_R	ripple steepness
δ_D	dune steepness
ς_R	parameter used to determine $\Re$ in δ_R
ς_D	parameter in δ_D equation
η_*	relative flow intensity
η_{*d}	parameter in δ_D equation
Λ	bed form length
Λ_D	dune length
Λ_R	ripple length
λ_c	ratio between c and c_f
ν	fluid kinematic viscosity
Ξ	material number

^{0}	measurement cross-section superscript labeled in ascending numerical order
ρ	fluid density (= 1000 kg/m^3 for water)
ρ_s	sediment density
τ_0	bed shear stress
υ_*	shear velocity
ϕ	Einstein's dimensionless bed-load function
Ψ_D	function of X in δ_D equation
Ψ_R	function of X in δ_R equation
$\Re$	parameter depended on ς_R

List of Appendices

Chapter 1

1 Introduction

1.1 Motivation

Sediment transport in rivers and streams occurs due to a complex relationship between the stream bed and banks and hydraulic forces that produce the overall morphology of the channel. Under steady flow conditions sediment transport and bed morphological development achieves equilibrium conditions. However, natural processes and anthropogenic activities cause short-term changes in riverine discharge and can disrupt this equilibrium. Changes in discharge, such as those due to extreme rainfall events, seasonal variation in precipitation patterns, or reservoir flushing, can result in substantial and rapid adjustments in the sediment transport regime and stream morphology. In addition to an increased risk of flooding and erosion hazards, such alterations in flow can also cause degradation of aquatic habitats, re-mobilization of pollutants, and damage to in-stream infrastructure (Booth et al., 2004; Cockerill and Anderson, 2013; Jongman et al., 2014). The majority of intense sediment transport occurs during flash flood events (Rowinski and Czernuszenko, 1998; Huygens et al., 2000). Flash floods occur when the river system is incapable of transporting the volume of runoff that was induced by an intense precipitation event (Bagatur and Hamidi, 2014). During these periods of unsteady flow the relationship that exists between hydraulic and sediment transport processes becomes increasingly complex. As a result, the morphological response to changes in flow prove challenging to accurately predict and quantify. Knowledge of this response is imperative to improve river management during flood events and to ensure the protection of hydraulic structures.

River flooding is projected to increase in frequency in the coming years and may result in catastrophic damage (Prettenhaler et al., 2015). In recent years, many regions around the world, including Dresden (Saxony, Germany), Calgary (Alberta, Canada), Toronto (Ontario, Canada), and Longmont (Colorado, United States of America) have experienced extreme flooding events that resulted in substantial morphological consequences to the river. Extreme rainfall inundated the Elbe River in Dresden on June 5, 2013 causing an influx of discharge and sediment transport that destroyed flood control dykes (Munich Re, 2013). The extent of this

flood affected nineteen different countries and damages in Dresden alone were estimated at EUR $16 billion (Munich Re, 2013). The most damaging natural disaster in Canadian history is a flash flood that occurred in Calgary's Bow River on June 19, 2013 (Wake, 2013). The upstream portion of the Bow River has a network of twelve dams and reservoirs that simultaneously lost a large volume of storage capacity due to sediment accumulation during the flood event. The Government of Alberta has since committed CAD $116 million to flood erosion control projects to stabilize river banks, repair damaged property or infrastructure, and restore dykes and berms (Water Canada, 2013). Toronto experienced Ontario's most costly natural disaster during a flash flood event in the Don River on July 8, 2013 (Toronto Region Conservation Authority, 2014). The combined sewer systems and outlet channels were unable to convey the volume of runoff, causing an influx in riverine discharge that resulted in erosion and incision that damaged stormwater infrastructure. On September 11, 2013 a rainfall event resulted in dam and bank breaches along the St. Vrain River in Longmont, Colorado (Natural Hazards Center, 2013). There were four known fatalities and damages to public infrastructure reached USD $150 million (Boulder County, 2014). In response to this flood, a coalition of stakeholders have developed a restorative plan to mitigate erosion damage caused by the flood and design a more flood resistant river (Boulder County, 2014).

Engineers and hydrologists have attempted to mitigate the damaging effects of changes in flow due to flash floods through river management, engineering, and restoration efforts. These efforts rely on a variety of sediment transport prediction formulae that were developed from laboratory experiments and field investigations (Sturm, 2011). These formulae were primarily developed based on the transport of non-cohesive, uniform sediments, steady and uniform flow conditions, and a straight, rectangular stream geometry (De Sutter et al., 2001; Yang, 2013). Considering this, these formulae clearly fail to appropriately describe real world conditions, such as the unsteady flow events described above (De Sutter, 2001; Warmink et al., 2012). Investigation into sediment transport mechanisms during unsteady flow conditions of varying magnitude and duration is required in order to understand the dynamic stream morphological response to temporal changes in discharge and depth (Montes, 1998; Comiti and Mao, 2012).

Gee (1973), Allen (1976), Griffiths and Sutherland (1977), Fredsoe (1979), Parker and Klingeman (1982), Wijbenga and Klaasen (1983), Graf and Suszka (1985), Wijbenga and Van Nes (1986), Dietrich et al. (1989), Kuhnle (1989), Williams (1989), and Lisle et al. (1993)

were among some of the pioneering studies to investigate the riverine response to unsteady flow events. These authors conducted experimental laboratory studies, computational modeling and field investigations to formalize the concept of a hysteretic time-lag between the discharge and sediment transport rates during unsteady flow events. Over the last fifteen years, there has been a substantial increase in research investigating the behaviour of sediment transport during unsteady flow events, as greater attention is given to the morphological response of rivers to changes in flow, such as those due to extreme flood events. Despite considerable research, further insight into the mechanics of stream bed adjustment and sediment transport during unsteady events is required in order to accurately predict future river behaviour and design appropriate preventative infrastructure to mitigate the damaging morphological consequences of flood events (Buffington, 2012; Vietz et al., 2013). In particular, systematic experimental research is required in order to quantify the effect of various characteristics of unsteady flow event hydrographs (e.g., event duration, event magnitude, hydrograph shape) on stream bed morphological response.

1.2 Goal and objectives of the thesis

The goal of this thesis is to investigate the morphodynamic response of alluvial stream beds to alterations in flow caused by unsteady flow events. This research will meet the following objectives:

1) Conduct a comprehensive review and analysis of recent experimental laboratory research on the morphological response of stream beds to unsteady flow events and identify recommendations and strategic opportunities for future research;
2) Quantify the morphodynamic response (alteration to sediment transport rates and adjustment in bed morphology) to unsteady flow events of varying magnitude and duration; and
3) Quantify the effect of unsteady flow events of varying hydrograph shape (i.e., time-to-peak flow) on stream bed morphodynamic response.

The first objective will be achieved with a focus on recent literature published between 2000 and 2013. In order to achieve the second and third objectives, experimental laboratory research is performed in the sediment transport flume at the University of Western Ontario in London, Ontario, Canada. While unsteady flow events can also result in plan form morphological

response (e.g., erosion of the stream banks), the focus of this thesis will be on stream bed response alone, as the morphology of stream beds has traditionally been studied by assuming rigid, fixed banks since the bank deformation occurs on a much greater time-scale than that of the bed deformation. In addition, while the most extreme unsteady flow events (i.e., flash floods) typically involve flows that overtop the main channel banks, in order to examine the effect of these unsteady flow event hydrograph characteristics in a systematic, controlled manner, only unsteady flow events confined to the main channel will be investigated. As such, the change in discharge will only involve variation in flow depth; the width of the channel remaining invariant.

1.3 Structure of the thesis

This thesis is presented in integrated article format. Following Chapters 1 and 2, three separate manuscripts are presented in Chapter 3 through 5. The five chapters of the thesis are structured as follows:

Chapter 2 is entitled "Fundamentals of the present work". This Chapter presents an overview of the fundamentals of river mechanics as it pertains to the present thesis. A review of the mechanics of flow, sediment transport and bed morphological development in alluvial streams during steady flow conditions is discussed. The concept of hysteresis, which describes the effect of unsteady flow on sediment transport and bed morphological response, is also introduced.

Chapter 3 presents the manuscript entitled "Morphological response of stream beds to unsteady flow events: a review of recent laboratory experiments". This Chapter includes a comprehensive literature review of recent laboratory experiments investigating the effect of unsteady flow events on sand and gravel beds. Recommendations and strategic opportunities for future research are identified.

Chapter 4 presents the manuscript entitled "Quantification of stream bed morphological response to unsteady flow event hydrographs of varying peak flow magnitude and duration". This Chapter presents the results from an extensive series of laboratory experimental runs seeking to evaluate the effect of peak flow duration and magnitude on stream bed morphological response.

Chapter 5 presents the manuscript entitled "Quantification of stream bed morphological response to variation in hydrograph shape". This Chapter presents the results from a series of experimental laboratory runs investigating the effect of the hydrograph shape (i.e., time-to-peak flow) of an unsteady flow event on stream bed morphological response.

Chapter 6 is entitled "Conclusions and recommendations". This Chapter discusses the results of Chapters 3 through 5 and summarizes the main contributions of this thesis. Engineering implications of the thesis and recommendations for future research in this area are also discussed.

1.4 References

Allen JRL. 1976. Time-lag of dunes in unsteady flows: an analysis of Nasner's data from River Weser, Germany. *Sedimentary Geology* **15**:309-321.

Bagatur T and Hamidi N. (2014). Evaluation with stream characteristics of downstream flood problems after dam construction. *Journal of Environmental Engineering and Landscape Management* **22**(2):96-104. DOI:10.3846/16486897.2013.852555

Booth DB, Karr JR, Schauman S, Konrad CP, Morley SA, Larson MG, Burges SJ. 2004. Reviving Urban Streams: Land Use, Hydrology, Biology, and Human Behaviour. *Journal of American Water Resources Association.* **40**(5):1351-1364. DOI: 10.1111/j.1752-1688.2004.tb01591.x

Boulder County 2014. Saint Vrain Creek watershed master plan. Boulder County Colorado. 93 pages.

Buffington JM. 2012. Changes in channel morphology over human time scales. In Gravel-Bed Rivers: Processes, Tools, Environments, Church M, Biron PM, Roy AG (eds). Wiley: Chichester; 433-463.

Cockerill K and Anderson WP. 2013. Creating false images: stream restoration in an urban setting. *Journal of American Water Resources Association.* **50**(2): 468-482. DOI: 10.1029/2005WR003985

Comiti F and Mao L 2012. Recent advances in the dynamics of steep channels. Gravel-Bed Rivers: Processes, Tools, Environments. Wiley-Blackwell: Chichester; 351-377.

De Sutter R, Verhoeven R, Krein A. 2001. Simulation of sediment transport during flood events: laboratory work and field experiments. *Hydrological Sciences Journal* **46**(4):599-610. DOI:10.1080/02626660109492853

Dietrich WE, Kirchner JW, Ikeda H and Iseya F. 1989. Sediment supply and the development of the coarse surface layer in gravel-bed rivers. *Nature* **340**(6230):215-217.

Fredsoe J. 1979. Unsteady flow in straight alluvial streams: modification of individual dunes. *Journal of Fluid Mechanics* **91**(3):497-512.

Gee DM. 1973. Sediment transport in non-steady flow. *University of California Report* **4EC**:22-23.

Graf WH, Suszka L. 1985. Unsteady flow and its effects on sediment transport. *Proceedings 21st IAHR Congress* August 1985, Melbourne, Australia 540-544.

Griffiths GA and Sutherland AJ. 1977. Bedload transport by translation waves. *Journal of the Hydraulics Division*. Proceedings of the American Society of Civil Engineers **103**(HY11):127901291.

Huygens M, Verhoeven R and De Sutter R 2000. Integrated river management of a small Flemish river catchment. *The Role of Erosion and Sediment Transport in Nutrient and Contaminant Transfer: Proceedings of a Symposium Held at Waterloo, Ontario, Canada* **263**:191-198.

Jongman B, Hochrainer-Stigler S, Feyen L, Aerts JCH, Mechler R, Botzen WJW, Bower LM, Pflug G, Rojas R and Ward PJ. 2014. Increasing stress on disaster-risk finance due to large floods. *Nature Climate Change* **4**:264-268. DOI:10.1038/nclimate2124

Kuhnle RA, Willis JC and Bowie AJ. 1989. Variations in the transport of bed load sediment in a gravel-bed stream, Goodwin Creek, Mississippi, USA. *Proceedings of the 4th International Symposium on River Sedimentation*. Beijing, China 539-546.

Lisle TE, Iseya F and Ikeda H. 1993. Response of a channel with alternate bars to a decrease in supply of mixed-size bed load: a flume experiment. *Water Resources Research* **29**(11):3623-3629. DOI:10.1029/93WR01673

Montes S. 1998. Hydraulics of Open Channel Flow. *American Society of Civil Engineers*. United States of America.

Munich Re 2013. Floods dominate natural catastrophe statistics in first half of 2013. Munchener Ruckversicherungs-Gesellschaft.

Natural Hazards Center 2013. The 2013 Colorado Floods: Longmont's Response. University of Colorado at Boulder.

Parker G and Klingeman PC. 1982. On why gravel bed streams are paved. *Water Resources Research* **18**(5):1409-1423.

Prettenthaler F, Kortschak D, Hochrainer-Stigler S, Mechler R, and Urban H. 2015. Economic evaluation of climate change impacts. Springer Interational Publishing Switzerland. 349 pages.

Rowinkski RM and Czernuszenko W. 1998. Experimental study of river turbulence under unsteady conditions. *Acta Geophysical Polonica* **46**(4):461-480.

Sturm TW. 2010. Open channel hydraulics. McGraw Hill: New York, New York.

Toronto and Region Conservation Authority (TRCA). 2014. The history of flood control and the Toronto and Region Conservation Authority.

Vietz GJ, Sammonds MJ, Walsh CJ, Fletcher TD, Rutherfurd ID, and Stewardson MJ. 2013. Ecologically relevant geomorphic attributes of streams are impaired by even low levels of watershed effective imperviousness. *Geomorphology* **206**:67-78. DOI:10.1016/j.geomorph.2013.09.019

Wake B. 2013. Flooding costs. *Nature Climate Changes* **3**:778.

Warmink JJ, Schielen RMJ, Dohmen-Janssen CM. 2012. Bed form evolution under varying discharges, flume versus fields. *Proceedings River Flow 2012,* Costa Rica.

Water Canada. 2013. Alberta invests $116 million in flood erosion control. *Complete Water Magazine.*

Wijbenga A and Van Nes X 1986. Flow resistance and bedform dimensions for varying flow conditions; results of flume experiments with flood waves. *Delft Hydraulics Research Report*. R657. M1314 Part XIII.

Wijbenga JHA and Klaassen GL. 1983. Changes in bedform dimensions under unsteady flow conditions in a straight flume. *Modern and ancient fluvial systems: Special Publications of the IAS* **6**:35-48.

Williams GP. 1989. Sediment concentrations versus water discharge during single hydrologic events in rivers. *Journal of Hydrology* **111**(1):89-106.

Chapter 2

2 Fundamentals of the present work

This Chapter provides an overview of the fundamentals of river mechanics as it relates to the present thesis. The mechanics of flows, sediment transport and bed morphological development in alluvial streams under steady flow conditions are discussed. The effect of hysteresis during periods of unsteady flow on sediment transport and bed morphological response, and the factors responsible for this phenomenon, are also discussed.

2.1 Mechanics of flow

Traditional sediment transport equations were developed based on the assumption of steady (discharge does not change over time) and uniform (discharge does not change along the stream-wise direction) flow. Tranquil (or subcritical) flow is also assumed, meaning the flow is deep and slow moving. This can be defined according to the Froude number (Fr) following:

$$Fr = \frac{u_{av}}{\sqrt{gh}}, \tag{1}$$

where u_{av} is the mean velocity, g is the acceleration due to gravity and h is the flow depth. Froude numbers less than 1 represent subcritical flow conditions. Turbulent flow is also assumed. The Reynolds number is defined as follows:

$$R = \frac{u_{av} h}{\nu}, \tag{2}$$

where ν is the fluid kinematic viscosity (assumed to be 10^{-6} m^2/s for water). Turbulent flow occurs when the Reynolds number is greater than ≈ 600 in open channel flows. Turbulent flow can be further classified into three regimes that affect the velocity distribution according to the roughness Reynolds number of the flow at the bed (R_*). R_* can be defined as:

$$R_* = \frac{\upsilon_* k_s}{\nu}. \tag{3}$$

In Eq. (3) υ_* is the shear velocity and defined as:

$$\upsilon_* = \sqrt{Sgh}\ , \tag{4}$$

where S is the longitudinal bed slope. When R_* is less than 5, then the flow is classified as being in the hydraulically smooth regime. When R_* is between 5 and 70, the flow is considered to be in the transitional flow regime. When R_* is greater than 70 the flow is in the rough turbulent regime. Traditional sediment transport equations assume that the flow is in the rough-turbulent regime as this is the flow regime typical of most natural rivers. However, in many cases in laboratory flume studies the flow is in the transitional flow regime due to experimental constraints. Comparison of laboratory and field data has shown that this has negligible effect on morpholological processes.

2.2 Sediment transport

There are two types of sediment discharge: bed-material discharge (stream bed sediment) and wash load (fine sediments that have eroded from the watershed). Bed-material discharge can be broken down into two categories: (1) bed load, being the portion of sediment that is carried near the bed by physical processes such as intermittent rolling, saltating, or sliding, and (2) suspended load, being composed of sediment particles that are lifted into the main body of the flow by turbulence and transported downstream (Sturm, 2001). Wash load consists of very small sediment grains that remain in suspension and have little to no effect on the bed morphology (ASCE, 2008). Considering this, this thesis will focus on bed-material discharge. Occurrence of bed-material discharge can be defined according to the relative flow intensity (η_*) defined by Yalin and da Silva (2001) as:

$$\eta_* = \frac{Y}{Y_{cr}}. \tag{5}$$

No sediment transport occurs when $\eta_* < 1$. Only bed load occurs when $1 < \eta_* < 10$ and suspended load (in addition to bed load) occurs when $\eta_* > 10$. Y and Y_{cr} are dimensionless parameters (related to the Shields parameter) that represent the mobility number and critical mobility number (corresponding to the initiation of motion stage), respectively. Y is defined as:

$$Y = \frac{\rho \upsilon_*^{\ 2}}{\gamma_s D_{50}}, \tag{6}$$

where ρ is the fluid density (= 1000 kg/m^3 for water), γ_s is the specific weight of grains in fluid (= 16186.5 N/m^3 for the present sediment material and fluid) and D_{50} is the average grain size. Y_{cr} is a function of the dimensionless material number (Ξ) and obtained from the modified Shields' curve (Yalin, 2001). Ξ is defined as:

$$\Xi = \sqrt[3]{\frac{\gamma_s D_{50}^{\ 3}}{\nu^2 \rho}}. \tag{7}$$

Existing sediment transport formulae quantify bed load and suspended load, either individually or combined, with the majority of the equations developed based on steady and uniform flow conditions. Results from the various sediment transport formulae can drastically differ which make selection of an appropriate equation for a particular application challenging. It is uncertain which formula will yield results closest to the natural environment in current engineering practice (ASCE, 2008). The focus of this thesis will be on bed load transport. Examples of commonly used bed load transport equations include, but are not limited to: Meyer-Peter and Müller (1949), Yalin (1963), Bagnold (1968), and van Rijn (1984). These equations all solve for the parameter ϕ proposed by Einstein (1950), which can then be used to solve for the specific volumetric bed load transport rate (q_{sb}), and is defined as:

$$\phi = \frac{q_{sb} \rho^{1/2}}{\gamma_s^{\ 1/2} D_{50}^{\ 3/2}}. \tag{8}$$

Meyer-Peter and Müller (1949) defined ϕ according to:

$$\phi = 8\left(Y - Y_{cr}\right)^{3/2}. \tag{9}$$

Yalin (1963) defined ϕ according to:

$$\phi = 0.635 s \sqrt{Y}\left[1 - \frac{1}{As}\ln\left(As\right)\right], \tag{10}$$

where A is defined as:

$$A = 2.45 \frac{Y_{cr}^{1/2}}{W^{0.4}}, \tag{11}$$

W is defined as:

$$W = \frac{\rho_s}{\rho}, \tag{12}$$

and s is defined as:

$$s = \frac{Y - Y_{cr}}{Y_{cr}}. \tag{13}$$

Bagnold (1968) defined ϕ according to:

$$\phi = B_s \beta Y^{1/2} \left(Y - Y_{cr}\right), \tag{14}$$

where β is a constant dependent on D_{50} and B_s can be calculated from R_* following:

$$B_s = \left(2.5 \ln R^* + 5.5\right) e^{-0.0705\left(\ln \mathrm{Re}^*\right)^{2.55}} + 8.5\left(1 - e^{-0.0594\left(\ln R^*\right)^{2.55}}\right). \tag{15}$$

van Rijn (1984) defined ϕ according to:

$$\phi = 0.053 \Xi^{-0.3} \left(\eta_* - 1\right)^{2.1}. \tag{16}$$

The presence of bed forms requires, the sediment transport equations to be modified by taking into account the increased resistance to flow due to the bed forms. For undulated beds, this causes the q_{sb} to be reduced. In bed load transport equations the parameter Y_Δ is used in place of Y. Y_Δ is defined as:

$$Y_\Delta = Y \lambda_c^{\,2}, \tag{17}$$

where λ_c is defined as:

$$\lambda_c = \frac{c}{c_f}, \tag{18}$$

the resistance factor, c, is defined as:

$$c = \sqrt{\frac{1}{\left(\frac{1}{c_f^{\,2}} + \frac{1}{c_\Delta^{\,2}}\right)}}, \tag{19}$$

c_f, the pure friction component of c, is defined as:

$$c_f = \frac{1}{\mathrm{K}} \ln\left(0.368 \frac{h_{av}}{k_s}\right) + B_s, \tag{20}$$

and c_Δ, the bed form component of c, is defined as:

$$c_\Delta = \sqrt{\frac{1}{\frac{1}{2}\delta^2 \frac{\Lambda}{h}}}. \tag{21}$$

In Eq. (20) K is the von Karman constant (= 0.4), k_s is the height of the granular roughness ($k_s = 2D_{50}$) and B_s is defined following Eq. (15). In Eq. (21) δ is the bed form steepness and Λ is the bed form length.

In general, non-uniform sediment transport and any subsequent alterations of the mobile bed is governed by the sediment transport continuity (Exner-Polya) equation, defined as:

$$(1-p)\frac{\Delta z_b}{\Delta t} = -\frac{\Delta q_{sb}}{\Delta x}, \tag{22}$$

where p is the porosity of the granular material, Δz_b is the change in bed elevation, Δt is the change in time, Δq_{sb} is the change in the specific volumetric bed load rate, and Δx is the distance along the streamwise direction.

2.3 Bed morphological development

As mentioned in Section 2.2, bed load transport can cause deformation of an alluvial stream bed determined by Eq. (22). This bed deformation can result in the development of mobile bed morphological features. Determining the geometry of bed morphological features is of importance to determine their influence on resistance to flow and to ensure the protection of hydraulic structures.

Turbulent eddies which form due to non-uniformities in the flow field are responsible for the stream bed morphological development (Bridge, 2003). Typical bed forms include dunes, ripples and bars. Other bed development processes, such as armoring, can also result from the interaction between the flow and stream bed. A summary of the flow conditions responsible for these bed forms and bed development processes are summarized in Table 1. The existence of dunes, ripples or ripples superimposed on dunes can be determined by the relationship between the relative flow intensity η_* and the dimensionless grain size Reynolds number (X) defined as:

$$X = \frac{\upsilon_* D_{50}}{\nu}. \tag{23}$$

Eddies, and in turn, bed forms, will grow until they reach the maximum dimensions for the hydraulic and boundary conditions. The maximum length of dunes (Λ_D) is approximately six times the flow depth (h) while the maximum ripple length (Λ_R) is approximately 1000 times the average grain size (D_{50}). Numerous equations have been proposed to determine the steepness, height and length of bed forms (see, e.g., Allen, 1970; Yalin, 1977; Fredsoe, 1982; van Rijn, 1984; Ashley, 1990; Yalin, 1992).

Table 1: Summary of bed forms and bed development processes

Bed form/ process type	Geometry	Occurrence
Flat bed	A flat bed is void of any significant bed forms as a result of	Flat beds occur at a variety of flow depths and grain sizes if the rate of flow or sediment transport is too low

	minimal sediment transport (ASCE, 1966; 1977).	(Yalin and da Silva, 2001). They can also develop at high flow rates when sediment transport capacity is too large, and thus, sediment transport is dominated by suspended load with no significant bed form development.
Ripples	Ripples have a longitudinal profile that is triangular in shape with a convex upstream slope and downstream slope equal to the angle of repose (ASCE 1966; 1977). In relation to other bed forms (e.g., dunes) they are relatively short crested.	A ripple dominated bed occurs when the grain size Reynolds number is less than 2.5 (Yalin and da Silva, 2001). Ripples will superimpose on top of dunes when the grain size Reynolds number is between 2.5 and 35 (Yalin and da Silva, 2001). Generally, ripples will form in sediments with D_{50} less than 0.6 mm and will migrate downstream at a velocity slower than that of the flow (ASCE 1966; 1977).
Dunes	The longitudinal profile of dunes is of similar shape to ripples, but with larger lengths and heights (ASCE 1966; 1977). The length (Λ_D) is proportional to the flow depth (h) where the maximum length is approximated by $\Lambda_D = 6h$ (Yalin and da Silva, 2001).	Dunes will form independently of other bed forms when the grain sized Reynolds number is larger than 35 (Yalin and da Silva, 2001). Dunes will allow ripples to superimpose on the upstream slope of dunes when the grain size Reynolds number is between 2.5 and 35 (Yalin and da Silva, 2001). Similar to ripples, dunes migrate downstream at a velocity slower than the flow (ASCE 1966; 1977).
Bars	Bars have a longitudinal profile of similar shape to ripples and dunes (ASCE 1966; 1977). Bar lengths (Λ_B) are proportional to the flow width (B) where the maximum length is approximated by $\Lambda_B = 6B$ (Yalin and da Silva, 2001). Alternate or multiple bars can form across a channel (Yalin and da Silva, 2001).	Bars occur when B/h is significantly large and burst eddies are in contact with the bed (Yalin and da Silva, 2001). Bars, similar to ripples and dunes, migrate downstream at a velocity slower than the flow (ASCE 1966; 1977).

Armor	Armoring of the bed is a vertical sorting of the sediment (Karmin and Holly, 1986). This vertical sorting allows for larger particles to form a protective layer at the surface of the bed inhibiting smaller particles from being transported (Karmin and Holly, 1986).	Armoring is most commonly found in gravel bed riverine systems (Karmin and Holly, 1986). Armor typically forms during phases of sediment starvation (Karmin and Holly, 1986).

Dune length (Λ_D) is defined by Yalin (1977; 1992) as:

$$\Lambda_D = 6h\left[1+\frac{(Z-40)(Z-400)}{Z}e^{-m_\Lambda}\right], \tag{24}$$

where

$$Z = \frac{h}{D_{50}}, \tag{25}$$

and

$$m_\Lambda = 0.055\sqrt{Z} + 0.04X. \tag{26}$$

Dune steepness (δ_D) is defined by Yalin (1977; 1992) as:

$$\delta_D = \psi_D(X)\left(\delta_D e^{1-\varsigma_D}\right)^{m_\delta}, \tag{27}$$

where

$$\psi_D(X) = 1-e^{-\left(\frac{X}{10}\right)^2}, \tag{28}$$

$$\varsigma_D = \frac{\eta_* - 1}{\eta_{*d} - 1}, \tag{29}$$

$$\eta_{*d} = 35\left(1-e^{-0.074Z^{0.4}}\right)-5, \tag{30}$$

and

$$m_{\delta} = 1 + 0.6e^{-0.1(5-\log Z)^{3.6}}. \tag{31}$$

Dune height (Δ_D) is defined by Yalin (1977; 1992) with the following relationship:

$$\Delta_D = \delta_D \Lambda_D. \tag{32}$$

According to Yalin (1977; 1985; 1992), ripple length (Λ_R) is defined as:

$$\Lambda_R = \frac{3000 D_{50}}{\Xi^{0.88}\sqrt{\eta_*}\left(1 - 0.22\sqrt{\eta_*}\right)}. \tag{33}$$

Ripple steepness (δ_R) is defined by Yalin (1977; 1985; 1992) as:

$$\delta_R = \psi_R(X)0.014\Re(\eta_* - 1)e^{(1.1-0.1\eta_*)}, \tag{34}$$

where

$$\psi_R(X) = e^{-\left[\frac{(X-2.5)}{14}\right]^2} \; if \; X > 2.5, \tag{35}$$

$$\psi_R(X) = 1 \; if \; X < 2.5, \tag{36}$$

and

$$\varsigma_R = 0.1(\eta_* - 1). \tag{37}$$

The quantity $\Re$ in Eq. (34) is defined according to:

$$\begin{aligned} \Re &= 1 \; if \; \varsigma_r \le 1 \\ \Re &= 0 \; if \; \varsigma_r > 2 \\ \Re &= \varsigma_r(2 - \varsigma_r) \; if \; 1 < \varsigma_r \le 2. \end{aligned} \tag{38}$$

Ripple height (Δ_R) is defined by Yalin (1977; 1985; 1992) following:

$$\Delta_R = \delta_R \Lambda_R. \tag{39}$$

2.4 Hysteresis

During unsteady flow events, sediment transport rates can experience hysteretic behaviour. Hysteresis is a retardation effect that occurs when the forces acting on a body change. Hysteresis during unsteady flow events results in a lag-in-time between the discharge and the rate of sediment transport (ASCE, 2008). In such cases, the sediment transport rate will have a different value for an identical discharge during the ascending and descending stages of a flood hydrograph (Brownlie, 1981). The effect of hysteresis is more prominent on alluvial beds that have a lower longitudinal bed slope. Hysteresis can be classified according to the following behaviour: (1) clockwise, (2) anti- or counter-clockwise, (3) single value, (4) single value with a loop, and (5) figure eight shaped (Williams, 1989; Ahanger et al., 2008). The most commonly observed classifications of hysteretic behaviour are clockwise and counter-clockwise (see Appendix A for a schematic of clockwise and counter-clockwise hysteresis). Clockwise hysteresis, appearing more frequently in literature, is characterized by greater sediment transport occurring during the rising limb of the flow hydrograph compared to the falling limb (Asselman, 1999; De Sutter et al., 2001). On the other hand, counter-clockwise occurs when there is a lower sediment transport rate in the rising limb compared to the falling limb of the flow hydrograph. Engineers seek to understand the mechanics of sediment transport during unsteady flow event in order to incorporate and advance river management and dam operation decisions. For example, predicting the time-to-peak and rate of sediment transport downstream of a dam during a reservoir flushing event will allow engineers to determine the duration required for the sediment to be deposited at specific locations downstream.

Many factors have been suggested to contribute towards creating hysteresis in sediment transport rates. Hysteretic behaviour is thought to be, in part, a function of the availability of sediment in the river that can be transported (Singh et al., 2011). Typically, clockwise hysteresis is observed when there is a lack of sediment being fed to the stream and counter-clockwise hysteresis is more prevalent if there is a steady or increased supply of sediment (Wood, 1977; Williams, 1989). In real world applications a lack of sediment supply could be attributed to the presence of an upstream engineered structure, such as a dam, that inhibits the natural transport of sediment. Although this circumstance may not always be the case, clockwise hysteresis is generally observed when the maximum sediment transport rate is reached prior to the hydrograph peak due to sediment depletion (ASCE, 2008; Singh et al.,

2011). However, if there is not an upstream disruption, sediment will continue to be naturally fed at a steady or pulsed rate allowing for counter-clockwise hysteresis to occur. During a flood event there may also be excess sediment being supplied to the river by means of runoff, wash load or sediment from banks. Considering this, the conditions of sediment starvation and sediment availability alone cannot be used as predictive measurements for the hysteretic behaviour of the sediment transport rate during unsteady flow events.

Other factors that affect sediment transport hysteresis include bed structure, variation in sediment composition of the river bed, and the mode of transport (i.e., bed load or suspended load) (Reesink and Bridge, 2007; Reesink and Bridge, 2009; Humphries et al., 2012). The development of geometric bed forms (e.g., dunes and ripples) is more common in rivers with sand-beds while gravel bed rivers are prone to the development of an armor layer. Adjustments in average geometry of bed forms as flow and sediment transport rates change can also experience a lagged effect (Bridge, 2003). This lag, often referred to looped hysteresis, occurs due to the fact that a large volume of sediment (i.e., the sediment composing an individual bed form) is required to be transported in order to cause an observable change in bed morphology (Allen, 1982). Bed form lag depends on the bed shear stress and is not solely a function of the behaviour of the discharge. The mode of sediment being transported by the flow also influences the type of hysteresis that occurs. According to several studies suspended sediment transport typically results in clockwise hysteresis while bed load more commonly results in counter-clockwise hysteresis (Lopes and Ffolliott, 1993). Many stream beds are composed of a combination of these characteristics, which can make it difficult to isolate and determine the direct effect of each characteristic on the hysteretic behaviour of sediment transport and bed response during unsteady flow events.

2.5 References

Ahanger MA, Asawa GL, Lone MA. 2008. Experimental study of sediment transport hysteresis. *Journal of Hydraulic Research* **46**(5):628-635. DOI:10.3826/jhr.2008.3185

Allen JRL. 1970. Sand waves: a model of origin and internal structure. *Sedimentary Geology* **26**(4):281-328. doi:10.1016/0037-0738(80)90022-6

Allen JRL. 1982. Sedimentary structures: their character and physical basis, volume 1. Developments in sedimentology 30. Elsevier Science Publishers: Amsterdam

American Society of Civil Engineers (ASCE) Task Committee. 1966. Nomenclature for bedforms in alluvial channels. *Journal of Hydraulics Division* **92**:HY3 Process Paper 5408:51-64.

American Society of Civil Engineers (ASCE) Task Committee. 1977. Sedimentation Engineering Manuals and Reports on Engineering Practice.

American Society of Civil Engineers (ASCE) Task Committee. 2008. Sedimentation engineering manuals and reports on engineering practice 110.

Asselman NEM. 1999. Suspended sediment dynamics in a large drainage basin: the River Rhine. *Hydrological Processes* **13**(10):1437-1450.

Ashley GM. 1990. Classification of large-scale subaqueous bedforms – a new look at an old problem – bedforms and bedding structures. *Journal of Sediment Petrology* **60**:160-172.

Bagnold RA. 1968. An approach to the sediment transport problem from general physics. Geologic Survey Professional Paper 422(I).

Bridge. JS. 2003. Rivers and floodplains: forms, processes and sedimentary record. Blackwell Publishing. John Wiley and Sons.

Brownlie. WR. 1981. Prediction of flow depth and sediment discharge in open channels. Keck Laboratory of Hydraulics & Water Resources, Caltech.

De Sutter R, Verhoeven R, Krein A. 2001. Simulation of sediment transport during flood events: laboratory work and field experiments. *Hydrological Sciences Journal* **46**(4):599-610. DOI:10.1080/02626660109492853

Fredsoe J. 1979. Unsteady flow in straight alluvial streams: modification of individual dunes. *Journal of Fluid Mechanics* **91**(3):497-512.

Einstein HA. 1950. The bed-load function for sediment transportation in open channel flows. *Technical Bulletin USDA Soil Conservation Service* **1026**:1-71.

Engelund F and Hansen E. 1967. A monograph on sediment transport in alluvial streams. Technical University of Denmark. Teknisk Forlag. Copenhagen, Denmark.

Humphries R, Venditti JG, Sklar LS and Wooster JK. 2012. Experimental evidence for the effect of hydrographs on sediment pulse dynamics in gravel-bedded rivers. *Water Resources Research* **48**:1-15. DOI: 10.1029/2011WR010419

Kamphuis, JW. 1974. Determination of sand roughness for fixed beds. *Journal of Hydraulic Research* **12**(2):193-203.

Karmin F and Holly FM. 1986. Armoring and sorting simulation in alluvial rivers. *Journal of Hydraulic Engineering* **112**(8):705-715.

Lopes VL and Ffolliott PF. 1993. Sediment rating curves for a clearcut ponderosa pine watershed in northern Arizona. *Journal of the American Water Resources Association* **29**(3):369-382. DOI: 10.1111/j.1752-1688.1993.tb03214.x

Meyer-Peter E and Müller R. 1949. Formula for bed load transport. Proc 2nd Meeting IAHR 6.

Reesink AJH and Bridge JS. 2007. Influence of superimposed bedforms and flow unsteadiness on formation of cross strata in dunes and unit bars. *Sedimentary Geology* **202**(1):281-296. DOI:10.1016/j.sedgeo.2007.02.005

Reesink AJH and Bridge JS. 2009. Influence of superimposed bedforms and flow unsteadiness on formation of cross strata in dunes and unit bars – Part 2, further experiments. *Sedimentary Geology* **222**(3):274-300. DOI:10.1016/j.sedgeo.2009.09.014

Rouse H. 1937. Modern conceptions of the mechanics of fluid turbulence. Trans *American Society of Civil Engineers* **102**:463-543.

Singh VP, Singh P, and Haritashya UK. 2011. Encyclopedia of Snow, Ice and Glaciers. Springer: Dordrecht, Netherlands.

Sturm TW. 2010. Open channel hydraulics. McGraw Hill: New York, New York.

van Rijn. 1984. Sediment transport part I: bed load transport. Journal of Hydraulic Engineering **110**(10):1431-1456.

Wang Z, Lin B, and Nestmann F. 1997. Prospects and new problems of sediment research. *International Journal of Sediment Research* **12**(1):1-15.

Williams GP. 1989. Sediment concentrations versus water discharge during single hydrologic events in rivers. *Journal of Hydrology* **111**(1):89-106.

Wood PA. 1977. Controls of variation in suspended sediment concentration in the River Rother. *Sedimentology* **24**(3):437-445.

Yalin MS. 1963. An expression for bed load transport. *Journal of Hydraulics Division* **89**(3):221-250.

Yalin MS. 1977. Mechanics of sediment transport. Pergamon Press, Oxford.

Yalin MS. 1985. On the determination of ripple geometry. *Journal of Hydraulic Engineering* **111**(8):Aug.

Yalin MS. 1992. River mechanics. Pergamon Press, Oxford.

Yalin MS and da Silva AMF. 2001. Fluvial Processes. IAHR Monograph. IAHR. Delft, The Netherlands, 197 pages.

Chapter 3

3 Morphological response of stream beds to unsteady flow events: a review of recent laboratory experiments

3.1 Introduction

Natural processes and anthropogenic activities, such as extreme rainfall events and reservoir flushing, can result in substantial and rapid alterations to sediment transport and stream bed morphology. These morphological adjustments can have widespread environmental and economic consequences, such as stream bank instability, transport of contaminated sediments, and damage to hydraulic structures. While knowledge of morphological response to changes in flow is necessary in order to lead to improved river management, our present ability to predict morphological change is hindered due to the complex relationship that occurs between hydraulics and sediment transport in response to unsteady flow events. Numerous laboratory, computational and field-based pioneering studies have been conducted on the morphological response of streams to unsteady flow events since the 1970s. In recent years, the morphodynamic response of stream beds to unsteady flow events has received a considerable increase in experimental laboratory research as greater attention is paid to the sensitivity of rivers and streams to the effects of such unsteady flow events as extreme flood events.

The goal of this Chapter is to provide a comprehensive review of recent experimental laboratory research into the morphodynamic response of alluvial stream beds to unsteady flow scenarios. The findings and contributions from these studies will be compared and analyzed, and from this, recommendations and strategic opportunities for future research will be identified. While unsteady flow events also result in plan form morphological response, the focus of this review will be on stream bed response alone, as the morphodynamics of stream beds has traditionally been studied experimentally by assuming rigid, fixed banks.

3.2 Review of recent laboratory experiments

This section aims to provide a comprehensive review of recent laboratory research from the literature. This review will be presented in two categories: sand and gravel bed streams. In order to distinguish between different experimental approaches, each category will be further sub-divided into sediment starved and sediment fed laboratory conditions. For each study, a

brief outline of objective of the research, experimental results, and major contributions are reported. Table 2 presents an overview of all studies reported in this Chapter. This table includes a summary of laboratory conditions (e.g., flume width and length), hydraulic parameters, (e.g., discharge, longitudinal bed slope, etc.) and observed sediment transport and bed morphological behaviour (e.g., bed morphology).

3.2.1 Sand bed streams

3.2.1.1 Sediment starved conditions

De Sutter et al. (2001) validated a laboratory flume investigation with an artificial flood simulation in the field. With the use of trapezoidal hydrographs these authors analyzed suspended sediment transport during an unsteady flow scenario representative of a snowmelt event. The maximum discharge was held constant for all hydrographs and the time to the peak discharge was varied. The stream bed of the flume was composed of a cohesionless sand and results were compared to the previous findings of experimental runs of De Sutter et al. (1999) using cohesive sediment. Bed morphological adjustments in response to the experimental hydrographs, which were run over the stream bed three consecutive times, were analyzed. Overall, the bed exhibited discontinuous, scattered bed forms during the first run of the hydrographs. However, this erosion pattern did not persist during the second and third repetition of the hydrograph. Rather, vertical sorting of the grains formed a protective structure over the bed, inhibiting any further degradation, consistent with patterns observed by De Sutter et al. (1999). De Sutter et al. (2001) concluded that hydrographs with a shorter time to peak discharge had the largest transport capacity. The influence that the unsteadiness of the hydrograph (variation in discharge over time) has on sediment transport rate was previously defined with equations proposed by Suszka (1987) and Nezu et al. (1997), who considered the duration of both the rising and falling limbs of the hydrograph in the

Table 2: Summary of laboratory conditions, hydraulic parameters and morphological response reported in experimental research from recent literature

Author	Maximum discharge [m^3/s]	Flume width [m]	Flume length [m]	Slope	Sediment	Hydrograph shape	Transport mode	Feeding conditions	Bed morphology	Hysteresis
Hassan and Church (2000)	-	0.80	10.0	0.0062 - 0.0066	G	T	BL	F	AM	CC,C
De Sutter et al. (2001)	4.02E-02	0.39	18.6	0.006	S	Z	SL	SS	D,R	C
Lee et al. (2004)	6.19E-02	0.60	21.0	0.03	S	T	BL	SS	D	CC
Hassan et al. (2006)	6.19E-02	0.60	9.0	-	G	T,Z	BL	SS	AM	C
Wong and Parker (2006)	5.16E-02	0.50	22.5	0.0089 - 0.014	G	T	BL	F	-	C
Reesink and Bridge (2007; 2009)	6.29E-02	0.61	7.6	-	S	A	BL	F	D,R,B	-
Ahanger et al. (2008)	1.03E-01	1.00	24.0	0.002 - 0.009	S	T	SL	F	D,R	C
Madej et al. (2009)	7.73E-02	0.75	12.0	0.01	G	T	-	F	AM,B	CC
Bombar et al. (2011)	8.25E-02	0.80	18.0	0.005	S	T, Z	BL	SS	D,R	CC
Nelson et al. (2011)	2.58E-02	0.25	6.0	0.0001	S	T, A	BL	SS	D,R	-
Humphries et al. (2012)	8.87E-02	0.86	28.0	0.0079	G	T	BL	F	B	C
Mao (2012)	3.09E-02	0.30	8.0	0.01	G	T,Z	BL	F	AM	CC,C
Piedra et al. (2012)	9.28E-02	0.90	7.0	0.007	G	T	BL	SS	AM	CC
De Costa and Coleman (2013)	-	-	-	-	S	A	-	SS	D,R	CC
Guney et al. (2013)	4.96E-02	0.80	18.6	0.006	G	T	BL	SS	AM	CC,C
Martin and Jerolmack (2013)	5.70E-02	0.92	15.0	-	S	T	BL	F	D,R	CC
Reesink et al. (2013)	3.10E-02	0.50	16.0	-	S	A	SL	SS	D,R	-

Legend: G = gravel; S = sand; T = triangular hydrograph; Z = trapezoidal hydrograph; A = alternate hydrograph formation; BL = bed load; SL = suspended load; F = sediment feeding; SS = sediment starved; AM = armored; D = dunes; R = ripples; B = bars; CC = counter-clockwise; C = clockwise

formulation of their expressions. Extending upon these expressions, De Sutter et al. (2001) proposed an unsteadiness parameter that only considered the rising limb of the hydrograph to demonstrate that as the unsteadiness of the discharge increases, the shear velocity (and hence the sediment transport rate) becomes a function of the time gradient of the flow alone.

Lee et al. (2004) applied triangular shaped hydrographs to investigate bed load transport for unsteady scenarios of varying magnitudes to replicate flood events representative of a hilly watershed. These authors sought to expand on the lag-time routing method of Marcus (1989), which accounts for differences in measured and calculated sediment transport during a flood-like event. Lee et al. (2004) analyzed the lag-time between the hydrograph and sediment transport rate peak values and compared observed bed load transport rates in both steady and unsteady flow experiments. Counter-clockwise hysteresis was observed during the experimental runs with a lag-time between 6% and 15%. The migration of pre-existing dunes was found to highly influence the sediment transport rate as sediment went through a series of aggradation and degradation stages during the unsteady event. Dunes grew in length and height during stages of increasing discharge and subsequently decreased in size during periods of decreasing discharge. Hydrographs with lower magnitudes produced a greater frequency of fluctuation in bed load transport rate while dune heights remained relatively small. On the other hand, in runs with hydrographs with higher peak discharges, the average dune height was greater and there was a lower frequency of fluctuation in the bed load transport rate. Lee et al. (2004) conducted a regression analysis to develop an accurate method of bed load transport prediction. The authors proposed an unsteadiness parameter, which was observed to increase with the bed load rate independently of the total flow-work index. According to Lee et al. (2004), the total bed load transport rate can be predicted using empirical sediment transport formulas suited for steady flow conditions by applying a suitable ratio ranging from 1:4 to 1:6 in order to estimate unsteady flow sediment transport conditions. Based on these results, Lee et al. (2004) proposed that steady flow could be used to estimate unsteady flow sediment transport in practical applications.

Nelson et al. (2011) also investigated bed load transport using triangular shaped hydrographs, however, the shape of their hydrographs simulated more rapid changes in discharge with time compared to the hydrographs of Lee et al. (2004). Hydrographs were either symmetrical or

started at maximum discharge and gradually decreased to base flow conditions. Nelson et al. (2011) examined the initiation of bed forms and the time required for equilibrium conditions of the bed to be reached based on bed form geometry. These authors sought to predict the drag created by bed forms and subsequent effect of this drag on sediment transport rates during flood-like events. Initial hydraulic conditions resulted in the formation of individual and incomplete ripples across the width of the flume. During the rising limb of the symmetrical hydrograph runs the length and height of the ripples increased. This caused the average step length of the entrained particles to increase and inhibited the growth of shorter features. As the discharge decreased, bed forms decreased in height or were observed to completely flatten. A shorter step length was observed on the lee side and trough areas of the bed forms, while a longer step length was observed at the upper crests. The step length was observed to increase to forty times the grain diameter as the flow increased. The opposite pattern was observed during decreasing flow periods. During varying flow regimes the dimensions of bed forms fluctuated significantly, both spatially and temporally, resulting in temporal variations in drag and local roughness. Nelson et al. (2011) analyzed the three-dimensional interaction occurring between the smaller-scale bed forms and larger scale crests. This occurred when the bed form crests transitioned to a cusp-like shape during the high flow periods. The authors suggested that this may be the result of the top of the crests growing too fast relative to the lower parts of the stoss side of the dunes as the crests transformed to more cusp-like shapes during the peak flow events. Their findings are in agreement with real world observations, demonstrating that bed forms are rarely in equilibrium during flood events, but rather constantly evolving with time. Nelson et al. (2011) concluded that flood hydrographs will result in longer and taller bed forms which will assist in the development of a more accurate representation of local roughness which is commonly misrepresented in many current computational flow models.

Bombar et al. (2011) used both triangular and trapezoidal hydrographs to investigate the effect of hydrograph shape on bed load transport rate. The hydrographs were obtained manually from depth-averaged velocity measurements and a numerical algorithm to smooth the velocity data. Bombar et al. (2011) found that trapezoidal hydrographs demonstrated greater counter-clockwise hysteretic lag-times than triangular hydrographs. The total sediment yield increased exponentially with the total flow-work index, while the total flow-work index had an inverse exponential relationship with the observed hysteresis. Bombar et al. (2011) compared their

results to De Sutter et al. (2001) and Lee et al. (2004) in order to improve upon the unsteadiness parameter developed by those authors. The new parameter, based on the concept of net acceleration, was developed based on their experimental findings and validated against a numerical model. Overall, the validated model produced sediment yield errors for the triangular and trapezoidal hydrographs of 7% and 15%, respectively.

Reesink et al. (2013) investigated the effect of free surface slope and flow depth on pre-existing dunes during suspended load transport experiments. These authors varied the flow depth and free surface slope to simulate naturally occurring features, such as deeper areas of the bed (i.e., stream thalweg), shallower areas (i.e., bars), and transitional areas (i.e., river mouth connections). When the water depth increased, a successive decrease in free surface slope, Froude number, dune migration, and trough scour was observed. A series of superimposed bed forms developed on the stoss slope of the pre-existing dunes, which, in turn, caused upstream bed forms to merge and increase in size. Although the presence of superimposed bed forms is naturally occurring, it can be considered to be a function of the discontinuity observed between the flow passing over the dune stoss slope and the initial dune geometry. This suggests that any antecedent bed morphology, sediment transport rates and bed form kinematics will affect the degradation of large dunes and the formation of smaller bed forms. When the water depth decreased the Froude number still decreased but in contrast to the first run, the trough scour and dune lengths were observed to increase. However, there was no development of a bed form train and downstream superimposition did not occur. The third run conducted by Reesink et al. (2013) increased the discharge with a fixed depth which resulted in an overall increase in dune migration, scour depth, Froude number, and dune crest height. The number of superimposed bed forms was observed to decrease in this run. In the final run, the water depth was decreased and the opposite effects that occurred in the third run were observed. Reesink et al. (2013) concluded that variations in water depth had a greater influence on the morphology of the bed than alterations in free surface slope. According to these authors, bed forms are controlled by four key factors: bed form stability range, variability in bed form stability, bed form kinematics, and relative magnitude of free surface slope and depth.

De Costa and Coleman (2013) also investigated the temporal and spatial changes in developed dunes as a result of alterations in flow in alluvial laboratory streams. Their results were used together with those of Allen (1976) and Julien and Klaasen (1995) to develop a stochastic

model to represent the time required for changes in dune morphology to occur as a response to alterations in discharge. These authors experimentally developed a stochastic model by measuring the depth and shape of the dunes and velocity distribution to create a three-dimensional representation of the bed forms. The experimental results of De Costa and Coleman (2013) demonstrated counter-clockwise hysteretic behaviour between the bed form geometry, however, hysteretic loops observed during experimental and computed runs varied significantly. The experimental results regarding sediment transport rates in response to the varying discharges appeared to be either sharply peaked or steady during stages of low discharge. In contrast, the developed computer model produced smoother transitions in sediment transport rates. De Costa and Coleman (2013) found that average dune height and wavelength can respond differently over the distance a dune travels before it degrades. The experimental range of average dune length and height was a near-identical match to the theoretically-calculated values for the smallest experimental dunes. To accurately represent the differences observed during experimentation and computational modeling, De Costa and Coleman (2013) proposed a new parameter (referred to as gross bed form-normal transport parameter), in order to account for bed form alignment issues.

3.2.1.2 Sediment feeding conditions

Reesink and Bridge (2007; 2009) conducted a two-part study to determine the influence of superimposed bed forms during unsteady flow events on the formation of subsequent bed forms. This research sought to investigate the grain sorting that occurs during bed-load transport and pre-sorting observed on the back of dunes that form superimposed bed forms or unit bars. The work of Reesink and Bridge (2007) included: (1) simulating cross strata over dunes and unit bars in a sandy gravel bed during steady and unsteady flow conditions; (2) determining the geometry, sorting, porosity and permeability of the formed cross strata; (3) determining the controls of the cross strata formation; and (4) investigating the use of cross strata to interpret the flow conditions in which they developed. Cross-stratification features are the most common structure in depositional areas of rivers that are created by dunes and unit bars and have been used to determine historic flow and sediment regimes (Bridge, 2003). Reesink and Bridge (2007) found an increase in the dilation of the bed material, which resulted in a decrease in the effectiveness of the kinetic sieving and consequentially an increase in the effect of differential settling. Dilation is the process of reorganization of larger particles within

the bed structure to be packed more loosely (Marquis and Roy, 2012) and kinetic sieving is the process that allows grains of different sizes to segregate into graded layers resulting in larger particles on top of finer particles (Bridgwater, 1976). A field study conducted by Marquis and Roy (2012) in Beard Creek, Quebec, Canada, validated the experimental behaviour observed by Reesink and Bridge (2007). Overall, the grain size was observed to increase on cross strata and the finest grained sediments of the re-circulated sediment was deposited on the lee side of previously existing unit bars. Reesink and Bridge (2007) concluded that the grain size variation responsible for the development of cross strata had three controlling factors: 1) pre-sorting caused by superimposed bed forms and unsteady flow conditions; 2) the bed load transported is sorted and deposited on the lee side of the bed forms; and 3) due to the previous two factors, the slope reworks itself. These three controlling factors result in considerable variation in cross strata geometry, grain-size sorting and permeability and can be used to quantitatively interpret river-channel deposits. Reesink and Bridge (2009) determined that the pre-sorting pattern responsible for the formation of cross strata on the superimposed bed forms can be used to interpret the pre-existing and superimposed bed form geometries. However, these authors observed that the pre-sorting pattern is no longer present if there is less sediment available than there was during the re-sorting of the sediment on the lee side. Reesink and Bridge (2009) concluded that because the plan-view shape of the pre-existing bed forms lee slope controls the geometry of the cross strata, the cross strata can then be used to determine the type, size and geometry of the antecedent and superimposed bed forms. The unsteady flow conditions and the associated sediment transport rates morphologically control the geometry of the lee-side of pre-existing bed forms.

Ahanger et al. (2008) investigated the hysteretic effects of asymmetrical and symmetrical triangular hydrographs on suspended load sediment transport. In these runs the authors fed sediment to the stream at a rate equal to that of which the sediment was transported during a steady flow event of similar magnitude. Fourteen different hydrographs were simulated. Changes in water discharge, depth and suspended sediment concentration were measured. Each hydrograph was run over the bed of the flume for four different slopes ranging between 0.002 and 0.009 and all experiments were completed for two different sand sizes. Ahanger et al. (2008) observed that clockwise hysteresis of the suspended load was evident during all hydrographs and for both sand sizes. Multiple regression analysis of the laboratory results was

applied to relate the variables and develop two independent equations for the rising and falling limbs of the hydrographs. The experimental and computed sediment load parameters were nearly similar, suggesting a high level of accuracy of these expressions. More specifically, the peak sediment discharge and the time to peak were found to be accurate but highly sensitive to changes in flow depth, particularly those experienced during the falling limb of a hydrograph. The equations developed by Ahanger et al. (2008) were then validated against a series of hydrographs and results indicate that these expressions are a promising approach to predict sediment transport rates during unsteady flow events.

Martin and Jerolmack (2013) conducted a series of experiments with hydrographs of varying magnitudes to determine the morphological response of pre-existing dunes to bed load transport rates during unsteady events. Some suspended load occurred during higher flows but this was neglected as it had little influence on the bed morphological development. Two time series for the stepped hydrographs were used in these runs: (1) hydrograph time steps that lasted for the time required for equilibrium to be reached; and (2) time step adjustments of prescribed durations (either 20 minute time steps over a total of eight hours, or five minute time steps over a total of two hours). Throughout the experiments, an abrupt increase in discharge resulted in the rapid dune growth by collision and merging that proceeded to migrate with varying celerities. The dune growth rates slowed as the bed forms approached equilibrium under each respective discharge regime. During periods of decreasing discharge, bed form decay occurred due to the formation of smaller secondary bed forms. Once these bed forms reached their subsequent equilibrium geometry, the original bed form features were completely degraded. Martin and Jerolmack (2013) concluded that hydrographs with shorter durations produced a greater magnitude of hysteresis. Furthermore, these authors suggested that the hysteresis that was observed between the bed form geometries and discharge were dependent upon the time scale over which the discharge varied.

3.2.2 Gravel bed streams

3.2.2.1 Sediment starved conditions

Hassan et al. (2006) conducted laboratory experiments representative of unsteady flow events typically observed in gravel bed streams situated in humid and snowmelt areas that experience armoring. Hassan et al. (2006) used trapezoidal and sharply peaked hydrographs of varying

durations to determine their effects on the bed load transport rate and the bed armoring process. Asymmetrical and symmetrical hydrographs had either a constant duration and varying magnitudes or a constant magnitude and a varying duration. Experimental results in the asymmetrical hydrograph runs showed a large amount of sediment sorting occurring during the falling limb and winnowing of the bed material for the first ten hours of experimentation. Clockwise hysteresis was observed in the sediment transport rates in the symmetrical hydrograph experimental runs and the particle size distribution of transported material was observed to be finer than the original bed composition. In contrast to the findings of Gomez (1994), Hassan et al. (2006) concluded that winnowing is not a dominant control of armoring, and rather, grain size distribution should be used as an indicator of armor development.

A recent experimental study conducted by Piedra et al. (2012) applied triangular, stepped hydrographs of varying durations to quantify coarse bed development and investigate the associated sediment transport mechanisms. The total surface area occupied by the clustered coarse grains and the areas of accumulation of the connected grains were related to the threshold values of shear stress during entrainment. It was observed that as the magnitude of the discharge increased, the overall size of these accumulations was larger. Lower critical bed shear stress values occurred for beds with higher degrees of clustering. Bed structures were found to be more stable when the coarse grains were distributed more evenly over the bed surface. Piedra et al. (2012) determined that bed surface composition and the spatial distribution of the coarsest grains could be used as an indicator of bed resistance to sediment transport and degradation during unsteady events. Image analysis software was used to determine size classes and particle clusters from digital images in conjunction with ultraviolet light. Due to its ease of application and short processing time Piedra et al. (2012) suggest the use of this technique to be promising for a variety of sediment transport applications.

Guney et al. (2013) used symmetrical hydrographs to examine the effect of armoring on bed load and grain size distribution of the transported material. Similar to De Sutter et al. (2001) and Nelson et al. (2011), hydrographs were run three consecutive times over the deforming bed. In order to determine the dimensionless reference shear stress, Guney et al. (2013) applied the equation developed by Wilcock and Southard (1988) that incorporated the theories of Einstein (1950) and Parker (1979). These authors also determined the armor ratio for their experiment to analyze the influence of the total bed load. An armor ratio is the ratio of surface

median grain size to substrate median grain size and was used to determine the degree and formation of armoring of the bed. After the first run, clockwise hysteresis was observed as sufficient supply of upstream sediment existed during this period. During the second run this hysteretic behaviour was not present. By the third run, an armored bed had developed and counter-clockwise hysteresis was observed in the bed load transport rate. Guney et al. (2013) concluded that the maximum bed load transport rates observed during the experiments depended on the antecedent flow and the degree of coarseness of the bed. Following the experiments, the authors used the total bed load equation developed by Bombar et al. (2011) to demonstrate that the coarse surface created during the antecedent flows is an influencing factor on the bed morphology and total sediment transport rates.

3.2.2.2 Sediment feeding conditions

Hassan and Church (2000) investigated the changes in surface texture and structure of a static, armored sediment bed using triangular and trapezoidal hydrographs during periods of both sediment starvation and sediment supply. In order to create the pre-existing armored state of the bed, the authors conducted preliminary experiments using steady flow. Low rates of sediment feeding were used over a developed bed to investigate the influence of feeding rates on sediment transport. Hassan and Church (2000) re-circulated the sediment through the flume at various percent intervals (i.e., 50%, 75%, 100% and 150%). The majority of the bed re-organization occurred during the early stages of the experiments, irrespective of the percentage of sediment fed to the flume. When the triangular hydrographs were introduced to the system the bed load exhibited contrasting types of hysteresis. The symmetrical hydrograph produced clockwise hysteresis while the asymmetrical hydrograph created counter-clockwise hysteresis. The armored bed structure resulted in stone clusters that trapped smaller sediment from being entrained causing the overall bed structure to remain fairly stable throughout the experiment. According to Hassan and Church (2000) the bed surface texture depends on the size of entrained sediments and the discharge rate. Hassan and Church (2000) concluded that the majority of the bed shear stress is either carried by the structure of the bed or absorbed by the transport load, with the remaining portion of the bed shear stress being absorbed by the bed grains.

Wong and Parker (2006) analyzed the bed load transport response to the repetition of symmetrical and asymmetrical hydrographs of varying durations and shape. These experiments were conducted until a state of mobile-bed equilibrium was observed under constant feeding conditions. Three different scenarios were used to investigate the effect of varying the total duration of the hydrographs, the length of the falling limb and the peak discharge values. Overall, clockwise hysteresis was observed in terms of aggradation and degradation of the bed surface. Aggradation began to occur near the peak flow of the hydrograph. Degradation of the bed surface was observed to occur at a lower rate in the falling limb of the hydrograph compared to the rising limb. However, similar to Griffiths and Sutherland (1977), Wong and Parker (2006) reported very little or no lag in the total bed load transport rate. In the initial reach of the flume the bed elevation and bed slope were observed to fluctuate cyclically with the changing discharge. The transport rate remained nearly equivalent to the constant feeding rate. In the downstream section, while the bed elevation and slope did not fluctuate substantially in response to the changes in discharge, the amount of transported bed load was affected. Considering this, Wong and Parker (2006) concluded that gravel-bed rivers subjected to hydrograph peaked flows will adjust accordingly to minimize the response of changes in bed structure and maximize the response observed in the bed load transport rate. The slope of the initial bed was found to be of critical importance to the number of hydrograph cycles required to achieve a state of mobile-bed equilibrium. Wong and Parker (2006) attributed the bed elevation fluctuations to the stochastic nature of entrainment, similar to the transport processes described by Yalin (1977).

Madej et al. (2009) examined the response of an armored laboratory stream bed to varying sediment inputs. The experiments were modelled after flood events that affected Redwood Creek and Emerald Creek in northern California, USA. Sediment feeding rates were based on rates associated with 12, 20 and 50-year flood events within this northern Californian watershed. The authors measured changes of overall bed slope, sediment storage, morphological changes and bed texture during their experimental runs. During the initial stages of the bed development process mid-channel bars were observed to form as a response to the sediment feeding. Bed morphology was investigated by conducting cross-sectional transects to quantify channel processes such as incision, fill or the growth and decay of lateral bars. Counter-clockwise hysteresis was observed with a lag-in-time of one hour. The bed roughness

decreased during the rising limb (periods of aggradation). The bed surface became finer when the sediment feeding rate was high which allowed for greater subsequent sediment transport. During the falling limb (periods of degradation), the sediment transport rate remained relatively high because sediment accumulated within the bed forms during the phase of aggradation. The transport rate demonstrated an observable relationship to the rate at which sediment was fed into the flume. As the feed rate was increased, the bed became less armored and subsequent bed morphological adjustments occurred. Laboratory results of Madej et al. (2009) were very similar to field surveys of Redwood Creek that also produced changes to bed slope, sediment aggradation and degradation, channel morphology, and bed texture in response to flood events. Madej et al. (2009) concluded that alterations in the sediment transport rate at the end of the flume was found to be a function of the rate of sediment feeding, storage within the bed and bed mobility.

Humphries et al. (2012) extended the research of Hassan and Church (2000) and Madej et al. (2009) by investigating effect of pulsed inputs of sediment on armored gravel beds. In contrast to other authors, Humphries et al. (2012) based their experiments on the stream restoration methodology of gravel augmentation. Their flume bed was consequently altered to create a pool-bar morphology. Gravel augmentation is a restoration method used to control sediment releases near a dam that has depleted the stream of its natural ability to transport sediment. The pool-bar morphology lessens the effects of incision, coarsening and sediment immobility. The peak discharges for hydrographs of varying durations all occurred after two and a half hours. The hydrographs produced a definitive pattern of clockwise hysteresis of sediment transport and the pulsed sediment inputs tended to accumulate at the point bars. This process can be projected to eventually lead to channel migration in the natural environment. Hydrographs with lower magnitudes resulted in dispersion of the sediment pulses and very little translation. On the other hand, the hydrographs with larger magnitudes caused dispersion and some sediment translation. The findings of Humphries et al. (2012) contributes to more effective stream restoration through developing a better understanding of the sediment transport and morphological response of forced pool-bar morphology to unsteady flow events.

Mao (2012) investigated the effect of stepped triangular and trapezoidal hydrographs (typical of extreme rainfall and snowmelt events, respectively) on bed load and spatial arrangement of the bed structure. The sediment composition of the bed was manually re-circulated every one

to 10 minutes throughout the experiments, allowing for an armored bed to develop. Clockwise hysteretic effects on the bed load transport rates were observed during the experiments. This trend was seen most prominently during low magnitude flow hydrographs. In contrast, the size of the sediment grains transported exhibited counter-clockwise hysteresis. An increase in the reference shear stress for sediment entrainment was observed in the falling limb, and as a result, there was reduced sediment mobility. Mao (2012) suggested that this effect of hysteresis appeared to be caused by a change in the surficial structure of the bed sediments. Changes in the degree of structure and complexity of the bed surface are likely the cause of the reduced mobility of sediments resulting in a reduced sediment transport rate during the falling limb of the hydrographs.

3.3 Discussion and strategic opportunities

Results and contributions from the experimental studies discussed in this Chapter make it evident that a full understanding of the morphological response of alluvial stream beds to unsteady (flood-like) events remains incomplete. Although some studies reported conflicting results, several general trends and similarities arose after comparison of the main contributions from the previous experimental research. This section begins with a discussion of the various factors responsible for hysteresis. Following this, a discussion of proposed predictive models of morphological response is discussed. This section concludes with a summary of strategic opportunities for further investigation.

3.3.1 Factors affecting hysteresis

While there is not yet complete agreement regarding the factors responsible for alterations in sediment transport and bed morphology during unsteady flow events, many previous studies have reported specific causes of hysteresis from their respective experimental results. In the following section contributions from previous research regarding hysteretic behaviour of sediment transport during unsteady flow events are discussed according to the following four factors: 1) sediment composition; 2) hydrograph shape; 3) sediment supply; and 4) bed morphological development. These factors can have counteracting effects on the sediment transport and bed morphological responses to unsteady flow events, making it difficult to assess the influence of factors responsible for hysteresis individually.

3.3.1.1 Sediment composition

Sediment classification and grain size are important factors to consider when evaluating the effects of unsteady flow events on sediment transport rates and bed morphological response. No clear trend in the type of hysteresis occurring in sand bed streams was evident. De Sutter et al. (2001) and Ahanger et al. (2008) observed clockwise hysteresis while the majority of other authors observed counter-clockwise hysteresis (e.g., Lee et al., 2004; Bombar et al., 2011; De Costa and Coleman, 2013; Martin and Jerolmack, 2013). Lee et al. (2004) and Bombar et al. (2011) reported different types of hysteresis but similar lags-in-time between the hydrograph and peak sediment transport rate. Gravel beds exhibited both clockwise (e.g., Hassan et al., 2006; Wong and Parker, 2006; Humphries et al., 2012) and counter-clockwise (e.g., Piedra et al., 2012; Madej et al., 2009) hysteresis. In some gravel bed experiments, both clockwise and counter-clockwise hysteresis were observed (e.g., Hassan and Church, 2000; Mao, 2012; Guney et al., 2013). For example, Mao (2012) reported clockwise hysteresis in the total bed load transport rate, but the size of the sediment being transported demonstrated counter-clockwise hysteresis. Experiments of Wong and Parker (2006) and Martin and Jerolmack (2013) reported the occurrence of little or no hysteresis.

3.3.1.2 Hydrograph shape

The type of hydrograph associated with the unsteady event is also an important factor affecting the type of hysteresis occurring in the sediment transport rate and bed development. It is known that hydraulic conditions, in part, control sediment transport rates and bed morphological development. These can be accurately calculated for steady-flow conditions. During unsteady flow events, the effect of specific changes in discharge over time on sediment transport rates and bed morphology cannot be accurately predicted due to hysteresis. It is important to consider the effect of the hydrograph discharges by considering peak flow magnitudes, duration of hydrograph, hydrograph shape (triangular or trapezoidal), time-to-peak flow, and the distribution of rising and falling limbs over the duration of the total hydrograph (symmetrical or asymmetrical skewness). In general, it is known that sediment transport rates and bed morphology generally follow the trends of the hydrograph but as noted in the Section 3.3.1. there has been no general relationships established.

Antecedent flow conditions considered as prior to, or part of, the flood hydrograph play an important role. According to Mao (2012), the consideration of antecedent flow during unsteady bed load transport experiments remains one of the most neglected areas of study associated with this phenomenon. Stream beds that are subjected to larger and longer discharges, yet remained below the threshold for entrainment, required greater shear stresses to entrain sediment than beds that were not subjected to antecedent flows (Monteith and Pender, 2005; Hayes and Pender, 2007). Studies by Piedra et al. (2012), Mao (2012) and Guney et al. (2013) support the need for further analysis of the effect of antecedent flow as their results were considered to be dependent upon antecedent flow conditions.

The majority of the experimental research summarized in this Chapter used triangular-shaped hydrographs (e.g., Ahanger et al., 2008; Madej et al., 2009; Nelson et al., 2011; Piedra et al., 2012; etc.). However, a variety of symmetrical and asymmetrical triangular shaped hydrographs of varying magnitudes and durations were also used. At present, there remains no direct relationship between hydrograph shape, sediment transport rates and bed morphological adjustments. De Sutter et al. (2001) used trapezoidal hydrographs to simulate the process of snowmelt. Other studies used a combination of triangular and trapezoidal hydrographs (e.g., Hassan et al., 2006; Bombar et al., 2011; Mao 2012). Bombar et al. (2011) quantified the difference in hysteresis that occurred from triangular and trapezoidal shaped hydrographs due to hydraulic differences. Due to shape variation, rising and falling limbs of the hydrographs should be considered separately (Ahanger et al., 2008; Nelson, 2011; Martin and Jerolmack, 2013). Several studies reported in this Chapter simulated changes in water depth and discharge but did not report the use of a traditional hydrograph (Reesink and Bridge, 2007; Reesink and Bridge, 2009; Nelson et al., 2011; De Costa and Coleman, 2013; Reesink et al., 2013).

In general, lower magnitude hydrographs resulted in a greater lag-in-time of sediment transport rates and bed morphological response (e.g., Lee et al., 2004; Martin and Jerolmack, 2013; Humphries et al., 2013) and larger magnitude hydrographs demonstrated smaller lag-in-times (Lee et al., 2004). The total duration of the hydrograph plays a prominent role in determining the type of hysteresis in the sediment transport rates (e.g., Hassan et al., 2006; Humphries et al., 2012; Mao, 2012). Lee et al. (2004) and Wong and Parker (2006) expressed contrasting views regarding the relationship between hydrograph peak discharges and duration of hydrographs. Lee et al. (2004), in agreement with Song and Graf (1997), suggest that if the

time steps of the hydrographs were too long then they are inaccurate in depicting unsteady flow behaviour associated with flood events. In contrast, Wong and Parker (2006) emphasize the importance of a hydrograph encompassing a substantial amount of time in order to capture the stream beds hysteretic morphological response to a flood event. Hydrographs with shorter time to peak flows are also found to generate larger time-lags in sediment transport rates (De Sutter et al., 2001). As expressed by Hassan et al. (2006), further investigation is required into the hydraulic factors of the hydrograph that control coarse bed armoring processes.

3.3.1.3 Sediment supply

Sediment availability has also been found to be a factor influencing the type of hysteresis observed in the sediment transport rates and bed development (Hassan et al., 2006; Mao, 2012). Sediment feeding is a complex process to replicate in an experimental setting. As a result, there remains great uncertainty regarding the effect of varying sediment supply on hysteresis during unsteady flow experiments. Few sand bed experiments applied sediment feeding conditions to their experimental runs (e.g., Reesink and Bridge, 2007; Reesink and Bridge, 2009; Martin and Jerolmack, 2013), while sediment feeding was more frequently applied in gravel bed experiments (e.g., Hassan and Church, 2000; Wong and Parker, 2006; Madej et al., 2009; Humphries et al., 2012; Mao, 2012).

Sediment feeding conditions and the associated traditional type of hysteresis were discussed previously in this thesis (see Section 2.5). However, results from certain studies, including De Sutter et al. (2001) and Ahanger et al. (2008), contradict these general claims. The effect of available sediment supply was identified by Guney et al. (2013) who reported two types of hysteresis in gravel bed load experiments with sediment starved conditions. Hysteretic behaviour was altered each time the same hydrograph was repeated over the bed. Clockwise hysteresis, no hysteretic transport and counter-clockwise hysteresis were observed for the three repetitions of the hydrograph over the bed, respectively. According to these authors, during the first run there was considerable upstream supply of sediment to entrain, allowing the bed to remain un-armored and as a result, clockwise hysteresis occurred. No hysteresis during the second repetition of the hydrograph could likely be attributed to a phase of transition, where upstream sediment supply was lessening and the armor layer was beginning to form. During

the third repetition, the supply of upstream sediment decreased in availability resulting in a completely armored bed and counter-clockwise hysteretic behaviour.

Further research to determine the effect of varying sediment feeding on armored beds is required (see, e.g., Hassan and Church, 2000; Hassan et al., 2006; Madej et al., 2009; Guney et al., 2013). Hassan and Church (2000) recommend that sediment feeding should be varied to analyze the effect of armoring during the falling limb of a hydrograph. Hassan et al. (2006) reported that a lack of sediment feeding allowed vertical sorting within the bed and counter-clockwise hysteresis to occur. Investigation into cyclical sediment supply (increasing or decreasing sediment feeding rates to correspond with the changes in discharge) or varying pulsed sediment supply is recommended for future studies (Wong and Parker, 2006; Reesink and Bridge, 2007; Madej et al., 2009; Bombar et al., 2011). Madej et al. (2009) recommended using a variety of sediment feeding rates in order to study the spatial relationship between transport capacity, storage of sediment and bed mobility: cyclical feeding rates would simulate the sediment introduced to a riverine system from overland runoff, whereas varying pulses of sediment would simulate bank collapse occurrences typical of flood events. Mao (2012) also recommended the investigation of an unlimited sediment supply while Wong and Parker (2006) and Bombar et al. (2011) recommended examination of a constant feed rate in conjunction with a trapezoidal-shaped hydrograph to simulate snowmelt. Based on these results, it is recommended that other factors, such as bed development and sediment feeding conditions, be considered and investigated independently to understand the apparent inconsistent hysteretic behaviour of the transported sediment.

3.3.1.4 Bed morphological development

The manner in which bed morphological development occurs in response to an unsteady event can also be a valuable indicator of the type of hysteresis likely to occur. For example, both sand and gravel beds exhibiting hysteresis attribute the lag-in-time between an adjustment, storage period or re-organization of the bed structure to bed morphology (Lee et al., 2004; Hassan et al., 2006; Madej et al., 2009; Humphries et al., 2012; Mao, 2012). Quantitative analysis of bed morphological development and adjustments during unsteady flow events has only started to be investigated within this last decade. Due to the differences between

morphological processes, sand and gravel beds will be discussed individually in the two sub-sections below.

3.3.1.4.1 Sand bed forms

In general, bed form height and length grow with increasing discharge and decrease in periods of decreasing discharge (e.g., Lee et al., 2004; Nelson et al., 2011; Martin and Jerolmack, 2013). Flow depth also plays a significant role in bed form development in sand bed streams. For example, Reesink et al. (2013) reported a decrease in dune migration rate with systematic increases in water depth. As the water depth decreased, the length of the dunes increased and superimposed ripples that were previously present disappeared. Martin and Jerolmack (2013) observed that as discharge was lowered, dune decay was accompanied by the formation of small secondary bed forms until the antecedent bed forms were completely degraded. Previous studies have concluded that further investigation into the effect of flow depth variation on the hysteretic behaviour of bed forms is required (see, e.g., Lee et al., 2004; Reesink et al., 2009; Reesink et al., 2013). Reesink et al. (2013) and Reesink and Bridge (2009) found the overall bed development to be more sensitive to changes in water depth than subtle changes in discharge due to the appearance of superimposed bed forms. On the other hand, Lee et al. (2004) considered flow depth variation and bed adjustment as complementary processes that simultaneously occur with changing discharges. Similar to Reesink et al. (2013), Lee et al. (2004) observed that flow depth adjustments resulted in the greatest amount of hysteretic behaviour in the bed load transport rate.

Cross strata and superimposed bed forms have only just started being investigated. Despite efforts by Reesink and Bridge (2007), further investigation is required into the kinetic sieving of sediment within bed forms in response to unsteady flow events. Reesink and Bridge (2007) suggested that a pulse of sediment may cause unit bars to migrate. Knowledge of three-dimensional bed form geometry, rate of migration and grain size sorting of pre-existing and superimposed bed forms is required in order to develop a greater understanding of the effects of long term unsteady flow on bed morphological response (Reesink and Bridge, 2007; Reesink and Bridge, 2009; Nelson et al., 2011; De Costa and Coleman, 2013; Unsworth et al., 2013). Nelson et al. (2011) also reported that determining the quantitative step length of bed load in relation to changing discharges over sand beds covered with dunes would allow for a

better understanding and representation of the geometry of three-dimensional dunes. The mechanics of the bed formation and bed form decay during more complex unsteady flow events is also required. Reesink et al. (2013) recommended further research into the mechanics responsible for the creation of a boundary layer on the stoss side of bed forms while Martin and Jerolmack (2013) recommend further studies to examine the spatial pattern of bed forms.

Martin and Jerolmack (2013) assumed that bed load drives the bed morphological development while suspended load has negligible effects due to a balance between sediment diffusion into the suspended load region and grain settling on the bed. However, the hydraulic conditions used during these authors' experiments allowed for substantial suspended load to occur over a dune-covered bed. Similarly, McElroy and Mohrig (2009) also adopted the use of this assumption. Neglecting significant suspended load may not be an entirely valid assumption, as the balance between sediment diffusion and settling will not be at equilibrium as the discharge varies throughout the hydrograph. As the flow begins to decrease, the sediment that was once in suspension may not have had time to exit the flume, and in turn, deposits on the bed of the flume and contributes to the bed morphological development. This would clearly also depend on the duration of the hydrograph and the size of sediment in suspension. For example, smaller grain sizes that are entrained as suspended load may become re-deposited on the bed and have negligible effect on the overall morphology, however, periods of increased flow rate may result in larger sediments entering suspension which, once re-deposited on the bed, may have considerable influence on the overall bed morphology.

3.3.1.4.2 Gravel bed forms

The majority of the gravel bed experiments summarized in this Chapter were conducted in conditions that allowed for the formation of armored beds. In general, previous research reveals that gravel bed rivers adjust (or armor) to minimize the effect of unsteady flow events on bed structure (Wong and Parker, 2006). Despite the type of hysteresis present, the majority of the bed structure was reorganized during the relative early stages of the experimental hydrographs. The majority of the results were based on the degree of armoring at the end of a flood-like event and as a result De Sutter et al. (2001) recommended further investigation to determine the effect of the rising limb of the hydrograph on an armored bed. However, other studies suggest that armoring was most dominant during the falling limb of the hydrographs (see, e.g.,

Hassan et al., 2006; Humphries et al., 2012). Overall, it was also observed that upstream sediment supply is the dominant process responsible for armoring (see, e.g., Hassan and Church, 2000; Hassan et al., 2006). However, Pender et al. (2001) and Guney et al. (2013) both report that unsteady flow and bed composition are not the only influencing factors affecting armoring, and emphasize the importance of also considering shear stress and winnowing of the bed surface material.

The ability to obtain accurate data in the laboratory may have inhibited the ability for further conclusions to be drawn regarding armored gravel bed structure. Hassan and Church (2000) suggest the development of a more direct experimental method of investigation to study the relationship between the stability and structure of the bed. Piedra et al. (2012) also acknowledged this need as the gravel clusters that formed during their laboratory experiments were due to a single coarse fraction from a limited number of short experiments. According to Hassan and Church (2000), the stability, structure and texture of armored gravel beds have yet to be successfully parameterized. Greater knowledge of gravel bed structure and stability will also allow for a more complete understanding of sediment transport during unsteady flow events, as transport is especially sensitive to the bed surface structure.

3.3.2 Prediction models of morphological response

Numerous theories, parameters and equations have been proposed to predict sediment transport behaviour during unsteady flow events. Sediment transport predictive equations were developed to incorporate the entire duration of the hydrographs (see, e.g., De Sutter et al., 2001; Lee et al., 2004; Bombar et al., 2013; Guney et al., 2013). In particular, Ahanger et al. (2008) proposed two separate equations for the rising and falling limbs of the hydrographs to better predict hysteretic sediment transport rates. Other predictive methods were created by Hassan et al. (2006), Reesink and Bridge (2007; 2009), Nelson (2011), Humphries et al. (2012) and De Costa and Coleman (2013).

De Sutter et al. (2001) proposed a parameter to represent the unsteadiness of the flow hydrographs for suspended load transport. Previous parameters developed by Suszka (1987) and Nuzu et al. (1997) considered both the rising and falling limbs of the hydrograph, however, De Sutter et al. (2001) proposed that only the duration of the rising limb is required in order to sufficiently represent the unsteady flow based on the observed effect on the suspended

sediment transport rate. The parameter was developed based on a calculated shear stress typical of steady flow in conjunction with the time lag observed during the experiments, and was found to be proportional to the parameters due to Suszka (1987) and Nezu et al. (1997). The De Sutter et al. (2001) parameter was further validated against the work of Kabir (1993), Bestaway (1997), Song and Graf (1997), De Sutter et al. (1999), and De Sutter et al. (2000). Lee et al. (2004) also proposed a parameter for unsteady flow. This parameter was related to the total bed load yield. Applying a regression analysis, a direct relation between the two parameters developed by Lee et al. (2004) and De Sutter et al. (1999) was observed for the experimental data collected by Lee et al. (2004).

Bombar et al. (2011) expanded upon the predictive parameters created by De Sutter et al. (2001) and Lee et al. (2004). Despite both studies reporting bed load transport in a counter-clockwise pattern, there was not good agreement observed between the experimental findings of Bombar et al. (2011) and the parameter created by Lee et al. (2004). The parameters did not yield realistic results and a very weak relationship was observed between the total bed load and the unsteadiness parameters for the experimental results of Bombar et al. (2011). Bombar et al. (2011) developed a dimensionless parameter based on the same concept of net acceleration followed by De Sutter et al. (2001). According to Bombar et al. (2011) the versatility of the proposed parameter and how it would respond to variations in hydrograph shape remain uncertain.

Based on peak and base flow measurements of flood-like hydrographs, Guney et al. (2013) applied the dimensionless total bed load parameter proposed by Bombar et al. (2011) for sand bed experiments to their gravel bed experiments. Guney et al. (2013) validated the Bombar et al. (2011) parameter on an armored bed and further developed two expressions to represent the interrelationships between the antecedent flow rate, maximum bed load transport rate, and total bed load. Guney et al. (2013) demonstrated a strong correlation between the Bombar et al. (2011) dimensionless bed load parameter and the armor ratio.

Other predictive methods were created for sand and gravel beds to better understand the relationship between post-event bed forms and variation in discharge. Reesink and Bridge (2007; 2009), Nelson et al. (2011) and De Costa and Coleman (2013) addressed sand bed predictive methods while Hassan et al. (2006) and Humphries et al. (2012) proposed predictive

methods for gravel bed streams. According to Reesink and Bridge (2007; 2009) cross strata development, grain size variation and geometry could quantitatively predict antecedent and superimposed river-channel deposits. Nelson et al. (2011) also developed a computational model for bed formation during unsteady flow events. Although the model predicted bed forms that were smaller than those observed, the model produced relatively accurate results. The model failed to accurately predict the rate of increase in wavelengths of bed forms during peak flows and towards the end of the falling limb of the hydrograph. With data from Allen (1976) and Julian and Klaasen (1995), De Costa and Coleman (2013) created a gross bed form normal transport parameter to estimate the time required for changes in dune morphology to respond to discharge fluctuations. According to Reesink and Bridge (2007; 2009), cross strata can be used to determine the type, size and geometry of the antecedent and superimposed bed forms. Hassan et al. (2006) reported that grain size distribution should be used as an indicator for the degree of armor development on a gravel bed.

3.3.3 Strategic opportunities for further investigation

Results and contributions from the experimental studies reported in this Chapter demonstrate that the nature of the morphological response of alluvial stream beds to unsteady (flood-like) events remains uncertain. There is a lack of complete understanding of the numerous interactions of the factors responsible for bed morphological adjustments in response to unsteady flow events and a more systematic experimental approach, where the effect of individual factors is studied in isolation, is recommended. The experiments summarized in this Chapter have made substantial advances in our understanding of this topic, however, the actual cause of the morphological response of the bed (and more specifically, the hysteretic behaviour in sediment transport rates) remains unknown.

The following recommendations and strategic opportunities for further experimental research are suggested:

1) Define a hierarchical framework of causes responsible for hysteresis of sediment transport rates and bed morphological adjustments. As outlined in this Chapter, bed composition, hydrograph shape, sediment supply, and antecedent bed morphology all play prominent roles in determining the type of hysteresis that occurs, however, the

degree of influence of each variable, and their inter-relationships, has yet to be determined.

2) Develop a methodology to more accurately predict bed morphological adjustments in response to unsteady flow events of varying hydrologic characteristics. Determining the influence of the duration and magnitude of unsteady flow events and the shape of hydrograph (i.e., time to peak flow) on bed morphological adjustments will assist in the development of more accurate predictive models and allow for extension of laboratory results to the field-scale.
3) Quantify the increased resiliency of non-uniform sediment bed composition to changes in flow rate associated with unsteady flow events.

The above recommendations will advance the state of knowledge on sediment transport rate and bed morphological responses during unsteady, flood-like, conditions in alluvial rivers and streams. This knowledge is of the utmost importance in order to develop more reliable predictive models to guide in river management strategies during flood events and to design river restoration and rehabilitation measures more resilient to the effects of unsteady flow scenarios, such as those due to extreme floods.

3.4 References

Ahanger MA, Asawa GL, Lone MA. 2008. Experimental study of sediment transport hysteresis. *Journal of Hydraulic Research* **46**(5):628-635. DOI:10.3826/jhr.2008.3185

Allen JRL. 1976. Time-lag of dunes in unsteady flows: an analysis of Nasner's data from River Weser, Germany. *Sedimentary Geology* **15**:309-321.

Bestaway A. 1997. Bedload transport and bedforms in steady and unsteady flows. PhD Thesis. Catholic University of Leuven. Belgium.

Bombar G, Elci S, Tayfur G, Guney SM and Bor A. 2011. Experimental and numerical investigation of bed-load transport under unsteady flows. *Journal of Hydraulic Engineering* **137**:1276-1282. DOI: 10.1061/(ASCE)HY.1943-7900.0000412

Bridge JS. 2003. Rivers and floodplains: forms, processes and sedimentary record. Blackwell Publishing. John Wiley and Sons.

Bridgwater J. 1976. Fundamental powder mixing mechanisms. *Powder Technology* **15**:215-236. doi:10.1016/0032-5910(76)80051-4

De Costa C and Coleman S. 2013. Temporal and spatial changes in bed-form due to change in flow in a flume environment. *International Conference on Sustainable Built Environments* **13**:111-116.

De Sutter R, Huygens M and Verhoeven R. 1999. Unsteady flow sediment transport in a sewer model. *Water Science and Technology* **39**(9):121-128.

De Sutter R, Verhoeven R, Krein A. 2001. Simulation of sediment transport during flood events: laboratory work and field experiments. *Hydrological Sciences Journal* **46**(4):599-610. DOI:10.1080/02626660109492853

Einstein HA. 1950. The bed-load function for sediment transportation in open channel flows. *Technical Bulletin USDA Soil Conservation Service* **1026**:1-71.

Gomez B. 1994. Effects of particle shape and mobility on stable armor development. *Water Resources Research* **30**(7):2229-2239.

Griffiths GA and Sutherland AJ. 1977. Bedload transport by translation waves. *Journal of the Hydraulics Division*. Proceedings of the American Society of Civil Engineers **103**(HY11):127901291.

Guney MS, Bombar G and Aksoy AO. 2013. Experimental study of coarse surface development effect on the bimodal bed-load transport under unsteady flow conditions. *Journal of Hydraulic Engineering* **139**(1):12-21. DOI: 10.1061/(ASCE)HY.1943-7900.0000640

Hassan MA and Church M. 2000. Experiments on surface structure and partial sediment transport on a gravel bed. *Water Resources Research* **36**(7):1885-1895. DOI: 10.1029/2000WR900055

Hassan MA, Egozi R and Parker G. 2006. Experiments on the effect of hydrograph characteristics on vertical grain sorting in gravel bed rivers. *Water Resources Research* **42**(9):W09408. DOI: 10.1029/2005WR004707

Hayes H and Pender G. 2007. Stress history effects on graded bed stability. *Journal of Hydraulic Engineering* **133**(4):343-349. DOI:10.1061/ASCE0733-94292007133:4343

Humphries R, Venditti JG, Sklar LS and Wooster JK. 2012. Experimental evidence for the effect of hydrographs on sediment pulse dynamics in gravel-bedded rivers. *Water Resources Research* **48**:1-15. DOI: 10.1029/2011WR010419

Julien PY and Klassen G. 1995. Sand-dune geometry of large rivers during floods. *Journal of Hydraulic Engineering* **121**:657-663.

Kabir MR. 1993. Bedload transport in unsteady flows. PhD Thesis. Catholic University of Leuven, Belgium.

Lee KT, Liu YL, and Cheng KH. 2004. Experimental investigation of bedload transport processes under unsteady flow conditions. *Hydrological Processes* **18**(13):2439-2454. DOI: 10.1002/hyp.1473

Madej MA, Sutherland DG, Lisle TE and Pryor B. 2009. Channel responses to varying sediment input: a flume experiment modeled after Redwood Creek, California. *Geomorphology* **103**(4):507-519. DOI:10.1016/j.geomorph.2008.07.017

Martin RL and Jerolmack DJ. 2013. Origin of hysteresis in bed form response to unsteady flows. *Water Resources Research* **49**(3):1314-1333. DOI:10.1002/wrcr.20093

Mao L. 2012. The effect of hydrographs on bed load transport and bed sediment spatial arrangement. *Journal of Geophysical Research* **117**:F03024. DOI:10.1029/2012JF002428

Marcus WA. 1989. Lag-time routing of suspended sediment concentration during unsteady flow. *Geological Society of American Bulletin* **101**(5):644-651.

Marquis GA and Roy AG. 2012. Using multiple bed load measurements: toward the identification of bed dilation and contraction in gravel-bed rivers. *Journal of Geophysical Research* **117**:F01014. DOI:10.1029/2011JF002120

McElroy B and Mohrig D. 2009. Nature of deformation of sandy bed forms. *Journal of Geophysical Research* **114**:F00A04. DOI:10.1029/200JF001.220

Monteith H and Pender G. 2005. Flume investigations into the influence of shear stress history on a graded sediment bed. *Water Resources Research.* **41**(12):W12401. DOI:10.1029/2005WR004297.

Nelson JM, Logan BL, Kinzel PJ, Shimizu Y, Giri S, Shreve RL and McLean SR. 2011. Bedform response to flow variability. *Earth Surface Processes and Landforms* **36**(14):1938-1947. DOI: 10.1002/esp.2212

Nezu I, Kadota A and Nakagawa H. 1997. Turbulent structure in unsteady depth-varying open-channel flows. *Journal of Hydraulic Engineering* **123**(9):752-763.

Parker G. 1979. Hydraulic geometry of active gravel rivers. *Journal of the Hydraulics Division* **105**(9):1185-1201.

Pender G, Hoey TB, Fuller C and McEwan IK. 2001. Selective bedload transport during degradation of a well sorted graded sediment bed. *Journal of Hydraulic Research* **39**(3):269-277. DOI:10.1080/00221680109499830

Piedra MM, Haynes H and Hoey TB. 2012. The spatial distribution of coarse surface grains and the stability of gravel river beds. *Sedimentology* **59**(3):1014-1029. DOI: 10.1111/j.1365-3091.2011.01290.x

Reesink AJH and Bridge JS. 2007. Influence of superimposed bedforms and flow unsteadiness on formation of cross strata in dunes and unit bars. *Sedimentary Geology* **202**(1):281-296. DOI:10.1016/j.sedgeo.2007.02.005

Reesink AJH and Bridge JS. 2009. Influence of superimposed bedforms and flow unsteadiness on formation of cross strata in dunes and unit bars – Part 2, further experiments. *Sedimentary Geology* **222**(3):274-300. DOI:10.1016/j.sedgeo.2009.09.014

Reesink AJH, Parsons D, Ashworth P, Hardy R, Best J, Unsworth C, McLelland S, and Murphy B. 2013. The response and hysteresis of alluvial dunes under transient flow conditions. *Marine and River Dune Dynamics (MARID IV)*, Bruges, Belgium.

Suszka B. 1987. Sediment transport at steady and unsteady flow; a laboratory study. PhD Thesis EPF Lausanne, Switzerland.

Song T and Graf WH. 1997. Experimental study of bed load transport in unsteady open-channel flow. *International Journal of Sediment Research* **12**(3):63-71.

Unsworth CA, Parsons DR, Reesink AJH, Best JL, Ashworth PJ and Hardy RJ. 2013. Flow structures over fixed 2D bedforms in transient states. *Marine and River Dune Dynamics (MARID IV).*

Wong M and Parker G. 2006. One-dimensional modeling of morphodynamic bed evolution in a gravel-bed river subject to a cycled flood hydrograph. *Journal of Geophysical Research* **111**:F03018. DOI: 10.1029/2006JF000478

Yalin MS. 1977. River Mechanics. 2nd edition, Pergamon Press, Sydney.

Chapter 4

4 Quantification of stream bed morphological response to unsteady flow event hydrographs of varying peak flow magnitude and duration

4.1 Introduction

River discharge naturally fluctuates, causing complex adjustments in sediment transport rates and bed morphology. Climatic processes such as rain, snowfall and runoff can intensify average daily, seasonal and annual maximum fluctuations in river discharge (Barrow et al., 2004; Intergovernmental Panel on Climate Change, 2014; Hirabayashiet al., 2013). Globally, climate change is causing more intense and frequent precipitation events that are altering the natural equilibrium of hydraulic and sediment regimes of rivers and streams resulting in catastrophic flooding (Brooks et al., 2001; Labat et al., 2004; Xenopoulos et al., 2005; Dankers and Geyan, 2009; Hirabayshi et al., 2013). While flooding is increasing globally (Dankers and Geyan, 2009), examples of Canadian locations that are subject to climate-induced flooding include Yukon, northern British Columbia, southern Ontario and Quebec (IPCC, 2014). Furthermore, flood events in rivers are projected to peak earlier in the year and last longer (Paasche and Storen, 2014; IPCC, 2014). The changing climate results in riverine flow events of varying peak flow magnitude and duration. Knowledge of the effects of peak flow magnitude and duration on sediment transport rates and bed morphological adjustments is presently incomplete.

Theoretical expressions to predict bed form dimensions and sediment transport rates have been studied for decades (e.g., Allen, 1970; Fredsoe, 1982; Yalin, 1963, Engelund and Hansen, 1967). Predictive equations developed through field, numerical and laboratory studies are relied on for river engineering and management projects. These equations often produce unrepresentative results of actual conditions due to the assumption of steady flow conditions. Few studies have attempted to develop a new set of sediment transport formulae or parameters to account for unsteady, non-uniform flow conditions. To address this deficiency, an extensive number of field studies have been conducted (e.g., Julien and Klaasen, 1995; Kleinhans et al., 2007; Aberle et al., 2010). However, field scale investigations are limited by their inability to accurately control hydraulic parameters. Numerical models assuming unsteady flow have also

been applied, however, the accuracy and validity of these models cannot be fully ascertained without complementary laboratory investigations for validation purposes (Marsooli and Wu, 2014; Sun et al., 2015). Field experiments and numerical models have offered little to the theoretical understanding of the mechanics of sediment transport and stream morphology during unsteady flow events due to the inability to control and evaluate parameters effectively in these settings. Furthermore, flood simulations in the field can be prohibitive due to safety and practical concerns.

According to Wang et al. (1997), while riverine flooding is a challenge to simulate in a laboratory setting, there is an urgency to develop a greater understanding of sediment transport and morphological response during unsteady, non-uniform flow events. Over the last decade, laboratory work has been conducted to further the understanding of stream bed and sediment transport alterations during unsteady flows (e.g., Hassan et al., 2006; Mao, 2011; Humphries et al., 2013). Unsteady, non-uniform flow events change sediment transport behaviour and influence bed forms and bed development processes. Based on these laboratory results, several equations and parameters to take into account unsteady flow conditions on sediment transport have been proposed (e.g., Lee et al., 2004; Bombar et al., 2011; Guney et al., 2013). However, without further investigation to examine their accuracy and generalize these expressions, application of these equations to real world applications remains limited.

Despite these considerable contributions, to date, no systematic effort to quantify the effects of altering the magnitude and duration of unsteady flow event hydrographs on the bed morphological and sediment transport response has been made. In order to satisfy some of the strategic opportunities outlined in Chapter 3, the goal of this Chapter is to quantify the stream bed morphological response to unsteady flow event hydrographs of varying magnitude and duration. This will be accomplished by conducting two systematic and distinct series of experimental laboratory runs to investigate the effect of varying the magnitude and duration of unsteady flow event hydrographs. The geometric changes in bed form dimensions and the hysteretic behaviour of the sediment transport rates in response to each stage of the experimental hydrographs are quantified.

4.2 Experimental set-up and hydraulic conditions of the runs

4.2.1 Laboratory set-up

Laboratory experimental runs were conducted in a sediment transport flume at the University of Western Ontario in London, Ontario, Canada (see Appendix B for a picture of the facility). The flume width (B), length (ℓ) and height ($h_{\max}$) were 0.31 m, 5.0 m and 0.45 m, respectively. An 1800 liter water supply tank beneath the rectangular flume supplied water to the flume through a hydraulic pump with a maximum capacity of 39.75 l/sec. Water entered the flume through a head tank and mesh flow dissipation structure to ensure uniform flow at the entrance of the flume. A sediment trap was installed at the flume exit to collect sediment that exited the flume and enable the volumetric determination of the sediment transport rates throughout the experiments. Within the water supply tank, three baffles and a mesh screen were installed to prevent excess fines from entering the hydraulic pump. A longitudinal, schematic of the flume is included in Appendix C.

The first metre (upstream reach) of the flume was covered with small stones to stabilize the flow and the downstream sediment bed. The rest of the flume contained a well-sorted, medium sand with an average grain size (D_{50}) of 0.36 mm, D_{10} of 0.20 mm and D_{90} of 0.80 mm. This non-uniform sand was sieved and fines below 0.11 mm were eliminated in order to ensure sediment was transported as bed load only during the laboratory runs. A sieve analysis of the present sand is included in Appendix D. The sand bed was sloped to yield a longitudinal slope (S) of 0.001 in all runs. At the flume exit a wooden sill was installed to stabilize the downstream-end of the stream bed. The sill was designed to maintain an average bed elevation (z_b) of 10.3 cm at the downstream-end, inhibit bed forms from scouring to the flume bottom, maintain bed saturation and free surface slope, and prevent washing out of the bed while allowing sediment in transport to freely exit the flume. The average flow depth (h_{av}) in the flume adjusted in response to the changing discharge. Constant flow depth values along the length of the flume were maintained due to the presence of the sill. The tail-gate at the flume exit was left open to eliminate backwater effects from extending upstream and avoid disrupting the bed morphological and sediment transport processes. Flow depths were averaged over the length of the flume and were found to vary by approximately +/- 5% along the length of the flume for any given flow rate.

4.2.2 Experimental procedure

In order to satisfy the objectives outlined above, two experimental groups, Series A (variation in magnitude of unsteady flow hydrographs) and Series B (variation in duration of unsteady flow hydrographs), were designed. Each series included experimental runs with different unsteady flow event hydrographs. Each run contained three stages: antecedent conditions (base-flow), unsteady event (flood), and post-flood conditions (return to antecedent conditions). Base-flow (BF) conditions had an average flow rate (Q) of 0.006 m^3/s (fluctuations from the prescribed flow rate of only +/- 4% were observed during the runs). The duration of antecedent and post-flood conditions was experimentally determined by a preliminary run using steady flow conditions for a duration of 70 min. In this run it was observed that the morphology of the bed, sediment transport rates, and the D_{50} of the transported material reached a state of equilibrium between 15 and 20 min. Considering this, antecedent conditions were experimentally determined to be 20 min. Post-flood conditions were selected to be 30 min in order to allow sufficient time for the analysis of the morphological recovery of the bed after the unsteady flow event. During the flood stage the magnitude and duration of the unsteady flow event hydrograph were systematically varied from run to run. The flood stages of all runs in Series A lasted for 10 min with peak discharge magnitudes of 1.25, 1.50, 1.75, and 2.00 times base-flow conditions in Runs A1, A2, A3, and A4, respectively. The flood stages of all runs in Series B had a constant discharge magnitude of 1.25 times base-flow conditions and had durations of 5, 10, 15, and 20 min in Runs B1, B2, B3, and B4, respectively. Each experimental run was repeated three times. Good agreement was observed between all repetitions, and therefore, results presented in this Chapter are averaged values. The standard deviation for the reported specific volumetric bed load transport rates for each experimental time step in each run are seen in Appendix E and F for the experimental runs of Series A and B, respectively. A summary of the unsteady flow event hydrograph conditions for all runs in Series A and B is displayed in Table 3.

Table 3: Unsteady flow event hydrograph conditions for experimental runs of Series A and B

Series	Run	Magnitude of flood stage	Duration of flood
A	A1	1.25 x *BF*	10 min
	A2	1.50 x *BF*	10 min
	A3	1.75 x *BF*	10 min
	A4	2.00 x *BF*	10 min
B	B1	1.50 x *BF*	5 min
	B2	1.50 x *BF*	10 min
	B3	1.50 x *BF*	15 min
	B4	1.50 x *BF*	20 min

To limit the influence of the upstream riprap and downstream sill on bed morphological development and ensure accurate representation of the bed morphological features, collection of bed elevation data (z_b) was restricted to the middle 3.0 m-long region of the flume, starting at a distance 1.0 m downstream from the sluice gate. Sediment was not fed to the flume throughout the runs (see Binns and da Silva, 2009 for justification of this experimental approach). In order to collect bed elevation and sediment transport data the flow was stopped at specified intervals throughout the experimental runs. Each time the flow was stopped the sluice gate and tailgate were closed to maintain a saturated bed and limit any possible disturbances to the bed morphology. Binns and da Silva (200) compared the final bed elevation topographies in experimental runs with and without stoppages in flow and determined that there was roughly no considerable difference between the final bed elevation topography. When the runs were resumed the flow was re-introduced gradually to also limit any possible disturbances to the bed. Bed elevation measurements were collected at the end of each experimental stage in order to monitor the stream bed. A point gauge device was used to collect bed morphological data (see Appendix G). This gauge was constructed of a rectangular steel prism that rested horizontally on the 0.45 m-tall flume walls. The device contained 17 equally-spaced (1.8 cm apart) vertical rods. The rods were lowered until they came in contact with the bed. As shown in Fig. 1, the point gauge was used to record bed elevations at 31 equally-spaced (10 cm apart) cross-sections along the length of the flume.

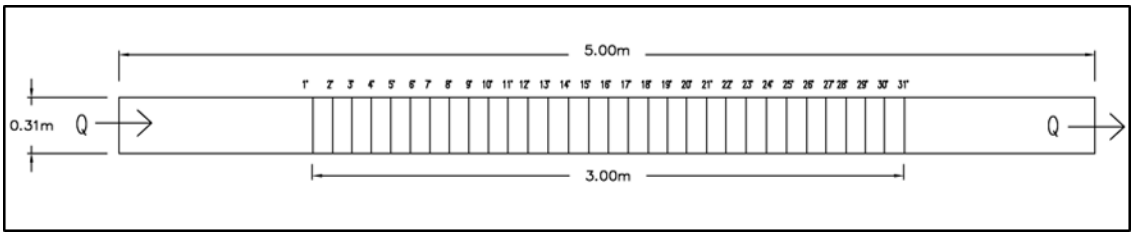

Figure 1: Location (planview) of 31 equally-spaced bed elevation data measurement cross-sections

Measurement cross-sections are labeled in ascending numerical order (e.g., 1^0, 2^0, 3^0,...), with cross-section 1^0 being the first measurement cross-section located a distance 1.0 m from the upstream-end of the flume. From these measurements, the elevation of the bed (z_b) was determined using the leveled flume bottom as datum (z_0). Bed elevation measurements were recorded to an accuracy of 0.1 cm.

Transported sediment was collected from the downstream sediment trap (see Appendix H) and measured volumetrically at various time intervals. Table 4 presents a summary of the sediment sampling times during each experimental run in Series A and B. During the antecedent stage, sediment samples were collected every 5 min. During flood and post-flood stages, sediment samples were measured every 1 min for the first 5 min of the flood stage and in any remaining time, sediment samples were collected every 5 min. An average error of +/- 2.19×10^{-07} m^2/s was determined for the specific volumetric bed load rates collected during experimentation. This value was determined by a collection of bed load that was not collected in the sediment trap, but rather, transported past and deposited in the holding tank of the flume.

Table 4: Sediment transport sampling times for experimental runs of Series A and B

Series	Run	Sample Times (min) of Specific Volumetric Bed Load Rates
A	**A1**	5 10 15 20 21 22 23 24 25 30 31 32 33 34 35 40 45 50 55 60
	A2	5 10 15 20 21 22 23 24 25 30 31 32 33 34 35 40 45 50 55 60
	A3	5 10 15 20 21 22 23 24 25 30 31 32 33 34 35 40 45 50 55 60
	A4	5 10 15 20 21 22 23 24 25 30 31 32 33 34 35 40 45 50 55 60
B	**B1**	5 10 15 20 21 22 23 24 25 26 27 28 29 30 35 40 45 50 55
	B2	5 10 15 20 21 22 23 24 25 30 31 32 33 34 35 40 45 50 55 60
	B3	5 10 15 20 21 22 23 24 25 30 35 36 37 38 39 40 45 50 55 60 65
	B4	5 10 15 20 21 22 23 24 25 30 35 40 41 42 43 44 45 50 55 60 65 70

At the beginning of each run, the upstream sluice gate was closed. The sluice gate was opened and the flow was set to base-flow conditions. Timing of the runs started when the water reached the downstream-end of the flume (at this time uniform flow depth conditions along the length of the flume were also approximately reached). During each time-step, h_{av} was recorded three times at locations within four equally-spaced zones of the flume (see Appendix I for zone locations). Qualitative observations of bed development were recorded throughout each time-step. In addition to bed elevation measurements, individual bed form heights (Δ) were also measured within each zone (see Appendix I) after each time-step. Bed form measurements were conducted three times and averaged ($\Delta_{avg,\exp}$) within the four equally spaced regions (see Appendix I). The manually-measured bed form heights were compared to the average of fifteen bedform heights that were extracted from the bed elevation contour-plots. Results from this comparison demonstrated near identical results. The measured sediment volumes were converted to specific volumetric sediment transport rates and the sediment was dried and sieved in order to obtain a grain size distribution of the transported material in each time-step of the experiment. This process was repeated for each experimental time-step.

4.2.3 Hydraulic conditions of runs

Hydraulic conditions for Series A and B are presented in Tables 5 and 6, respectively. Hydraulic conditions were selected so as to ensure that sediment was transported as bed load only during all three stages of the runs and for the bed forms to be ripples superimposed on dunes. The critical mobility number (Y_{cr}) for the hydraulic conditions was found to be 0.0365. During the experiments the values of the mobility number (Y) ranged from approximately 0.08 to 0.12, resulting in a variation in relative flow intensity (η_*) between 2.24 and 3.31. Tables 5 and 6 also include the following quantities that have not yet been defined: width-to-flow depth ratio $\left(\frac{B}{h_{av}}\right)$, relative depth $\left(\frac{h_{av}}{D}\right)$, channel-averaged Chézy resistance coefficient $\left(c_f\right)_{av}$, Reynolds number (R), Froude number (Fr), roughness Reynolds number (R_*), $\left(q_{sb,\exp}\right)_{avg}$ = average experimental specific volumetric bed load transport rate, and duration of each experimental stage (see Section 2.1 to 2.3 for a definition of these quantities). The average discharge of the antecedent stage of all eight runs was 0.006 m^3/s. Minor fluctuations (+/- 4%)

in discharge occurred due to the manual adjustment of the flow gauge. The average discharge in the post-flood stage of all eight runs was 0.006 m^3/s (with minor fluctuations of +/- 7%). The average flow depth h_{av} for all eight experimental runs was 5.22 cm (+/- 8%) during the antecedent stage and 5.57 cm (+/- 10%) during the post-flood stage. Fluctuations in h_{av} during the post-flood stage were higher than the antecedent conditions due to adjustments in water surface slope resulting from the morphological development of the bed. All experimental runs were in the transitional regime of turbulent flow with the roughness Reynolds number (R_*) approximately between 15 and 20.

Table 5: Hydraulic conditions of experimental runs in Series A

Run	Phase	Q [m^3/s]	h_{av} [cm]	S	u_{av} [m/s]	v_* [m/s]	B/h_{av}	h_{av}/D_{50}	$(c_f)_{av}$	R	Fr	R_*	η_* (= Y/Y_{cr})	$(q_{sb,exp})_{avg}$ [m^2/s]	Duration [min]
A1	*i*	-	-	0.001	-	-	-	-	-	-	-	-	-	-	-
	a	0.005	5.51	0.001	0.3215	0.0232	5.6261	153.1	13.8	17715	0.44	16.7	2.54	8.761E-06	20
	f	0.008	6.26	0.001	0.3921	0.0248	4.9521	173.9	15.8	24543	0.50	17.8	2.89	9.279E-06	10
	pf	0.006	5.93	0.001	0.3094	0.0241	5.2277	164.7	12.8	18349	0.41	17.4	2.74	4.352E-06	30
A2	*i*	-	-	0.001	-	-	-	-	-	-	-	-	-	-	-
	a	0.006	4.99	0.001	0.3553	0.0221	6.2078	138.7	16.1	17742	0.51	15.9	2.30	4.197E-06	20
	f	0.008	5.45	0.001	0.4910	0.0231	5.6852	151.5	21.2	26774	0.67	16.7	2.51	6.974E-06	10
	pf	0.005	4.85	0.001	0.3456	0.0218	6.3885	134.8	15.8	16769	0.50	15.7	2.24	3.798E-06	30
A3	*i*	-	-	0.001	-	-	-	-	-	-	-	-	-	-	-
	a	0.006	5.38	0.001	0.3598	0.0230	5.7621	149.4	15.7	19355	0.50	16.5	2.48	5.016E-06	20
	f	0.011	6.44	0.001	0.5403	0.0251	4.8137	178.9	21.5	34796	0.68	18.1	2.97	1.976E-05	10
	pf	0.006	6.17	0.001	0.3052	0.0246	5.0243	171.4	12.4	18828	0.39	17.7	2.85	4.384E-06	30
A4	*i*	-	-	0.001	-	-	-	-	-	-	-	-	-	-	-
	a	0.006	4.90	0.001	0.3937	0.0219	6.3265	136.1	18.0	19290	0.57	15.8	2.26	7.710E-06	20
	f	0.013	7.18	0.001	0.5670	0.0265	4.3175	199.4	21.4	40710	0.68	19.1	3.31	3.596E-05	10
	pf	0.006	5.94	0.001	0.3278	0.0241	5.2189	165.0	13.6	19473	0.43	17.4	2.74	4.828E-06	30

Table 6: Hydraulic conditions of experimental runs in Series B

Run	Phase	Q [m^3/s]	h_{av} [cm]	S	u_{av} [m/s]	v_* [m/s]	B/h_{av}	h_{av}/D_{50}	$(c_f)_{av}$	R	Fr	R_*	η_* (= Y/Y_{cr})	$(q_{sb,exp})_{avg}$ [m^2/s]	Duration [min]
B1	*i*	-	-	0.001	-	-	-	-	-	-	-	-	-	-	-
	a	0.006	5.21	0.001	0.3669	0.0226	6.0	144.6	16.2	19099	0.51	16.3	2.40	5.105E-06	20
	f	0.009	6.08	0.001	0.4699	0.0244	5.1	168.9	19.2	28570	0.61	17.6	2.80	8.746E-06	5
	pf	0.006	5.91	0.001	0.3166	0.0241	5.2	164.2	13.1	18720	0.42	17.3	2.72	5.541E-06	30
B2	*i*	-	-	0.001	-	-	-	-	-	-	-	-	-	-	-
	a	0.006	4.99	0.001	0.3553	0.0221	6.2	138.7	16.1	17742	0.51	15.9	2.30	4.197E-06	20
	f	0.008	5.45	0.001	0.4910	0.0231	5.7	151.5	21.2	26774	0.67	16.7	2.51	6.974E-06	10
	pf	0.005	4.85	0.001	0.3456	0.0218	6.4	134.8	15.8	16769	0.50	15.7	2.24	3.798E-06	30
B3	*i*	-	-	0.001	-	-	-	-	-	-	-	-	-	-	-
	a	0.006	5.40	0.001	0.3440	0.0230	5.7	150.0	14.9	18575	0.47	16.6	2.49	1.062E-05	20
	f	0.009	5.96	0.001	0.4905	0.0242	5.2	165.6	20.3	29240	0.64	17.4	2.75	1.201E-05	15
	pf	0.006	5.52	0.001	0.3538	0.0233	5.6	153.2	15.2	19511	0.48	16.7	2.54	7.609E-06	30
B4	*i*	-	-	0.001	-	-	-	-	-	-	-	-	-	-	-
	a	0.006	5.41	0.001	0.3519	0.0230	5.7	150.3	15.3	19046	0.48	16.6	2.49	7.113E-06	20
	f	0.010	6.47	0.001	0.4770	0.0252	4.8	179.6	18.9	30840	0.60	18.1	2.98	1.489E-05	20
	pf	0.006	5.42	0.001	0.3496	0.0230	5.7	150.4	15.2	18930	0.48	16.6	2.50	4.257E-06	30

4.3 Experimental observations and results

4.3.1 General

This section presents and discusses the results from the experimental runs. First, the antecedent conditions (which were similar in all runs) are discussed. Second, the results of the experimental runs of Series A and Series B are discussed separately followed by a summary of each respective experimental series.

In the presentation of the experimental results, the general trends in the measured $q_{sb,\exp}$ and $\Delta_{avg,\exp}$ values for each run are described. The experimental values are compared to predicted (calculated) $q_{sb,calc}$ and $\Delta_{avg,calc}$-values determined using established equations assuming steady flow conditions. Bed form geometry was represented by Δ and bedform δ and Λ where assumed to adjust in accordance with the bed form predictive equations (See Section 2.3) defined by Yalin (1971) as experimental Δ adjusted. For each run the hydrograph and sediment transport rate time-to-peak (t_r and t_s, respectively) are reported. From this the type of hysteresis of the sediment transport rate is assessed and discussed. Lastly, the variation in the average grain size (D_{50}) of the sediment in transport over the duration of the experimental hydrograph stages is investigated and discussed. Generally if the D_{50}-value peaks prior to t_r being reached then clockwise hysteresis of the average grain size of the sediment in transport has occurred. Contrarily, if the D_{50}-value peaks after t_r, then counter-clockwise hysteresis of the average grain size of the sediment in transport has occurred.

The bed load sediment transport equations initially considered included: Meyer-Peter and Müller (1949), Yalin (1963), Bagnold (1968) and van Rijn (1984). The results of these four expressions were compared to investigate the influence of the selected bed load transport equation on the calculated value. Due to the relatively small values of η_* and grain size Reynolds number (X), the five bed-load transport equations produced relatively similar results in each respective experimental runs. The results of this sensitivity analysis ranked the bed-load predictive equation from largest estimate to smallest as: Meyer-Peter and Müller (1949), van Rijn (1984), Yalin (1963), and Bagnold (1968). The results for this sensitivity

analysis for Series A and B can be found in Appendix J and K, respectively. Considering this, the Meyer-Peter and Müller (1949) bed load transport equation was selected to calculate $q_{sb,calc}$ -values for the remainder of the analysis in this thesis (refer to Section 2.2 for a review of bed-load transport calculations with this expression). This equation was selected since Meyer-Peter and M üller (1949) validated the equation using sediment that had an average grain size of 0.4 mm, flume widths ranging from 0.15 to 2 m, slopes varying from 0.0004 to 0.002 and realatively small flow depths (minimum flow depth of 1 cm). These conditions that were used by Meyer-Peter and Müller (1949) to develop the predictive specific volumetric bed load rate are similar to the experimental conditions for Series A and B. Furthermore, the Meyer-Peter and Müller (1949) equation was selected for comparison to experimental sediment transport rates because it predicted the highest specific volumetric bed load rates, giving a conservative comparison between the calculated and experimentally transported sediment.

The height of the bed forms ($\Delta_{avg,calc}$) were calculated using steady flow predictive equations by Yalin (1985) and Yalin and da Silva (2001) for ripples and dunes. The results of the $\Delta_{avg,calc}$ for ripples and dunes were averaged to give an approximate size of possible bed forms present during the given hydraulic conditions. It was experimentally observed that the majority of the bed was dominated by dunes at the end of each experimental stage. However, ripples did exist at the early stages of the antecedent stage and, in some cases, during phases of dune degradation during the flood stage. In order to represent the changes observed during experimentation, $\Delta_{avg,calc}$ presents an average of ripple and dune height (refer to Section 2.2 or a full description of the calculation of bed form geometry).

4.3.2 Antecedent conditions

The hydraulic conditions in the antecedent stage were identical in all experimental runs of Series A and B. Equilibrium sediment transport rates and bed geometry were achieved by the end of antecedent conditions in all runs of Series A and B. Antecedent conditions were computationally determined and experimentally validated. Specific volumetric sediment transport rates ($q_{sb,\exp}$) throughout the 20 min antecedent stage typically decreased with time. $q_{sb,\exp}$ -values are relatively large during the first 5 min due to the initial displacement of a large volume of sediment as the bed adjusted to the flow from its initial flate state. At the end of the

first 5 min of the antecedent stage the bed was observed to have quickly adapted to the hydraulic conditions. Partially-formed ripples were observed to develop on the bed in a relatively straight line across the width of the flume during this period. Over the remaining 15 min of the antecedent stage $q_{sb,\exp}$-values gradually decreased as the ripples fully formed, across the width of the flume and individual dunes began to form. At the end of the antecedent stage (at t = 20 min), $q_{sb,\exp}$-values and bed morphology reached an approximate state of equilibrium. It was observed during the steady state conditions that a bed form would migrate along the streamwise length of the flume much slower that the discharge. Generally, an individual bed form was observed to migrate approximately 1 to 2 m over a 20 min experimental period.

This state of equilibrium was also observed in the D_{50}-values of the sediment in transport. A preliminary steady-flow experimental run of 70 min in duration was conducted to investigate the change in the grain size composition of the sediment in transport with time. As observed in this Fig. 2, during the first 15 min of the experimental run, the D_{50}-value of the sediment in transport decreased from 0.37 mm to 0.35 mm. By 20 min into the experiment, the D_{50}-value reached equilibrium conditions at 0.36 mm, where it remained for the duration of the experimental run until t = 55 min where it decreased to 0.35 mm. This was likely due to a minor fluctuations in the discharge.

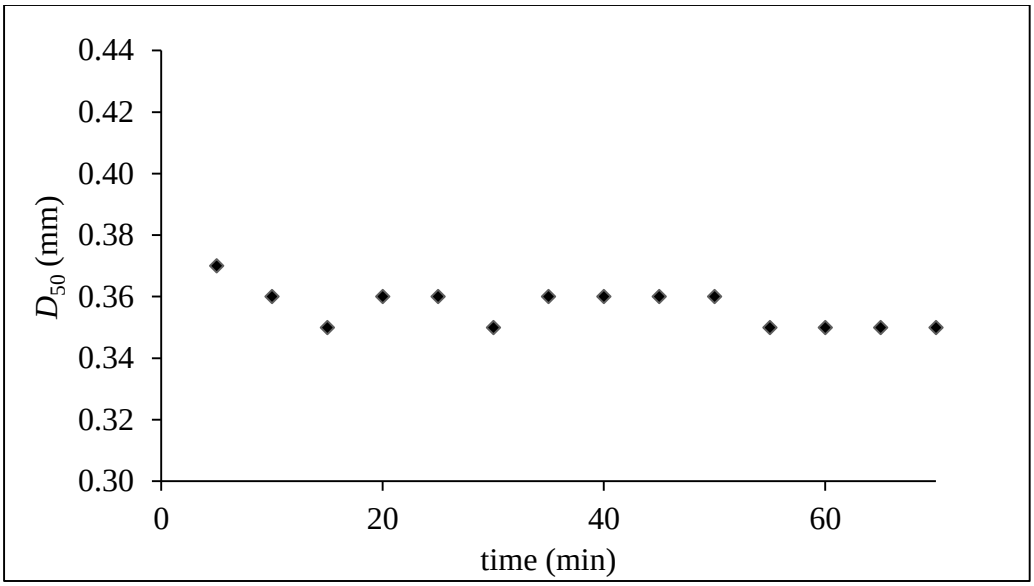

Figure 2: D_{50}-value versus time for the sediment in transport during a 70 min steady-flow preliminary experimental run

By the end of the antecedent stage, $q_{sb,\exp}$ and the bed geometry reached the predicted values using the traditional equations assuming steady flow conditions. Fully formed dunes dominated the bed with few ripples superimposed on top of the dunes. Values of $q_{sb,\exp}$ and $\Delta_{avg,\exp}$ at t = 20 min (end of the antecedent stage) were similar in all runs. The average $q_{sb,\exp}$ for the antecedent hydraulic conditions was 6.42×10^{-6} m^2/s and 6.76×10^{-6} m^2/s for Series A and B, respectively. The average values of $\Delta_{avg,\exp}$ at the end of the antecedent stage were 1.075 cm and 0.853 cm in Series A and B, respectively.

4.3.3 Series A results

4.3.3.1 Run A1

Run A1 contained a flood stage of 10 min in duration with a discharge magnitude of approximately 1.25 times base-flow conditions. Fig. 3 shows the bed elevation contour-plots for Run A1. This figure shows the bed morphology at the end of the antecedent stage (a), the end of the flood stage (f), and the end of the post-flood stage (pf). Generally, it is observed that during the antecedent stage the bed geometry is fairly uniform across the length of the flume. During the flood stage, the size of the bed forms increase and become more spread out. Finally,

during the post-flood stage, the bed forms were slightly smaller compared to the flood stage, but slightly larger compared to the antecedent stage.

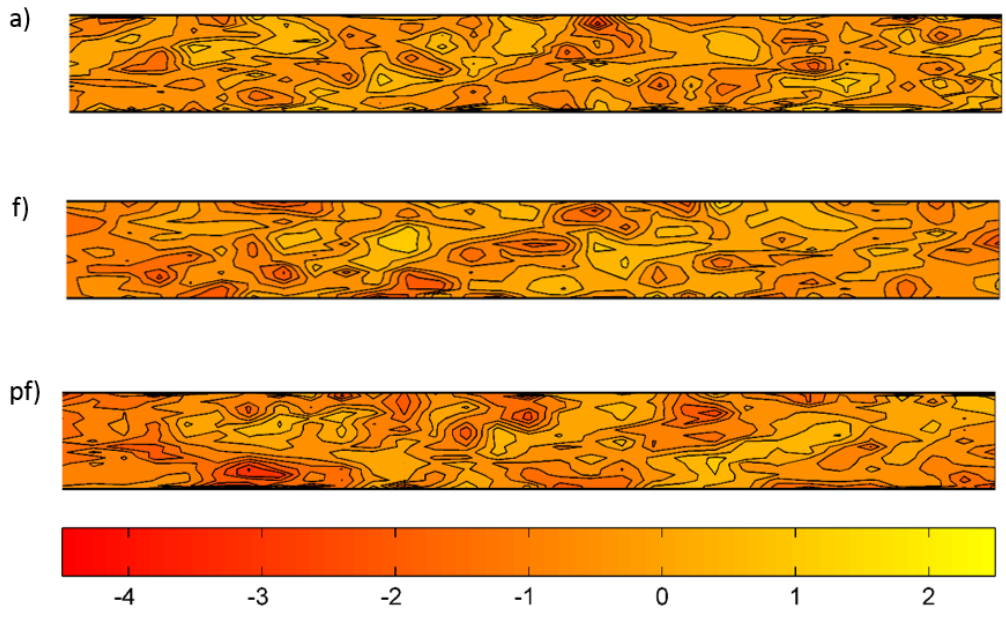

Figure 3: Bed elevation contour-plots for Run A1 (showing change in bed elevation from initial flat-bed conditions): antecedent (a); flood (f); and post-food (pf) stages [all values in cm]

Fig. 4a presents the sediment transport and discharge profiles for the entire duration of Run A1. As observed in this figure, $q_{sb,\exp}$ during the antecedent stage was observed to decrease, with minor fluctuations, until it reached a minimum value at 20 min. During the 10 min flood stage when the discharge was increased to be 1.25 times the base-flow conditions (0.0076 m^3/s), $q_{sb,\exp}$ peaked slightly at 21 min, decreased and then gradually increased again until the time-to-peak of the sediment transport rate (t_s) was reached at 24 min. A sharp decrease occurred at 25 min followed by a slight increase but relatively constant $q_{sb,\exp}$ at 30 min. The average bed load transport rate $\left(q_{sb,\exp}\right)_{avg}$ for the flood stage was 8.61×10^{-6} m^2/s. During post-flood conditions, $q_{sb,\exp}$ remained relatively stable with a slight decrease observed at 35 min. Clockwise hysteresis of the sediment transport rate (greater sediment transport during the rising limb compared to the falling limb of the hydrograph) was observed during the flood stage of the run since t_s (24 min) occurred prior to the time-to-peak of the unsteady flow event

hydrograph t_r (25 min). The antecedent $q_{sb,\exp}$-value approached the $q_{sb,calc}$-value at 20 min. The flood-stage $q_{sb,calc}$ was found to be 1.4 times greater than the $q_{sb,calc}$ predicted antecedent sediment transport rate, however, the flood-stage $q_{sb,\exp}$ was in fact observed to be 1.75 to 2.94 times the end of antecedent $q_{sb,\exp}$-value. During the post-flood stage $q_{sb,\exp}$ was found to be approximately equal to $q_{sb,calc}$ at each time step (some minor fluctuations were observed).

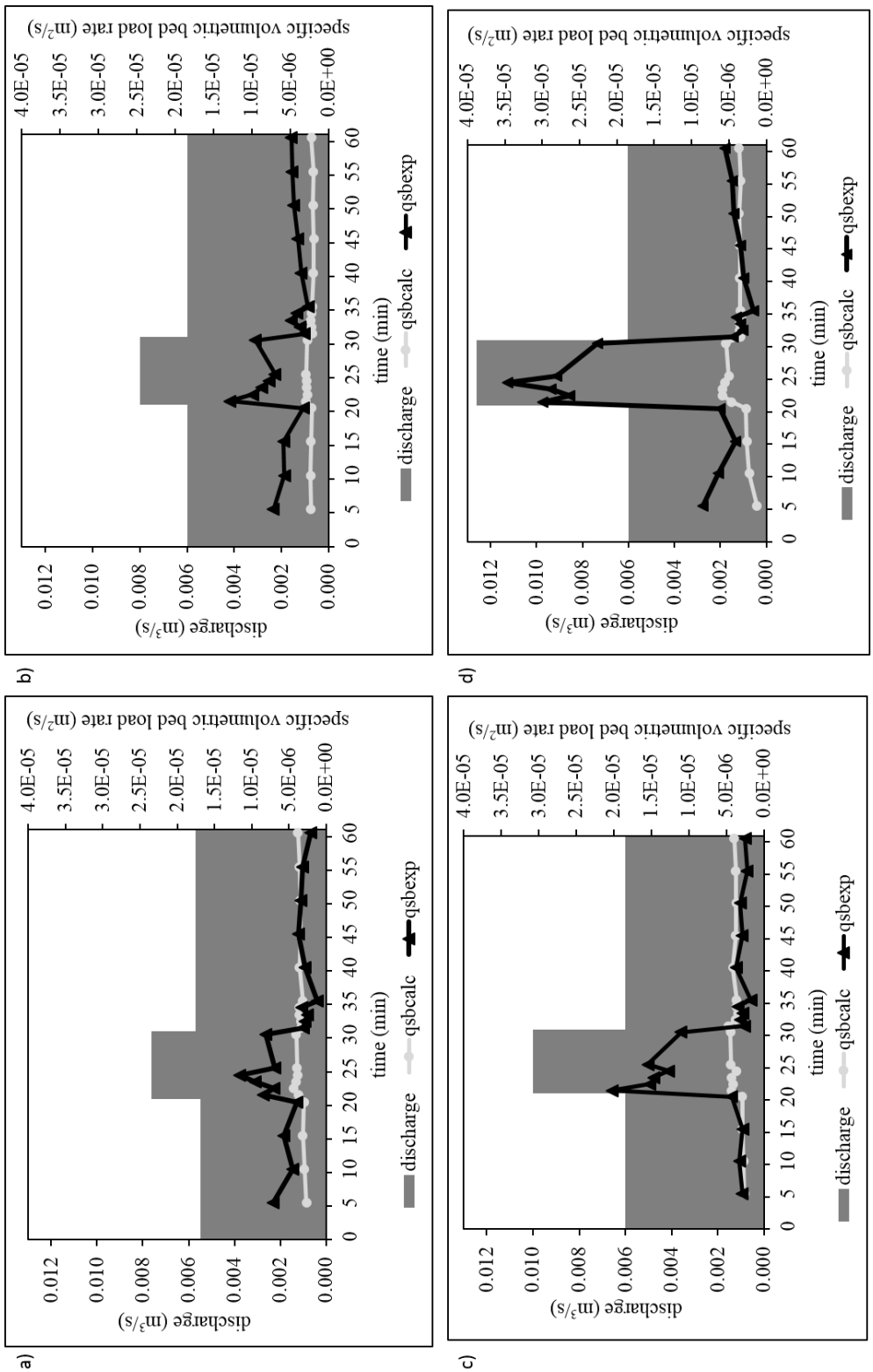

Figure 4: Sediment transport and discharge profiles for experimental runs of Series A: a) Run A1; b) Run A2; c) Run A3; and d) Run A4

Bed form average height and percent change in the average height of bed forms are seen in Tables 7 and 8 for $\Delta_{avg,\exp}$ and $\Delta_{avg,calc}$, respectively. At the end of the antecedent stage, the average bed form height $\Delta_{avg,\exp}$ was measured to be 1.25 cm, which increased by 45% by the end of the flood-stage to give a $\Delta_{avg,\exp}$-value of 1.81 cm. An 8% decrease in $\Delta_{avg,\exp}$ from the end of flood stage to the end of the post-flood stage was observed, giving a final post-flood $\Delta_{avg,\exp}$-value of 1.66 cm. Thus, a net increase in $\Delta_{avg,\exp}$ from the antecedent stage to the post-flood stage of 33% occurred. A similar trend was seen in the $\Delta_{avg,calc}$-values, however, slight variation in the dimensions of bed forms was noted. At the end of the antecedent stage, $\Delta_{avg,calc}$ was predicted to be 1.23 cm. There was a predicted increase in average bed form height of 31% at the end of the flood stage ($\Delta_{avg,calc}$ = 1.61 cm) and a predicted decrease in average bed form height of 12% from the end of the flood stage to the end of the post-flood stage ($\Delta_{avg,calc}$ = 1.43 cm). Overall, a net increase in average bed form height from the antecedent stage to the end of post-flood stage of 16% was predicted, which was considerably less than what actually occurred.

Table 7: Measured average bed form height for each experimental stage and percent change in average bed form height between experimental stages for the experimental runs of Series A and B

	Average bed form height (cm)			Change in average bed form height (%)		
Run	**a**	**f**	**pf**	**a to f**	**f to pf**	**a to pf**
A1	1.25	1.81	1.66	+45	-8	+33
A2	1.00	0.94	1.20	-6	+28	+20
A3	1.05	0.96	1.28	-9	+33	+22
A4	1.00	0.26	1.09	-74	+419	+9
B1	0.78	0.58	0.89	-26	+53	+14
B2	1.00	0.94	1.20	-6	+28	+20
B3	0.84	0.83	0.86	-1	+4	+2
B4	0.79	0.82	0.92	+4	+12	+16

Table 8: Calculated average bed form height for each experimental stage and percent change in average bed form height between experimental stages for the experimental runs of Series A and B

	Average bed form height (cm)			Change in average bed form height (%)		
Run	**a**	**f**	**pf**	**a to f**	**f to pf**	**a to pf**
A1	1.23	1.61	1.43	+31	-12	+16
A2	1.03	1.23	0.94	+19	-24	-9
A3	1.23	1.76	1.61	+43	-9	+31
A4	0.94	2.13	1.51	+127	-29	+61
B1	1.13	1.52	1.43	+35	-6	+27
B2	1.03	1.23	0.94	+19	-24	-9
B3	1.23	1.51	1.23	+23	-19	0
B4	1.23	1.76	1.23	+43	-30	0

As mentioned, a sieve analysis of the sediment collected at the end of each experimental time-step was performed to determine whether there were any changes to the composition of the sediment in transport over the duration of the experimental runs. The D_{50}-values of the sediment in transport for the entire duration of Run A1 are seen in Fig. 5a. At the first time-step of the flood stage (21 min) the D_{50} of the sediment in transport decreased considerably to 0.33 mm where it remained for the next time-step. The maximum D_{50} (0.36 mm) of the sediment in transport occurred at 30 min (i.e., at the end of the flood stage) in Run A1. This lag-in-time of the D_{50} of the sediment in transport demonstrated counter-clockwise hysteresis during the flood stage of the hydrograph.

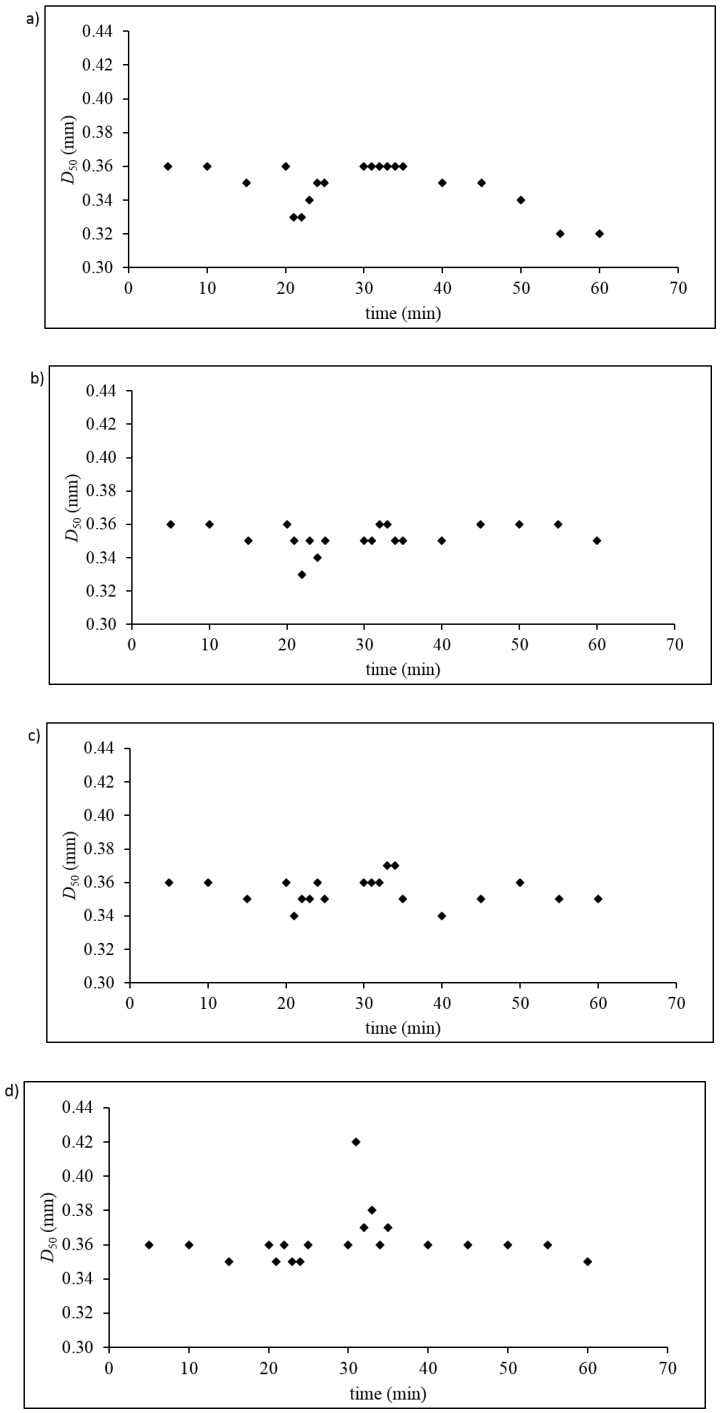

Figure 5: D_{50}-value versus time for the sediment in transport during the experimental runs of Series A: a) Run A1; b) Run A2; c) Run A3; and d) Run A4

4.3.3.2 Run A2

Run A2 contained a flood stage of 10 min in duration with a discharge magnitude of approximately 1.50 times base-flow conditions. Fig. 6 shows the bed elevation contour-plots for Run A2. The antecedent stage shows the bed at equilibrium with the flow conditions while the flood stage shows bed forms that are much more spread out and slightly smaller in size. The post-flood stage shows a recovery of the bed morphology, with slightly larger bed forms present than what is observed in the antecedent stage.

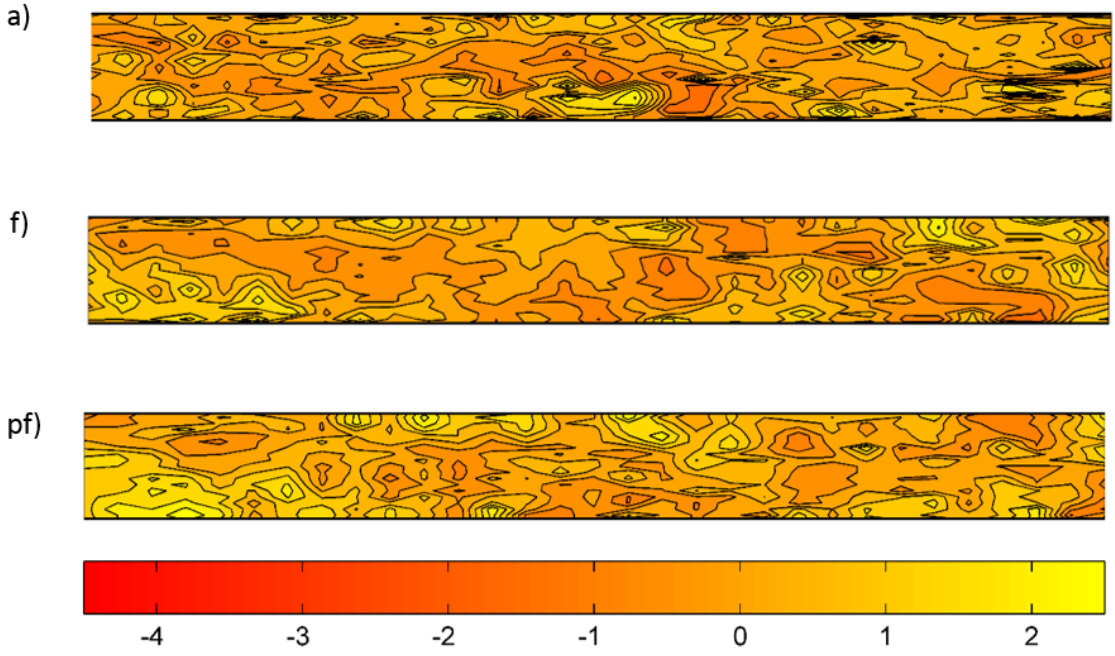

Figure 6: Bed elevation contour-plots for Run A2 (showing change in bed elevation from initial flat-bed conditions): antecedent (a); flood (f); and post-food (pf) stages [all values in cm]

Fig. 4b presents the sediment transport and discharge profiles for the entire duration of Run A2. As seen in this figure, $q_{sb,\exp}$ decreased gradually over the 20 min duration of the antecedent stage of Run A2. During the flood-stage t_s occurred at 21 min. $q_{sb,\exp}$ gradually decreased until it reached a minimum at 25 min and then increased again at 30 min. The flood stage $\left(q_{sb,\exp}\right)_{avg}$ was 9.31x10^{-6} m^2/s. During the post-flood stage, $q_{sb,\exp}$ had a slight peak at 33

min, decreased until 35 min, and then gradually increased for the duration of the post-flood stage. Clockwise hysteresis of the sediment transport rate occurred since t_s (21 min) occurred prior to t_r (25 min). The antecedent $q_{sb,\exp}$-value approached $q_{sb,calc}$-value by the end of the 20 min antecedent stage. The flood stage $q_{sb,calc}$ was predicted to be 1.40 times greater than the antecedent stage $q_{sb,calc}$. However, during the flood stage, $q_{sb,\exp}$ was 2.11 to 3.89 times greater than the corresponding antecedent values. During the post-flood conditions the $q_{sb,\exp}$ remained slightly greater than the $q_{sb,calc}$-values, with greater fluctuation observed in $q_{sb,\exp}$-values during the first 5 min of the post-flood stage.

Tables 7 and 8 show $\Delta_{avg,\exp}$ and $\Delta_{avg,calc}$, respectively, for Run A2. At the end of the antecedent stage, $\Delta_{avg,\exp}$ was approximately 1.00 cm. By the end of the flood stage $\Delta_{avg,\exp}$ had decreased by 6% with $\Delta_{avg,\exp}$ measuring 0.94 cm. From the flood to post-flood stage there was an 28% increase in bed form height to give a $\Delta_{avg,\exp}$ of 1.20 cm. Overall, there was a net increase of 20% in $\Delta_{avg,\exp}$ from the end of the antecedent stage to the end of the post-flood stage. The $\Delta_{avg,calc}$-values for the antecedent stage were predicted to be 1.03 cm and the flood stage conditions predicted a 19% increase in average bed form height to give a $\Delta_{avg,calc}$ = 1.23 cm at the end of the flood-stage. However, during the flood and post-flood stages, the $\Delta_{avg,calc}$ -values predicted the opposite trend to what was actually observed. A 24% decrease in average bed form height from the flood stage to the end of post-flood stage was predicted to give $\Delta_{avg,calc}$ = 0.94 cm at the end of the post-flood stage. Overall, a net decrease from antecedent to post-flood stage of 9% was predicted by the bed form expressions.

The D_{50}-values of the sediment in transport for the entire duration of Run A2 are seen in Fig. 5b. The D_{50} of the sediment in transport during Run A2 decreased during the flood stage to 0.35 mm for the majority of the 10 min duration of the flood stage. The D_{50} of the sediment in transport reached a minimum of 0.33-mm at 22 min. This reduction in the D_{50} of the sediment in transport is seen in Fig. 5b. The discharge increase of 1.50 times greater than base-flow conditions resulted in a counter-clockwise lag-in-time in the size of the sediment transported during the flood stage of the run. This pattern is similar to that observed in Run A1.

4.3.3.3 Run A3

Run A3 contained a flood stage of 10 min in duration with a discharge magnitude of approximately 1.75 times base-flow conditions. Fig. 7 shows the bed elevation contour-plots for Run A3. The antecedent stage shows the bed at equilibrium across the length of the flume. The flood stage bed contained slightly smaller and more spread out bed forms and the post-flood stage bed shows bed forms that are larger than the antecedent stage.

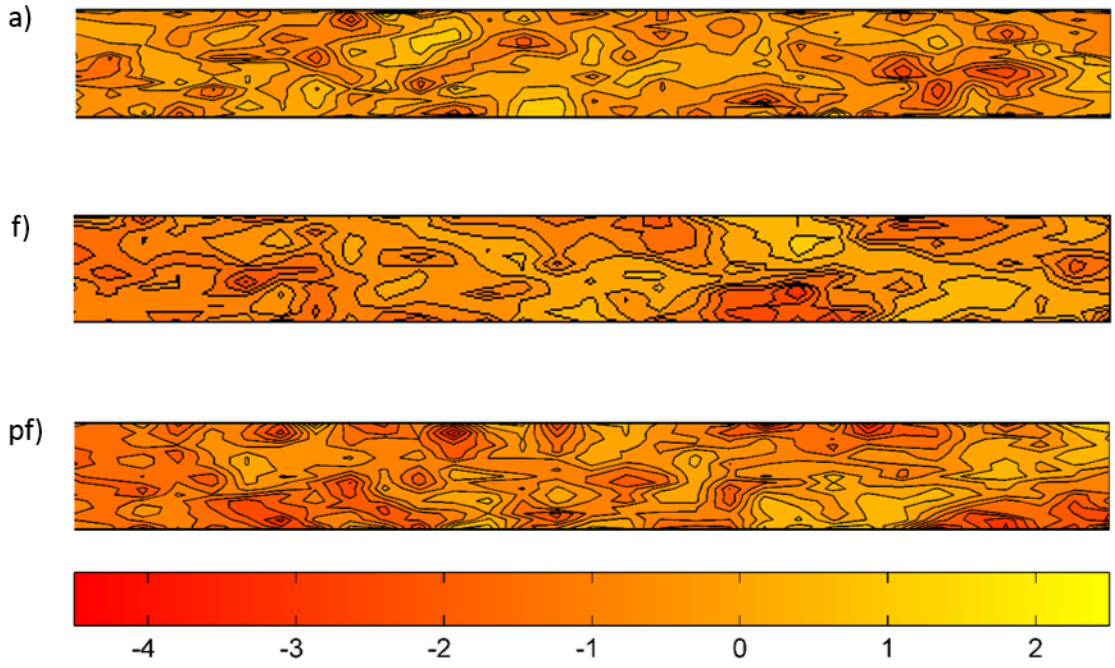

Figure 7: Bed elevation contour-plots for Run A3 (showing change in bed elevation from initial flat-bed conditions): antecedent (a); flood (f); and post-food (pf) stages [all values in cm]

Fig. 4c presents the sediment transport and discharge profiles for the entire duration of Run A3. In this run, $q_{sb,\exp}$ in the antecedent stage remained relatively low. During the flood stage t_s occurred at 21 min. $q_{sb,\exp}$ then decreased until 24 min, increased slightly at 25 min and then decreased again at 30 min. The flood stage $\left(q_{sb,\exp}\right)_{avg}$ was 1.49x10^{-5} m^2/s. During the post-flood stage, $q_{sb,\exp}$ fluctuated slightly from 31 min to 40 min but remained relatively consistent for the duration of the stage. Clockwise hysteresis of the sediment transport rate was

observed in the flood stage of this run since t_s (21 min) occurred prior to t_r (25 min). The antecedent stage $q_{sb,\exp}$-values fluctuated about the predicted $q_{sb,calc}$-values for the entire 20 min duration of the antecedent stage. $q_{sb,calc}$ during the flood stage was projected to be 1.57 times greater than the $q_{sb,calc}$ during the antecedent stage. In actuality, the flood-stage $q_{sb,\exp}$ was found to be 2.56 to 4.69 times greater than the corresponding antecedent values. During the entire duration of the post-flood stage $q_{sb,\exp}$ was approximately identical to $q_{sb,calc}$, with minor observed fluctuations.

Tables 7 and 8 show $\Delta_{avg,\exp}$ and $\Delta_{avg,calc}$, respectively, for Run A3. At the end of antecedent conditions $\Delta_{avg,\exp}$ was measured to be 1.05 cm. There was a 9% decrease in average bed form height at the end of the flood stage to give $\Delta_{avg,\exp}$ = 0.96 cm at the end of the flood stage. From the flood stage to the post-flood stage there was a 33% increase in average bed form height to give $\Delta_{avg,\exp}$ = 1.28 cm at the end of the run. Overall, there was a net increase in average bed form height of 22% from the end of antecedent to the end of the post-flood stage of the run. Variation in the predicted $\Delta_{avg,calc}$-values between stages of the run demonstrated a different pattern than the measured values. At the end of the antecedent stage $\Delta_{avg,calc}$ was predicted to be 1.23 cm and an increase in average bed form height of 43% was predicted to occur by the end of the flood stage (to give $\Delta_{avg,calc}$ = 1.76 cm). The post-flood stage predicted a 9% decrease in the average bed form height to give a $\Delta_{avg,calc}$-value of 1.61 cm at the end of the post-flood stage and give an overall net predicted increase in average bed form height of 31% from the end of the antecedent stage to the end of post-flood stage.

The D_{50}-values of the sediment in transport for the entire duration of Run A3 are seen in Fig. 5c. During Run A3, the D_{50} of the sediment in transport during the flood-stage of the run does not decrease. Rather, the D_{50} of the sediment in transport is maintained throughout the flood stage. During the post-flood stage the D_{50} of the sediment in transport increases to 0.37 mm at 33-34 min. This represents counter-clockwise hysteretic behavior of the grain size composition of the sediment in transport in response to the unsteady flow event hydrograph.

4.3.3.4 Run A4

Run A4 contained a flood stage of 10 min in duration with a discharge magnitude of approximately 2.00 times base-flow conditions. Fig. 8 shows the bed elevation contour-plots for Run A4. The antecedent stage shows bed forms of approximately uniform size that are at equilibrium with the hydraulic conditions. The flood stage shows bed forms that are comparatively much smaller and more spread out. This flood stage shows a considerable flattening of the bed. The post-flood stage shows bed forms that are larger compared to the antecedent stage but smaller compared to the flood stage.

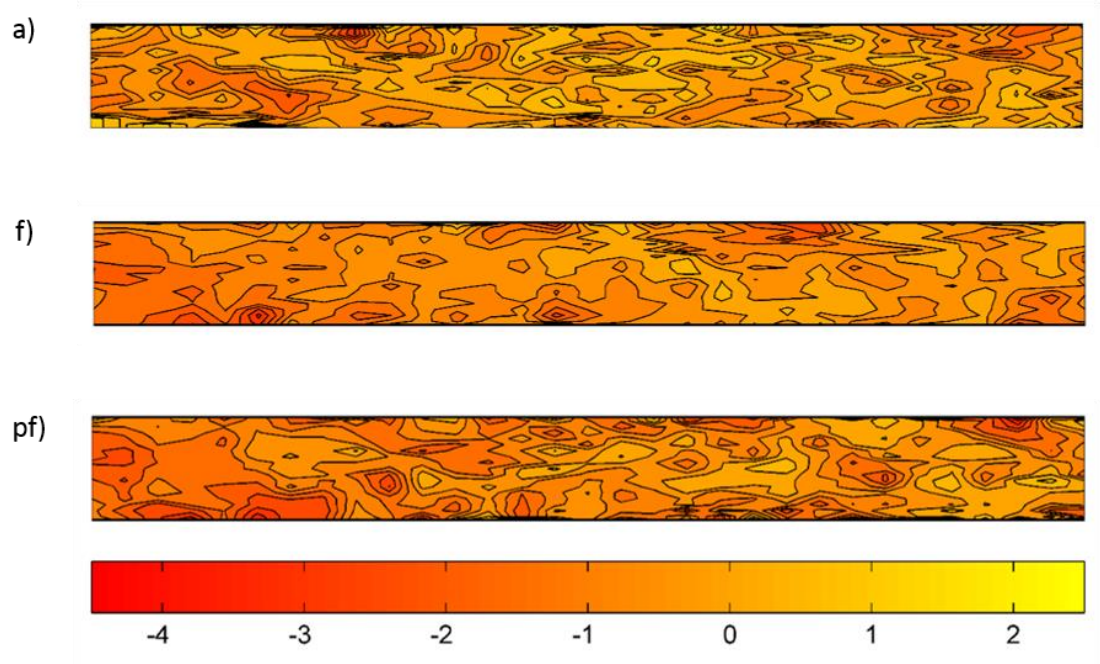

Figure 8: Bed elevation contour-plots for Run A4 (showing change in bed elevation from initial flat-bed conditions): antecedent (a); flood (f); and post-food (pf) stages [all values in cm]

Fig. 4c presents the sediment transport and discharge profiles for the entire duration of Run A4. In this run, $q_{sb,\exp}$ in the antecedent stage decreased until 15 min and then slightly increased for the last 5 min of the antecedent stage. During the flood stage, $q_{sb,\exp}$ initially peaked at 21 min, decreased at 22 min, and then gradually increased again until 24 min where t_s was reached. $q_{sb,\exp}$ was then observed to decrease over the remaining 6 min of the flood-stage.

The flood stage $\left(q_{sb,\exp}\right)_{avg}$ was determined to be 2.84x10^{-5} m^2/s. $q_{sb,\exp}$ during the post-flood stage remained relatively constant with a slight decrease observed at 35 min. Run A4 exhibited clockwise hysteresis in the sediment transport rates since t_s (21 min) peaked before t_r (25 min). The antecedent stage value of $q_{sb,\exp}$ was almost identical to the predicted $q_{sb,calc}$ throughout the 20 min antecedent stage. The predicted value of $q_{sb,calc}$ during the flood stage was projected to be 2.30 times greater than the predicted value of $q_{sb,calc}$ during the antecedent stage. During the flood stage, $q_{sb,\exp}$ varied from 3.64 to 5.58 times greater than the predicted $q_{sb,calc}$ values.

Tables 7 and 8 show $\Delta_{avg,\exp}$ and $\Delta_{avg,calc}$, respectively, for Run A4. At the end of the antecedent stage the average bed form height $\Delta_{avg,\exp}$ was measured to be 1.00 cm. By the end of the flood stage there was a 74% decrease in average bed form height with a $\Delta_{avg,\exp}$-value of 0.26 cm. From the end of the flood stage to the end of the post-flood stage the average bed form height increased by 419% to produce a $\Delta_{avg,\exp}$-value of 1.09 cm at the end of the post-flood stage. Overall, there was a net increase in average bed form height from the end of the antecedent stage to the end of post-flood stage of 9%. This trend between the hydrograph stages was not observed in the predicted $\Delta_{avg,\exp}$-values. The predicted average bed form height $\Delta_{avg,\exp}$ for the antecedent stage was 0.94 cm. A 127% increase in average bed form height was predicted by the end of the flood stage ($\Delta_{avg,calc}$ = 2.13 cm). There was a decrease of 29% in predicted average bed form height from the end of the flood stage to the end of the post-flood stage where $\Delta_{avg,calc}$ was 1.51 cm. Overall, a net increase of 61% from the end of the antecedent stage to the end of the post-flood stage was predicted by the bed form expressions, which was considerably greater than what was actually measured during the experimental run.

The D_{50}-values of the sediment in transport for the entire duration of Run A4 are seen in Fig. 5d. The D_{50} of the sediment in transport increased considerably during Run A4. During the flood-stage the D_{50} (0.36 mm) of the sediment in transport is approximately maintained. However, the D_{50} of the sediment in transport increased considerably during the post-flood

stage of the run. At 31 min the D_{50} of the sediment in transport reached 0.42 mm. This increase in the D_{50} of the sediment in transport demonstrated counter-clockwise hysteresis.

4.3.3.5 Summary of Series A

The experimental runs of Series A increased the magnitude of the unsteady flow event hydrograph from 1.25 to 2.00 times base-flow discharge from run to run while maintaining a constant unsteady flow event hydrograph duration of 10 min in each run. From the results described above, some clear trends regarding the effect of altering the magnitude of the flood-stage discharge on the sediment transport rates, average bed form heights, and composition of the sediment in transport were observed. As expected, $q_{sb,\exp}$ increased with increasing magnitude of the unsteady flow event hydrograph discharge. When the discharge was altered during the flood-stage to be 1.25, 1.50, 1.75, and 2.00 times base-flow conditions, $\left(q_{sb,\exp}\right)_{avg}$ was approximately 2.35, 3.00, 3.63, and 4.61 times greater than the corresponding antecedent value of $\left(q_{sb,\exp}\right)_{avg}$. Overall, the magnitude of average $q_{sb,\exp}$ increased with an increase in the magnitude of the flood stage discharge. A linear relationship was observed (see Fig. 9). $q_{sb,\exp}$ in the post-flood stages of the runs remained relatively constant among the runs in Series A with an average of 4.34×10^{-6} m^2/s. This value was approximately 32% lower than antecedent stage $q_{sb,\exp}$-value (where $q_{sb,\exp} = 6.42 \times 10^{-6}$ m^2/s). This was likely due to the initial adjustment of the bed from the initial flat bed conditions during the antecedent stage of the runs.

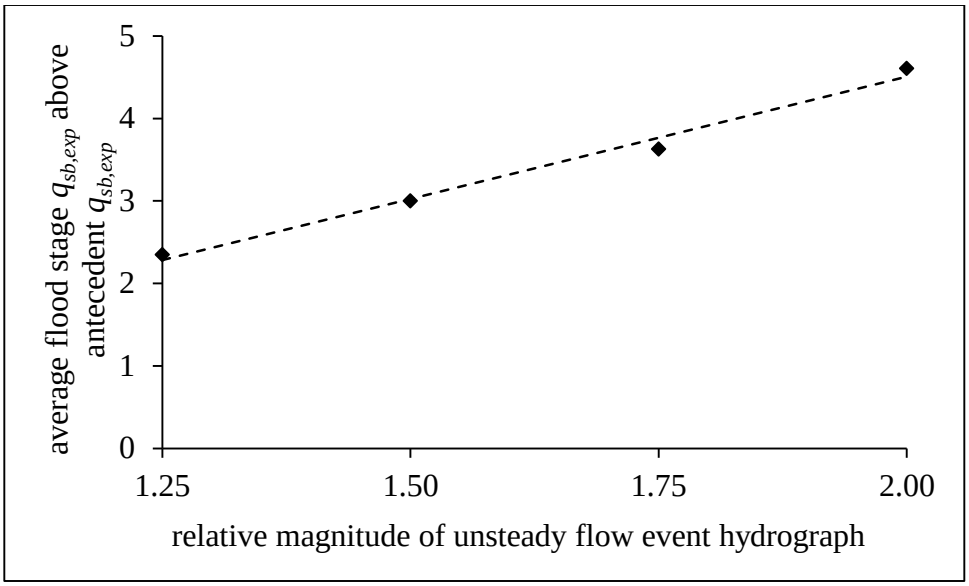

Figure 9: Relationship between relative magnitude of unsteady flow event hydrograph and average $q_{sb,exp}$ during the flood stage for the experimental runs of Series A

All four experimental runs demonstrated clockwise hysteresis in the sediment transport rates in response to the unsteady flow event hydrograph, meaning that t_s occurred prior to t_r. Since the unsteady flow event hydrograph is of the same duration in all runs in Series A, t_r remains constant at 25 min in each run. Although all experimental runs demonstrated clockwise hysteresis, t_s-values vary from run to run. In Run A1, A2, A3, and A4 t_s occurs at 24, 21, 21, and 21 min, respectively. Unsteady flow event hydrographs with greater discharge magnitudes (Runs A2, A3 and A4) emphasize a more pronounced effect of hysteresis in the sediment transport rate while unsteady flow event hydrographs with lower discharge magnitudes (Run A1) demonstrate a less pronounced effect of hysteresis.

It is also evident that $q_{sb,calc}$ considerably underestimates $q_{sb,\exp}$ in all runs of Series A. As previously discussed, the steady-flow preliminary experimental run had $q_{sb,\exp}$-values that fluctuated around the $q_{sb,calc}$ after equilibrium conditions were reached at t = 15 min. Table 9 presents a summary of the magnitude of the average flood stage $q_{sb,calc}$ above antecedent $q_{sb,calc}$ and the average flood stage $q_{sb,\exp}$ above antecedent $q_{sb,\exp}$. In Series A, it was observed that $q_{sb,calc}$ consistently under predicts the actual value of $q_{sb,\exp}$ by an average factor of 2.07 due

to the unsteadiness of the flow. As the discharge magnitude of the unsteady flow event hydrograph increased, the factor by which $q_{sb,calc}$ under predicts $q_{sb,\exp}$ also increased, with the exception of Run A4 when the factor decreased slightly.

Table 9: Predicted and experimental specific volumetric bed load transport rates for the experimental runs of Series A and Series B

Run	Description	$q_{sb,calc}$ flood magnitude above antecedent $q_{sb,calc}$	$q_{sb,exp}$ flood magnitude above antecedent $q_{sb,exp}$
A1	1.25 x base-flow for 10 min	1.40	1.75 – 2.94
A2	1.50 x base-flow for 10 min	1.40	2.11 – 3.89
A3	1.75 x base-flow for 10 min	1.57	2.56 – 4.69
A4	2.00 x base-flow for 10 min	2.30	3.64 – 5.58
B1	1.50 x base-flow for 5 min	1.42	2.40 – 3.84
B2	1.50 x base-flow for 10 min	1.40	2.11 – 3.89
B3	1.50 x base-flow for 15 min	1.31	2.92 – 4.44
B4	1.50 x base-flow for 20 min	1.86	3.25 – 4.74

In general, the average bed form height $\Delta_{avg,\exp}$ increased by the end of the post-flood stage. The plot of percent change in average bed form height versus the relative discharge magnitude of the unsteady flow event hydrograph is seen in Fig. 10. Trend lines are drawn on this figure to identify general patterns. Generally, from the antecedent stage to the flood stage, the bed forms showed a decrease in size as the magnitude of the event increased. From the flood stage to the post-flood stage the bed forms showed an increase in size as the magnitude of the event increased. Overall, from the end of the antecedent stage to the post-flood stage the bed form size decreased as the relative magnitude of the event increased. A larger net change in average bed form height from the end of the antecedent stage to the end of the post-flood stage was observed for smaller magnitude unsteady flow event hydrographs. Bed forms increase in size during the flood stage of unsteady flow event hydrographs of low magnitude, but decrease in size in response to larger events resulting in a flatter bed morphology. This is likely due to an excessive amount of sediment transport that occurs in response to unsteady flow event hydrographs of greater magnitude. These trends in $\Delta_{avg,\exp}$ are compared to $\Delta_{avg,calc}$. $\Delta_{avg,\exp}$ and $\Delta_{avg,calc}$ during antecedent conditions were near-identical. There was a greater observed difference between $\Delta_{avg,\exp}$ and $\Delta_{avg,calc}$ during the flood stage of larger magnitude events of

Series A. The predicted bed form geometry suggested that the flood stage $\Delta_{avg,calc}$ would increase with increasing magnitude of unsteady flow event hydrograph. However, the experimental flood stage $\Delta_{avg,\exp}$ was observed to decrease with increasing event magnitude. Both $\Delta_{avg,\exp}$ and $\Delta_{avg,calc}$ predicted an increase in the post-flood bed form height. $\Delta_{avg,calc}$ is greater during the post-flood stage than the antecedent stage in all runs in Series A due to minor differences in discharge which resulted in minor differences in average flow depth (h_{av}). Since bed forms generally scale by h_{av}, the value of $\Delta_{avg,calc}$ varied according to differences in h_{av}. The differences in $\Delta_{avg,\exp}$ are a result of the magnitude of the unsteadiness of the discharge which allowed h_{av} to fluctuate naturally, causing the subsequent hysteretic effect on $q_{sb,\exp}$.

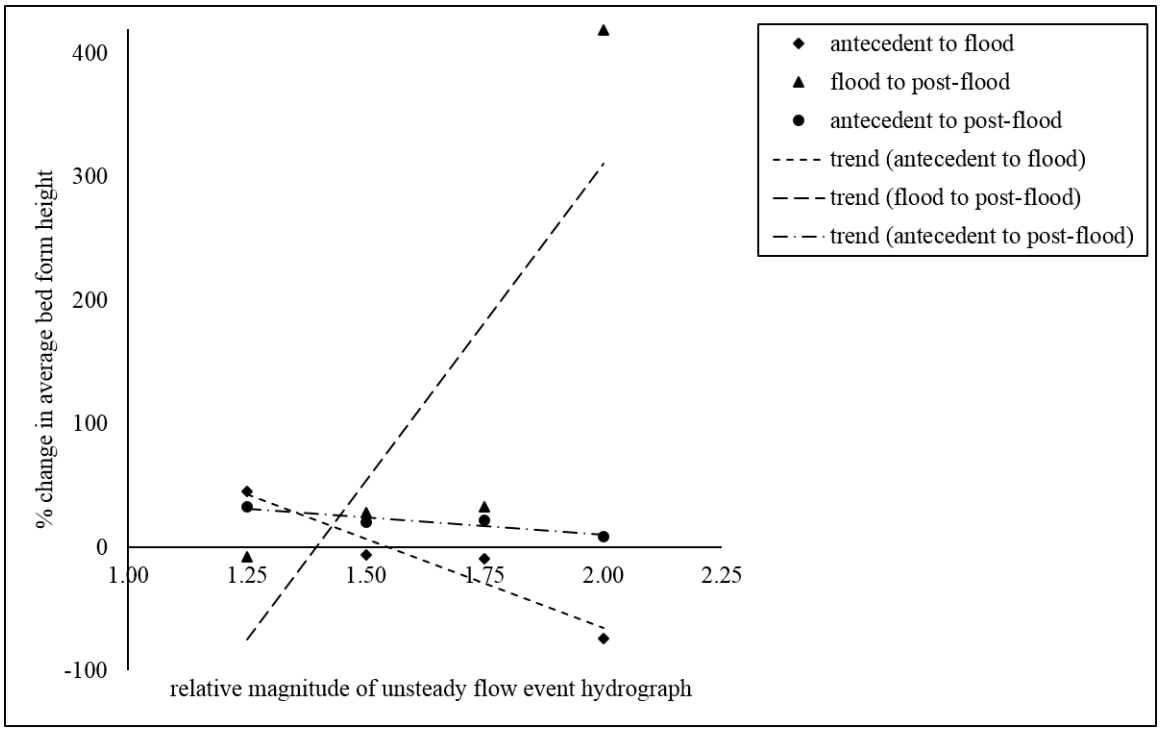

Figure 10: Percent change in average bed form height versus the relative magnitude of the unsteady flow event hydrographs in the experimental runs of Series A

Regarding the grain size composition of the sediment in transport during the experimental runs of Series A, a decrease in the D_{50} of the sediment in transport during the early stages of the unsteady flow event hydrograph was observed in Runs A1 and A2. A return to the antecedent stage D_{50}-value of the sediment in transport during the post-flood stage was observed in both

Runs A1 and A2, demonstrating counter-clockwise hysteresis of the grain size composition of the sediment in transport. In contrast, Runs A3 and A4 exhibited greater emphasis on counter-clockwise hysteresis as the D_{50} of the sediment in transport increased during the post-flood stage of the runs. In Run A3 and A4, the D_{50} of the sediment in transport did not increase until the post-flood stage. Run A4 had less of a lag-in-time than Run A3 but a larger change in the size of the D_{50} of the sediment in transport due to a larger magnitude of change in discharge during the flood stage of the run.

4.3.4 Series B results

4.3.4.1 Run B1

Run B1 contained a flood stage hydrograph discharge magnitude of 1.50 times base-flow conditions and a flood stage duration of 5.0 min. Fig. 11 shows the bed elevation contour-plots for Run B1. The antecedent stage contour-plot shows bed forms in equilibrium with the hydraulic conditions with bed forms of approximately uniform size across the entire length of the flume. The flood stage shows a considerable decrease in average bed form size. The post-flood stage shows regions of substantial scour, however, the bed forms are slightly larger than the antecedent stage.

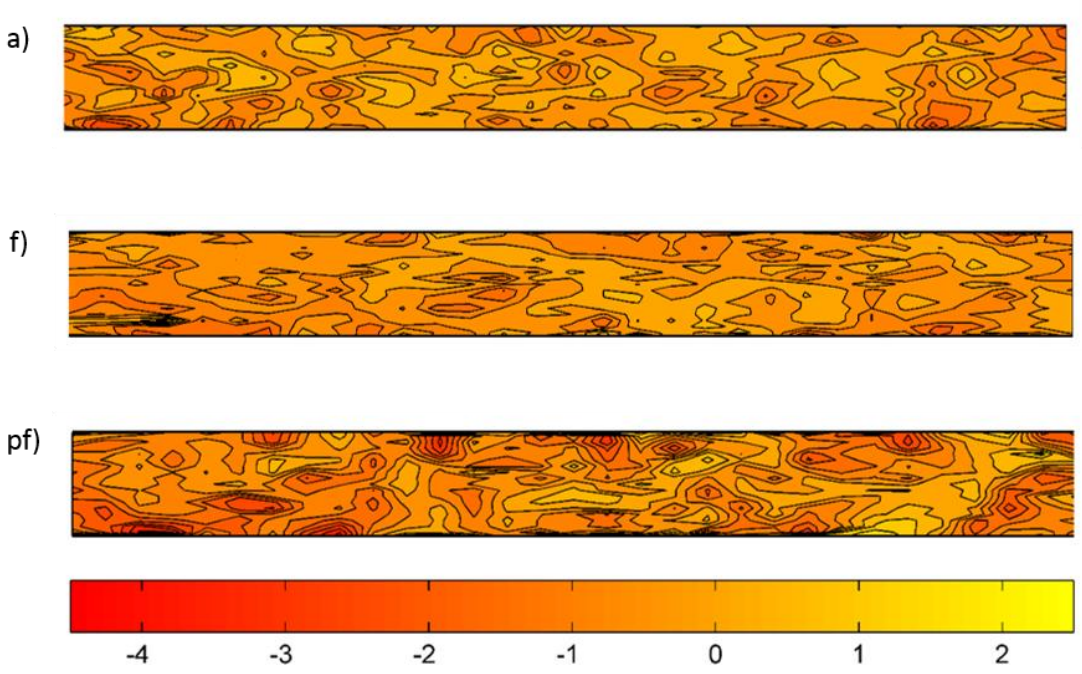

Figure 11: Bed elevation contour-plots for Run B1 (showing change in bed elevation from initial flat-bed conditions): antecedent (a); flood (f); and post-food (pf) stages [all values in cm]

Fig. 12a presents the sediment transport and discharge profiles for the entire duration of Run B1. In this run, $q_{sb,\exp}$ decreased over the 20 min duration of the antecedent stage. During the flood stage $q_{sb,\exp}$ increased until it reached t_s at 23 min and then gradually decreased for the remainder of the flood stage. The flood stage $\left(q_{sb,\exp}\right)_{avg}$ was 1.07x10^{-5} m^2/s. During the post-flood stage $q_{sb,\exp}$ fluctuated slightly, with peaks occurring at 30 and 40 min. Run B1 demonstrated counter-clockwise hysteresis since t_r (22.5 min) peaked before t_s (23 min). The flood stage $q_{sb,calc}$ was predicted to be 1.42 times greater than the antecedent stage $q_{sb,calc}$. However, the flood stage $q_{sb,\exp}$ was 2.40 to 3.84 times greater than the antecedent stage $q_{sb,\exp}$. During the post-flood stage $q_{sb,\exp}$ was slightly greater than the predicted $q_{sb,calc}$-value.

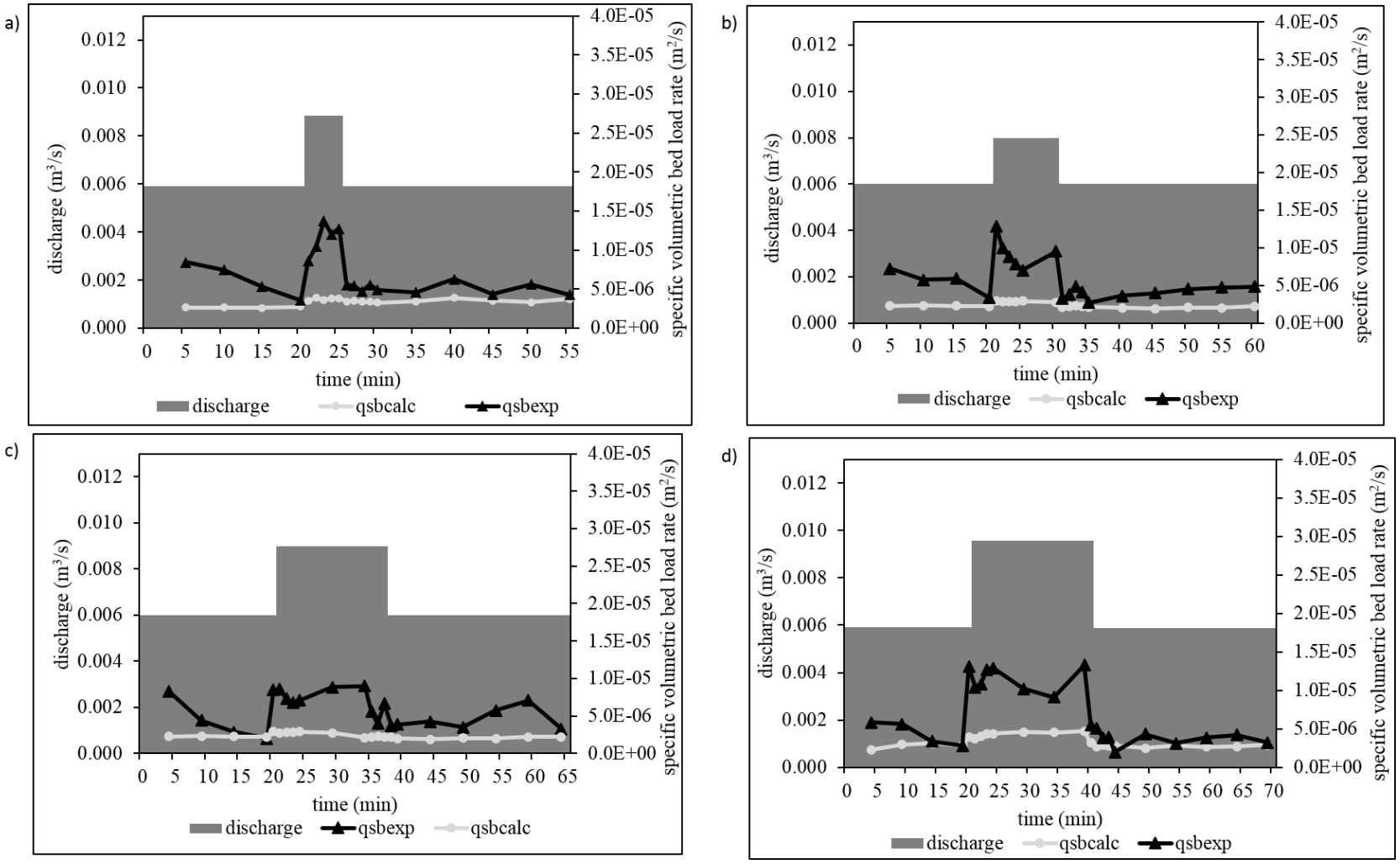

Figure 12: Sediment transport and discharge profiles for the experimental runs of Series B: a) Run B1; b) Run B2; c) Run B3; and d) Run B4

Tables 7 and 8 show $\Delta_{avg,\exp}$ and $\Delta_{avg,calc}$, respectively, for Run B1. At the end of the antecedent stage $\Delta_{avg,\exp}$ was measured to be 0.78 cm. By the end of the flood stage there was a decrease in average bed form height of 26% to give an end of flood stage $\Delta_{avg,\exp}$-value of 0.58 cm. From the flood stage to the post-flood stage there was an increase in average bed form height of 53% with $\Delta_{avg,\exp}$ measured to be 0.89 cm by the end of the post-flood stage. Overall, this represents a net increase in $\Delta_{avg,\exp}$ of 14% from the end of the antecedent stage to the end of the post-flood stage. This observed trend in the antecedent and flood stages was not seen in the predicted $\Delta_{avg,calc}$-values. By the end of the antecedent stage $\Delta_{avg,calc}$ was predicted to be 1.13 cm. From antecedent to flood stage there was a predicted increase in average bed form height of 35% to give a $\Delta_{avg,calc}$ = 1.52 cm at the end of the flood stage. From the flood to post-flood stage there was a decrease in average bed form height of 6%. At the end of the post-flood stage $\Delta_{avg,calc}$ was predicted to be 1.43 cm. Overall, this represents a predicted net increase in $\Delta_{avg,calc}$ of 27% from the end of the antecedent stage to the end of the post-flood stage. This value is considerably greater than the net increase in average bed form height that was actually observed in the experimental run.

The variation in D_{50} of the sediment in transport for the entire duration of Run B1 is seen in Fig.13a. In Run B1 the D_{50} of the sediment in transport reached a minimum (0.35 mm) within the first minute (t = 21 min) of the flood stage. The D_{50} of the sediment in transport is maintained at the antecedent size (0.36 mm) for the duration of the flood event. The D_{50} of the sediment in transport reached a maximum at 0.40 mm during the post-flood stage of the run. This observed trend represents counter-clockwise hysteresis of the D_{50} of the sediment in transport in response to the experimental unsteady flow event hydrograph.

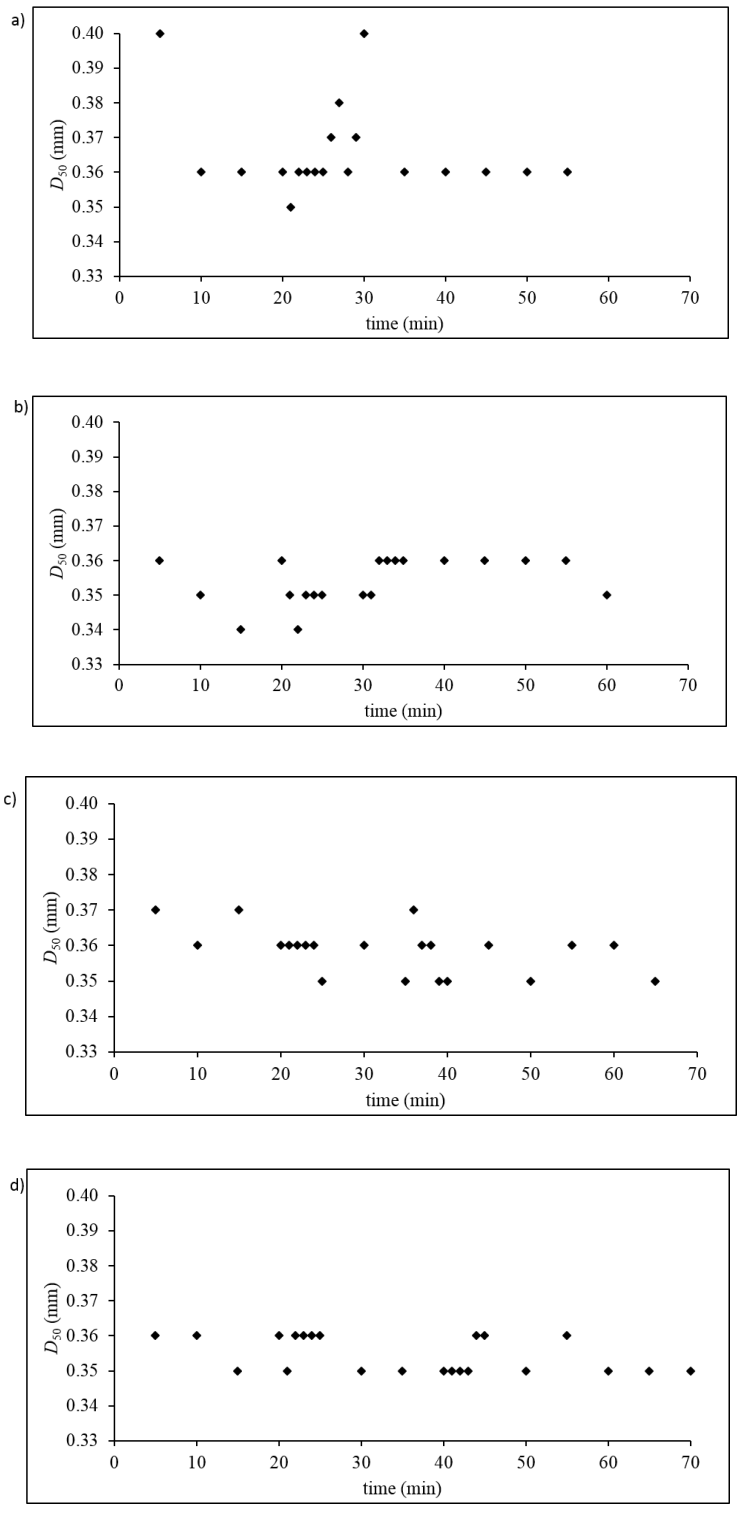

Figure 13: D_{50}-value versus time for the sediment in transport during Series B experiments: a) Run B1; b) Run B2; c) Run B3; and d) Run B4

4.3.4.2 Run B2

Run B2 contained a flood stage hydrograph discharge magnitude of 1.50 times base-flow conditions and a flood stage duration of 10.0 min. Fig. 14 shows the bed elevation contour-plots for Run B2. The antecedent stage shows approximately uniform bed forms across the length of the flume. The flood stage shows slightly smaller bed forms that are more spread out compared to the antecedent stage. The post-flood stage contour-plot shows bed forms that are larger compared to the antecedent stage across the entire length of the flume.

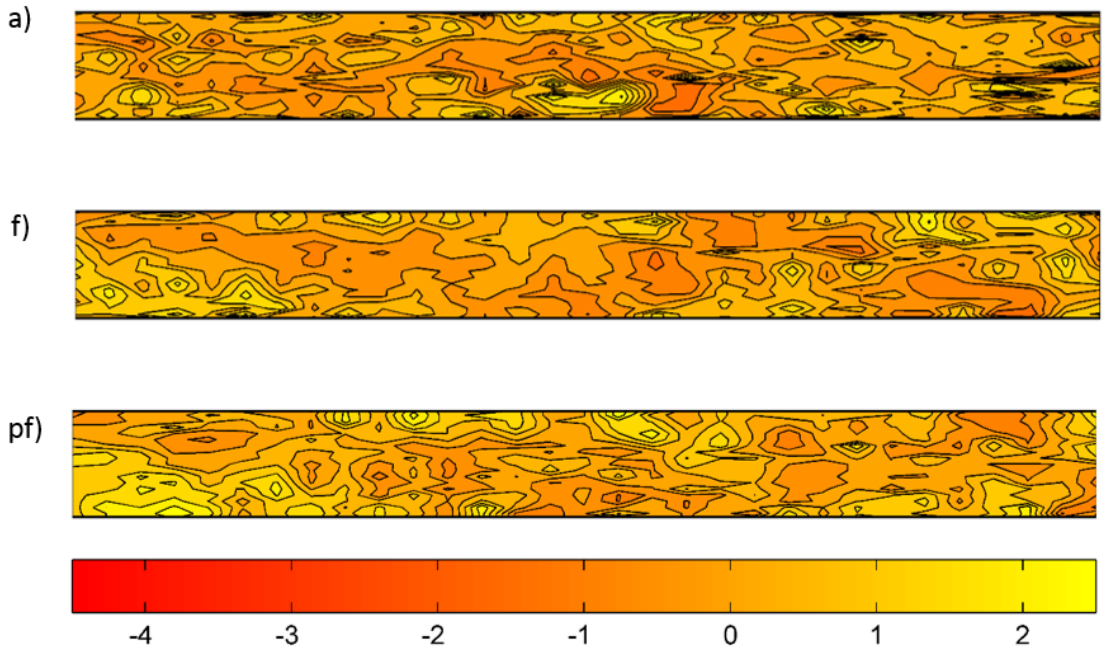

Figure 14: Bed elevation contour-plots for Run B2 (showing change in bed elevation from initial flat-bed conditions): antecedent (a); flood (f); and post-food (pf) stages [all values in cm]

Fig. 12b presents the sediment transport and discharge profiles for the entire duration of Run B2. In this run, $q_{sb,\exp}$ decreased over the 20 min duration of the antecedent stage. During the 10 min flood stage, $q_{sb,\exp}$ gradually increased until t_s occurred at 21 min, slightly decreased until 25 min, and then increased considerably again at 30 min. The flood stage $\left(q_{sb,\exp}\right)_{avg}$ was 9.31x10^{-5} m^2/s. During the post-flood stage $q_{sb,\exp}$ fluctuated slightly, with peaks occurring at 40 and 50 min. Run B2 exhibited clockwise hysteresis since t_s (23 min) peaked prior to t_r (25 min). The flood-stage $q_{sb,calc}$ was

predicted to be 1.40 times greater than the antecedent stage value of $q_{sb,calc}$. However, the flood-stage $q_{sb,\exp}$ was observed to be 2.11 to 3.89 times greater than the antecedent stage $q_{sb,\exp}$. During the post-flood stage, $q_{sb,\exp}$ was slightly greater than the predicted $q_{sb,calc}$-value at approximately 33 min and again from 35 min until the end of the experimental run.

Tables 7 and 8 show $\Delta_{avg,\exp}$ and $\Delta_{avg,calc}$, respectively, for Run B2. At the end of the antecedent stage, $\Delta_{avg,\exp}$ was measured to be approximately 1.00 cm. By the end of the flood-stage $\Delta_{avg,\exp}$ had decreased by 6% from antecedent conditions as $\Delta_{avg,\exp}$ was measured to be 0.94 cm. From the flood stage to the post-flood stage there was a 28% increase in average bed form height to give $\Delta_{avg,\exp}$ = 1.20 cm. Overall, this represents a 20% net increase in average bed form height from the end of the antecedent stage to the end of the post-flood stage. $\Delta_{avg,\exp}$ for the antecedent stage was predicted to be 1.03 cm. The flood-stage conditions predicted an increase in average bed form height of 19% to give a $\Delta_{avg,\exp}$ = 1.23 cm at the end of the flood stage. This increase in bed form geometry was also observed in the run. However, during the flood and post-flood stages, $\Delta_{avg,\exp}$ predicted the opposite trend to what was measured. A decrease of 24% in average bed form height from the flood stage to the end of post-flood stage was predicted as $\Delta_{avg,\exp}$ = 0.94 cm by the end of the post-flood stage. Overall, a net decrease in average bed form height of 9% from the antecedent to the post-flood stage was predicted, which is in contrast to what was actually observed in the runs.

The variation in D_{50} of the sediment in transport in Run B2 is seen in Fig.13b. In this run the D_{50} of the sediment in transport reached a minimum (0.34 mm) at t = 22 min. For the duration of the flood event the D_{50} of the sediment in transport was approximately maintained at the antecedent average grain size (0.36 mm). This observed trend represents counter-clockwise hysteresis of the D_{50} of the sediment in transport in response to the unsteady flow event hydrograph.

4.3.4.3 Run B3

Run B3 contained a flood stage hydrograph discharge magnitude of 1.50 times base-flow conditions and a flood stage duration of 15.0 min. Fig. 15 shows the bed elevation contour-plots for Run B3. The antecedent stage of the hydrograph showed a bed morphology at equilibrium with the hydraulic

conditions. The flood stage showed bed forms that are slightly smaller and more spread out across the flume. The post-flood stage bed forms are larger than both the antecedent and flood stage bed forms.

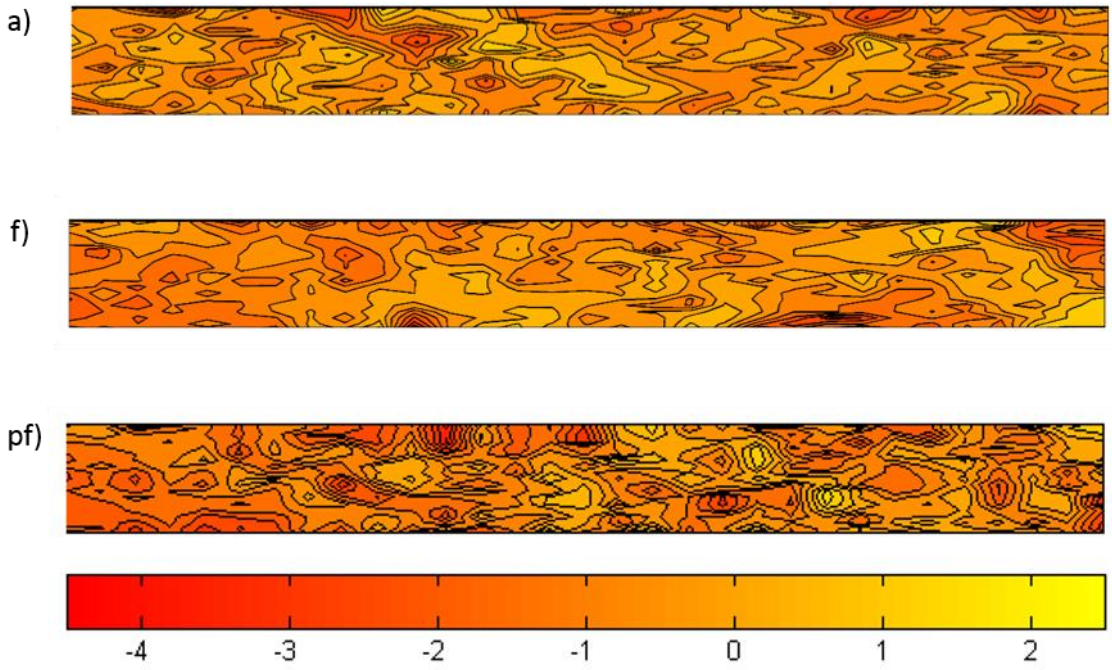

Figure 15: Bed elevation contour-plots for Run B3 (showing change in bed elevation from initial flat-bed conditions): antecedent (a); flood (f); and post-food (pf) stages [all values in cm]

Fig. 12c presents the sediment transport and discharge profiles for the entire duration of Run B3. As observed in this figure, $q_{sb,\exp}$ gradually decreased over the 20 min duration of the antecedent stage. During the 15 min flood stage, $q_{sb,\exp}$ peaked considerably at 21 and 22 min, decreased until it reached a flood stage minimum at 24 min, and then increased again until it reached a second peak at 30 min. The flood-stage $\left(q_{sb,\exp}\right)_{avg}$ was 1.20x10^{-5} m^2/s. During the post-flood stage $q_{sb,\exp}$ peaked at 34 min and again at 50 min. This run exhibited clockwise hysteresis since t_s (22 min) peaked prior to t_r (27.5 min). The second flood stage peak at 30 min is slightly less than the value of $q_{sb,\exp}$ at t_s. The flood stage $q_{sb,calc}$ was predicted to be 1.31 times greater than the antecedent predicted value of $q_{sb,calc}$. However, the flood-stage $q_{sb,\exp}$ was actually measured to be 2.92 to 4.44 times greater than the antecedent stage $q_{sb,\exp}$.

Tables 7 and 8 show $\Delta_{avg,\exp}$ and $\Delta_{avg,calc}$, respectively, for Run B3. At end of the antecedent stage $\Delta_{avg,\exp}$ was measured to be 0.84 cm. There was a 1% decrease in average bed form height by the end of the flood stage where $\Delta_{avg,\exp}$ was measured to be 0.83 cm. By the end of the post-flood stage $\Delta_{avg,\exp}$ was measured to be 0.86 cm, representing a 4% increase in average bed form height from the end of the flood stage to the end of the post-flood stage. Overall, a net 2% increase in average bed form height was observed from the antecedent to post-flood stage. $\Delta_{avg,calc}$ for the antecedent stage was predicted to be 1.23 cm. An increase in average bed form height of 23% (giving $\Delta_{avg,calc}$ = 1.51 cm) was predicted by the end of the flood stage. A 19% decrease in average bed form height from the end of the flood stage to end of the post-flood stage was predicted (giving $\Delta_{avg,calc}$ = 1.23 cm). Overall, there was no predicted net change in $\Delta_{avg,calc}$ from the antecedent stage to the post-flood stage, which was very close to what was actually observed in the run despite the fact that $\Delta_{avg,calc}$ over-estimated the averaged bed form height.

The variation in the D_{50} of the sediment in transport during Run B3 is seen in Fig.13c. The minimum D_{50} of the sediment in transport occurred at 25 and 35 min when the D_{50} reaches 0.35 mm. During the remainder of the flood stage, the D_{50} of the sediment in transport is maintained at the antecedent grain size of 0.36 mm, with the exception of at t = 36 min when the D_{50} of the sediment in transport increases slightly to reach a maximum value of 0.37 mm. This observed trend represents counter-clockwise hysteresis of the D_{50} of the sediment in transport in response to the experimental unsteady flow event hydrograph.

4.3.4.4 Run B4

Run B4 contained a flood stage hydrograph discharge magnitude of 1.50 times base-flow conditions and a flood stage duration of 20.0 min. Fig. 16 shows the bed elevation contour-plots for Run B4. The antecedent stage contour-plot shows the bed morphology having reached equilibrium with the hydraulic conditions. The flood stage contour-plot shows that bed forms have increased in size and are covering most of the bed. The post-flood stage bed shows bed forms that are larger in size than both the antecedent and flood stage, with slightly smaller bed forms situated at the upstream end of the flume.

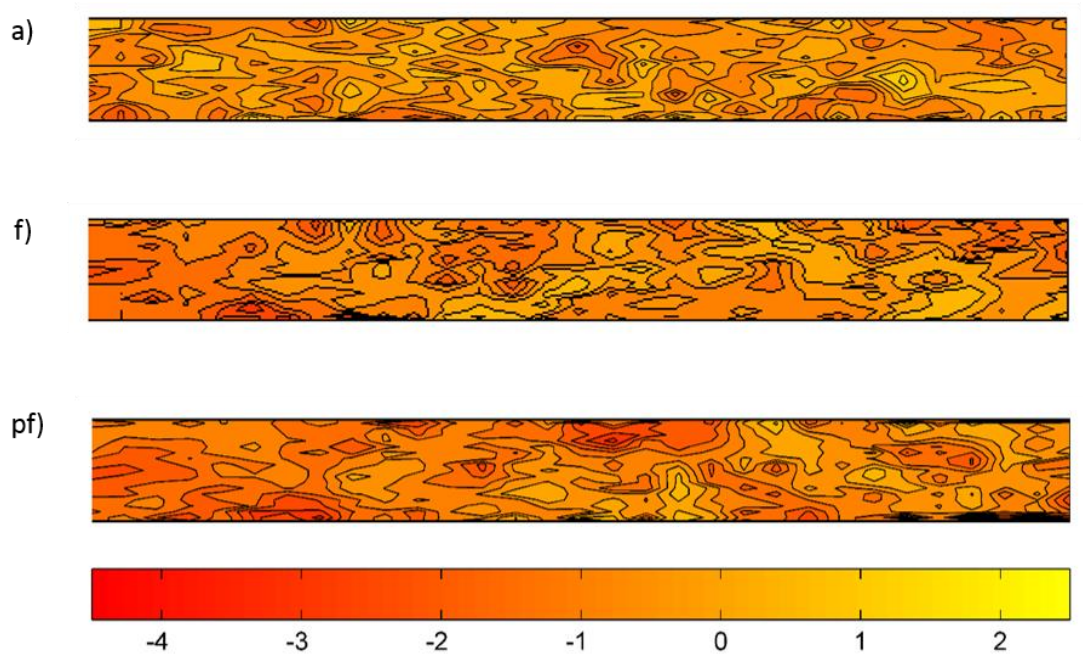

Figure 16: Bed elevation contour-plots for Run B4 (showing change in bed elevation from initial flat-bed conditions): antecedent (a); flood (f); and post-food (pf) stages [all values in cm]

Fig. 12d presents the sediment transport and discharge profiles for the entire duration of Run B4. As observed in this figure, $q_{sb,\exp}$ decreased gradually over the 20 min duration of the antecedent stage. During the 20 min flood stage, $q_{sb,\exp}$ peaked considerably at 21 min, decreased until it peaked again at 23 and 24 min, then gradually decreased again until 40 min. The flood-stage $\left(q_{sb,\exp}\right)_{avg}$ was 1.16x10^{-5} m^2/s. During the post-flood stage, there was a slight decrease in $q_{sb,\exp}$ at 45 min. This run demonstrates an equally, double-peaked sediment transport response (t_s occurring at 24 and 40 min) during the flood stage. However, due to the presence of multiple peaks in $q_{sb,\exp}$ that occurred at 21 and 25 min, Run B4 is considered to exhibit slightly clockwise hysteresis since t_r occurred at 30 min. The flood stage $q_{sb,calc}$ was predicted to be 1.86 times greater than the antecedent value of $q_{sb,calc}$. However, the flood stage $q_{sb,\exp}$ was actually measured to be approximately 3.25 to 4.74 times greater than the antecedent stage $q_{sb,\exp}$.

Tables 7 and 8 show $\Delta_{avg,\exp}$ and $\Delta_{avg,calc}$, respectively, for Run B4. At the end of the antecedent stage $\Delta_{avg,\exp}$ was measured to be 0.79 cm. There was a 4% increase in average bed form height to give

$\Delta_{avg,\exp}$ = 0.82 cm at the end of flood stage. At the end of the post-flood stage $\Delta_{avg,\exp}$ was measured to be 0.92 cm, representing a 12% increase in average bed form height from the end of the flood stage. Overall, a 16% net increase in average bed form height occurred from the antecedent stage to the post-flood stage. This trend was not predicted in the $\Delta_{avg,calc}$-values. At the end of the antecedent stage, $\Delta_{avg,calc}$ was predicted to be 1.23 cm. A 43% increase in average bed form height was predicted for the flood stage ($\Delta_{avg,calc}$ = 1.76 cm). By the end of the post-flood stage a 30% decrease in average bed form height was predicted ($\Delta_{avg,calc}$ = 1.23 cm). Overall, no net change in $\Delta_{avg,calc}$ from the antecedent stage to the post-flood stage was predicted which is in contrast to the measured bed forms observed in the experiment.

The variation of the D_{50} of the sediment in transport during Run B4 is seen in Fig.12d. The minimum D_{50} of the sediment in transport was 0.35 mm and this re-occurred numerous times throughout the run (i.e., at times t = 21, 30, 35, 40, and 41 min). During the remainder of the flood stage of Run B4, the D_{50} of the sediment in transport was maintained at 0.36 mm. The observed trend represents counter-clockwise hysteresis of the D_{50} of the sediment in transport in response to the experimental unsteady flow event hydrograph.

4.3.4.5 Summary of Series B

The experimental runs of Series B increased the duration of the unsteady flow event hydrograph from 5.0 min to 20.0 min while maintaining a constant unsteady flow event hydrograph discharge magnitude of 1.50 times base-flow conditions. Thus, Series B investigated the effect of the duration of the unsteady flow event hydrograph on $q_{sb,\exp}$, $\Delta_{avg,\exp}$ and the grain size composition of the sediment in transport during the runs.

While Series A showed a considerable increase in $q_{sb,\exp}$ from run to run as the discharge magnitude of the unsteady flow event hydrograph was increased, Series B did not show such a drastic trend. Rather, $q_{sb,\exp}$ during the flood stage of all four runs in Series B was observed to be less variable than that observed in Series A. For example, the flood stage $\left(q_{sb,\exp}\right)_{avg}$ was approximately 3.12, 3.00, 3.68, and 3.99 times greater than the corresponding antecedent $\left(q_{sb,\exp}\right)_{avg}$-values in Runs B1, B2, B3, and B4, respectively. The slight increase in $\left(q_{sb,\exp}\right)_{avg}$ from run to run in Series B was likely due to the

increase in duration of the flood stage as $\left(q_{sb,\exp}\right)_{avg}$ is generally observed to increase (slightly) as the duration of the event increases. This allowed more time for greater volumes of sediment to be entrained (i.e., greater opportunity for large peaks in sediment transport to occur during the flood stage). The duration of the flood stage and $q_{sb,\exp}$ showed a positive (increasing) linear relationship (see Fig. 17). Post-flood stage $\left(q_{sb,\exp}\right)_{avg}$ for all four runs of Series B fluctuated around an average value of 5.30x10^{-6} m^2/s. Some variation in $q_{sb,\exp}$ during post-flood stages was observed in Series B. In Run B1, an increase in $q_{sb,\exp}$ was observed at 40 and 50 min. $q_{sb,\exp}$ remained fairly constant during the post-flood stage of Run B2. The $q_{sb,\exp}$ in Run B3 increased from 50 min until the end of the run. Run B4 contained one $q_{sb,\exp}$ peak during the post-flood stage that lasted from 50 to 65 min.

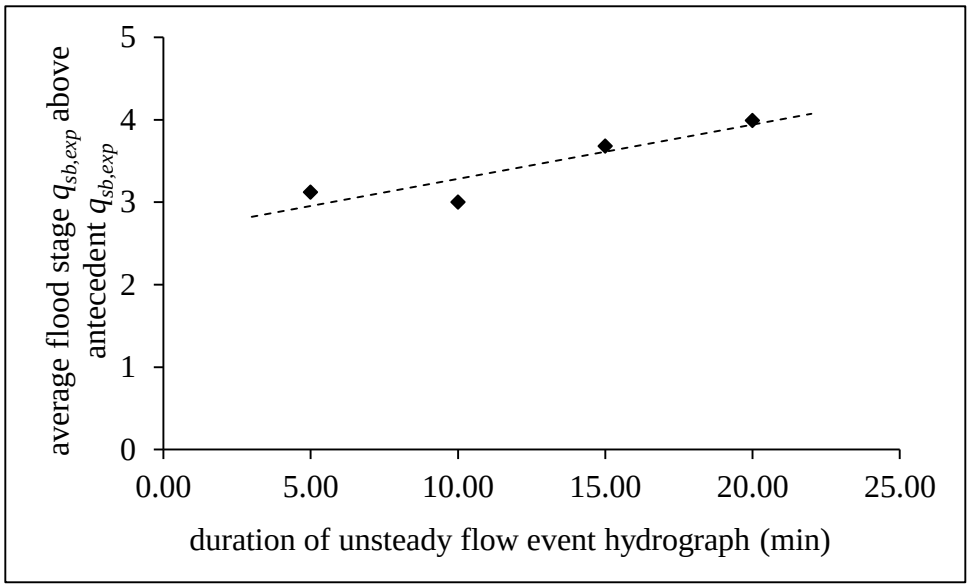

Figure 17: Relationship between duration of unsteady flow event hydrograph and average $q_{sb,exp}$ during the flood stage for the experimental runs of Series B

Since the experimental runs of Series B varied the duration of the flood stage from run to run, t_r of each run was unique. In contrast to the experimental runs of Series A, the same type of hysteresis was not observed in all runs in Series B. Run B1 demonstrated counter-clockwise hysteresis while Runs B2 and B3 demonstrated clockwise hysteresis (Run B3 started to show a second peak in $q_{sb,\exp}$, however, this run was still considered to exhibit clockwise hysteresis). Run B4 was double-peaked but was considered to display slightly clockwise hysteresis. In general, shorter duration unsteady flow

events exhibited counter-clockwise hysteresis (Run B1) and longer duration unsteady flow events exhibited clockwise hysteresis (Runs B2, B3 and B4).

The predicted $q_{sb,calc}$ considerably underestimated $q_{sb,\exp}$ in all runs of Series B. Table 9 presents a summary of the magnitude of both $q_{sb,calc}$ and $q_{sb,\exp}$ above the corresponding antecedent stage values. In Series B, $q_{sb,calc}$ under-predicts $q_{sb,\exp}$, on average, by a factor of 2.32 times the corresponding antecedent value due to the unsteadiness of the flow. While the variation between these factors is not excessive, it would be expected that they would be relatively constant since the magnitude of the flood stage discharge is near-identical. Despite efforts to manipulate the flow rate to create identical flood stage discharges in the experimental runs of Series B, the discharge and h_{av} varied slightly. This variation is likely responsible for the observed variation in $q_{sb,calc}$ and $q_{sb,\exp}$ in the experimental runs of Series B.

The percent changes in the average bed form height with increasing unsteady flow event durations are seen in Fig. 18. Trend lines are drawn on this figure to identify general patterns. Generally, the change in average bed form height from the antecedent stage to the end of the flood stage showed a decreasing trend as the duration of the unsteady flow event increased in the experimental runs of Series B. A more drastic decrease in the $\Delta_{avg,\exp}$ occurred between the flood and post-flood stages as the duration of the unsteady flow event increases. Overall, from the antecedent stage to the post-flood stage, $\Delta_{avg,\exp}$ is relatively constant as the duration of the unsteady flow event increases. On average, by the end of each experiment, $\Delta_{avg,\exp}$ increased by 13%. No clear relationship between the duration of the flood stage and the increase in the post-flood average bed form heights is evident. In all four experimental runs, $\Delta_{avg,\exp}$ increased from the flood to post-flood stage. These trends observed in the $\Delta_{avg,\exp}$ can also be compared to the $\Delta_{avg,calc}$-values. The antecedent $\Delta_{avg,\exp}$ and $\Delta_{avg,calc}$ were similar in that the $\Delta_{avg,\exp}$ deviated from the $\Delta_{avg,calc}$ by 25% for all Runs in Series B. No clear trend in relation to $\Delta_{avg,calc}$ and an increase in the flood stage duration exists as duration is not considered in the predictive bed form geometry equations. Fluctuations in $\Delta_{avg,calc}$ were due to slight variations in the experimental h_{av}. No net change is evident in the $\Delta_{avg,calc}$ for Runs B3 and B4 because h_{av} in the antecedent and post-flood stages were identical. However, the net change from antecedent to post-flood stages in $\Delta_{avg,\exp}$

$\Delta_{avg,\exp}$ for all runs in Series B show an increase due to the hysteresis of the sediment transport rates.

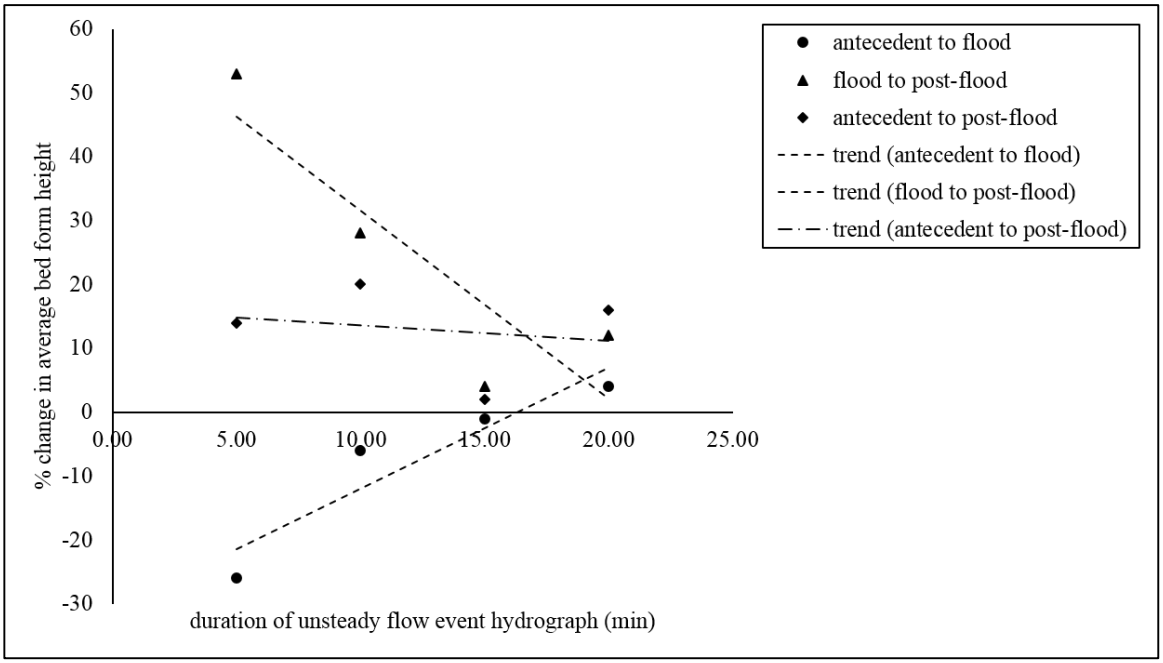

Figure 18: Percent change in average bed form height versus the duration of the unsteady flow event hydrographs in the experimental runs of Series B

Regarding the grain size composition of the sediment in transport during the experimental runs of Series B, there was very little variation in the D_{50} of the transported sediment from run to run due to the near-identical magnitude of discharge of the unsteady flow event hydrographs in these runs. In all runs, the D_{50} of the sediment in transport decreased early in the flood stage. All experimental runs exhibited a counter-clockwise hysteresis of the size of the transported sediment. The little variation in the D_{50} of the transported sediment for the experimental runs of Series B was likely due to near-identical magnitude of the flood-stage in all runs.

4.4 Discussion

This section analyzes and discusses the experimental results of Series A together with those from Series B in order to explore general trends regarding the effect of magnitude and duration of the unsteady flow event hydrograph on the stream bed morphological response. As discussed previously, hysteresis of the sediment transport rates is defined according to the time-to-peak of the hydrograph

(t_r) and the time-to-peak sediment transport rate (t_s). The parameter t_{lag} is used in order to define the lag-in-time occurring between t_r and t_s. This parameter is defined as:

$$t_{lag} = t_r - t_s . \tag{40}$$

Table 10 presents a summary of the relative magnitude of the flood stage (represented as the magnitude greater than base-flow discharge, flood stage duration, t_s, t_r, and t_{lag} for all experimental runs of Series A and B. Fig. 19 displays graphical relationships of the data presented in Table 10. Fig. 19a presents the relationship between t_{lag} and the relative magnitude of the flood stage for all runs of Series A and B and Fig. 19b presents the relationship between t_{lag} and the duration of the flood stage for all runs of Series A and B.

Table 10: Summary of t_{lag} in the experimental runs of Series A and B

Run	Relative magnitude of flood stage above antecedent	Duration of flood stage (min)	t_s (min)	t_r (min)	t_{lag} (min)	$q_{sb,exp}$ peak (m^3/s)
A1	1.25	10	24	25.0	1.0	1.16E-05
A2	1.50	10	21	25.0	4.0	1.29E-05
A3	1.75	10	21	25.0	4.0	2.03E-05
A4	2.00	10	24	25.0	1.0	3.46E-05
B1	1.50	5	23	22.5	-0.5	1.38E-05
B2	1.50	10	21	25.0	4.0	1.29E-05
B3	1.50	15	22	27.5	5.5	8.82E-06
B4	1.50	20	24	30.0	6.0	1.33E-05

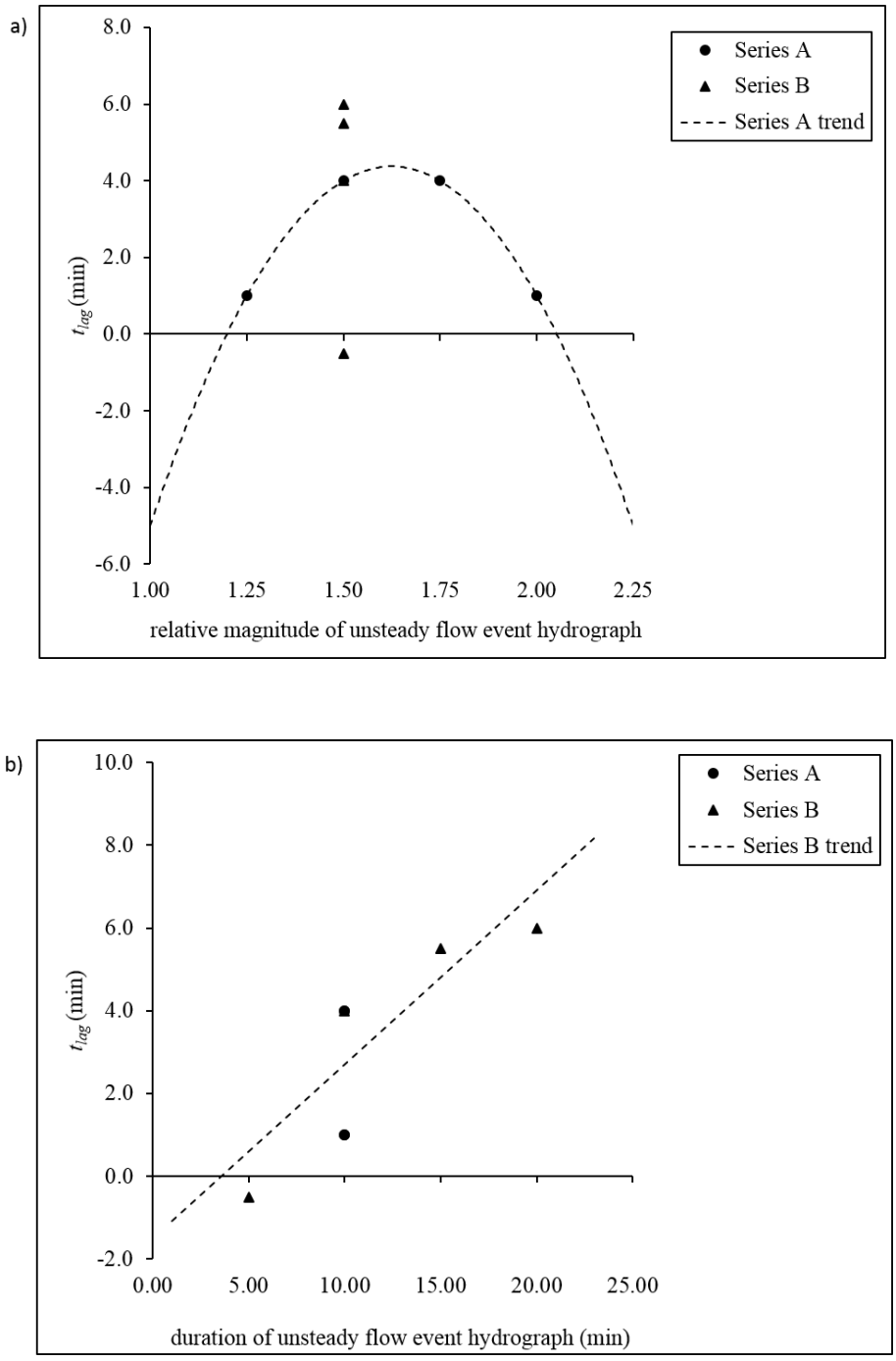

Figure 19: Relationship between t_{lag} and: a) the relative magnitude of the unsteady flow event hydrograph; and b) the duration of the unsteady flow event hydrograph (min)

All four experimental runs of Series A exhibit positive t_{lag} values (or clockwise hysteresis). As observed in Fig. 19a, the lowest and greatest discharge magnitude unsteady flow events of Series A

had relatively small t_{lag} -values. Runs A1 (lowest magnitude of unsteady flow event) and A4 (greater magnitude of unsteady flow event) had small values of t_{lag} (i.e., t_{lag} = 1.0 min). The "intermediate" magnitude events (i.e., Runs A2 and A3) had larger t_{lag} values, with both runs having values of t_{lag} = 4.0 min. In general, in the present experimental runs t_{lag} increased with increasing magnitude of unsteady flow event, reached a maximum at a certain point, after which it begins to decrease. This general trend in the experimental runs of Series A is displayed with a dashed line in Fig. 19a. Low magnitude unsteady flow events (Run A1) may have low t_{lag} - and $q_{sb,\exp}$ -values because bed forms grow (aggrade) between the antecedent and flood stages. Therefore, sediment is not transported out of the flume but rather, is deposited on the lee sides of the bed forms as they adjust to the change in discharge. Greater magnitude unsteady flow events (Run A4) have low t_{lag} -values but high $q_{sb,\exp}$ - values. During the early stages of the unsteady event, the amount of sediment being entrained increases and is deposited onto antecedent stage bed forms, causing an increase in average bed form height. As the unsteady event approaches t_r , the bed forms degrade as the bed adjusts to the hydraulic conditions and the amount of sediment being transported out of the flume increases. This results in an almost flat bed and a low t_{lag} -values as t_s occurs closer to t_r .

In Series B, while the relative magnitude of the unsteady flow event was constant in all runs, the value of t_{lag} varied from run to run. As shown in Table 10 and observed in Fig. 19b, t_{lag} increased for increasing duration of flood stage. A dashed line is included in Fig 19b to display this trend. This finding is expected considering the fact that the time-to-peak sediment transport rate (t_s) occurred very early in the flood stage and the duration of the flood stage was increased systematically from run to run. The value of t_r in Series B was 22.5, 25.0, 27.5, to 30.0 min, in Runs B1, B2, B3 and B4, respectively. The shorter duration event (i.e., Run B1) resulted in counter-clockwise hysteresis with a t_{lag} =-0.5 min, however, all other runs exhibited clockwise hysteresis with t_{lag} -values of 4.0, 5.5 and 6.0 min, for Runs B2, B3 and B4, respectively. The results for Series B are also included on Fig. 19a. From this figure, it is possible the displayed trend for Series A (dashed-curve) simply displaces upwards and downwards for increasing and decreasing unsteady flow event duration, respectively. Similarly, results for Series A are also included in Fig. 19b. From this figure, it is evident that there is a linearly increasing trend for the experimental runs of Series B. As the duration of the unsteady flow

event increases, the t_{lag} also increases. Generally, bed form change either displaces upwards and downwards for increasing and decreasing relative magnitude of unsteady flow event.

4.5 Concluding remarks

The main findings of this Chapter are summarized as follows:

1. The flood stage experimental specific volumetric bed load rate increases linearly with systematic increases in the magnitude of discharge above base-flow conditions of unsteady flow event hydrographs and remains relatively constant with increases in the duration of unsteady flow event hydrographs.

2. Greater magnitude and longer duration unsteady flow events emphasize clockwise hysteresis (sediment transport rate peaks prior to the hydrograph time-to-peak) in the sediment transport rates. Shorter duration events demonstrate counter-clockwise hysteresis (hydrograph peaks prior to the sediment transport rate time-to-peak) in the sediment transport rates in response to the unsteady flow event hydrograph.

3. In general, predicted specific volumetric bed load rates assuming steady flow conditions drastically under-predicts the experimental specific volumetric bed load rates actually observed during unsteady flow events. As the magnitude of the discharge of the unsteady flow event increases, the factor by which the calculated values under-predict the experimental rate also increases. As the duration of the unsteady flow event hydrograph increases, the factor by which calculated rates under-predicts experimental rates remains relatively constant.

4. A net increase in average bed form height from the antecedent stage to the end of the post-flood stage was observed in all experimental runs. During smaller magnitude events the average bed form height increased during the flood stage and decreased during the post-flood stage to follow the counter-clockwise hysteresis trend of the sediment transport rates. During larger magnitude events the average bed form height decreased during the flood stage and increased during the post-flood stage. Generally, the calculated bed form heights assuming steady flow conditions did not accurately predict the unsteady flow stage average bed form heights.

5. The average grain size of the sediment in transport during the flood-stage of the experimental runs decreased initially and then increased towards the end of the flood stage. Larger magnitude flood stage events exhibited greater emphasis in counter-clockwise hysteresis of the average grain size of the sediment in transport. The duration of the flood stage had a less pronounced effect on the average grain size of the sediment in transport in response to the unsteady flow event hydrograph.

6. Smaller and larger magnitude unsteady flow event hydrographs produced relatively small differences between the sediment transport rate and unsteady flow event hydrograph time-to-peaks, while intermediate magnitude unsteady flow event hydrographs had larger differences. This difference was also observed to increase for increasing durations of unsteady flow event hydrographs.

4.6 References

Aberle J, Nikora V, Henning M, Ettmer B, and Hentschel B. 2010. Statistical characterization of bed roughness due to bed forms: a field study in the Elbe River at Aken, Germany. *Water Resources Research* **46**(3). DOI: 10.1029/2008WR007406.

Allen JRL. 1970. Sand waves: a model of origin and internal structure. *Sedimentary Geology* **26**(4):281-328. doi:10.1016/0037-0738(80)90022-6

Bagnold RA. 1968. Deposition in the process of hydraulic transport. *Sedimentology* **10**(1):45-56.

Barrow EB, Maxwell B and Gachon P (Eds). 2004. Climate Variability and Change in Canada: Past, Present and Future. *ACSD Science Assessment Series No. 2*, Meteorological Service of Canada, Environment Canada, Toronto, Ontario, 114p.

Binns AD, da Silva AMF. 2009. On the quantification of the bed development time of alluvial meandering streams. *Journal of Hydraulic Engineering* **137**(5):350-360.

Binns AD, da Silva AMF. 2015. Meandering bed development time: formulation and related experimental testing. *Advances in Water Resources* **81**:152-160.

Bombar G, Elci S, Tayfur G, Guney SM and Bor A. 2011. Experimental and numerical investigation of bed-load transport under unsteady flows. *Journal of Hydraulic Engineering* **137**:1276-1282. DOI: 10.1061/(ASCE)HY.1943-7900.0000412

Brooks GR, Evans SG and Clague JJ. 2001. Flooding: A Synthesis of Natural Geological Hazards in Canada. *Geological Survey of Canada Bulletin* **548**:101-143

Dankers R and Feyan L. 2009. Flood hazard in Europe in an ensemble of regional climate scenarios. *Journal of Geophysical Research: Atmospheres* **114**(D16). DOI: 10.1029/2008JD011523

Engelund F and Hansen E. 1967. A monograph on sediment transport in alluvial streams. Technical University of Denmark. Teknisk Forlag. Copenhagen, Denmark.

Fredsoe J. 1982. Shape and dimensions of stationary dunes in rivers. *Journal of the Hydraulics Division* **108**(8):932-947.

Guney MS, Bombar G and Aksoy AO. 2013. Experimental study of coarse surface development effect on the bimodal bed-load transport under unsteady flow conditions. *Journal of Hydraulic Engineering* **139**(1):12-21. DOI: 10.1061/(ASCE)HY.1943-7900.0000640.

Hassan MA, Egozi R and Parker G. 2006. Experiments on the effect of hydrograph characteristics on vertical grain sorting in gravel bed rivers. *Water Resources Research* **42**(9):W09408. DOI: 10.1029/2005WR004707.

Hirabayashi Y, Mahendran R, Koirala S, Konoshima L, Yamazaki D, Watanabe S, Kanae S. 2013. Global flood risk under climate change. *Nature Climate Change* **3**(9):816–821. DOI:10.1038/nclimate1911.

Humphries R, Venditti JG, Sklar LS and Wooster JK. 2012. Experimental evidence for the effect of hydrographs on sediment pulse dynamics in gravel-bedded rivers. *Water Resources Research* **48**:1-15. DOI: 10.1029/2011WR010419.

Intergovernmental Panel on Climate Change. 2014. Climate change 2014: impacts, adaptation, and vulnerability. Cambridge University Press, Cambridge, United Kingdom and New York, NY, USA, 1-32.

Julien PY and Klassen G. 1995. Sand-dune geometry of large rivers during floods. *Journal of Hydraulic Engineering* **121**:657-663.

Kleinhans MG, Wilbers AWE and Ten Brinke WBM. 2007. Opposite hysteresis of sand and gravel transport upstream and downstream of a birfurcation during a flood in the River Rhine, the Netherlands. *Netherlands Journal of Geosciences* **86**(3):273-285.

Labat, D., Godd, Y., Probst, J. L., & Guyot, J. L. (2004). Evidence for global runoff increase related to climate warming. Advances in water resources, 27(6), 631–642.

Lee KT, Liu YL, and Cheng KH. 2004. Experimental investigation of bedload transport processes under unsteady flow conditions. *Hydrological Processes* **18**(13):2439-2454. DOI: 10.1002/hyp.1473

Mao L. 2012. The effect of hydrographs on bed load transport and bed sediment spatial arrangement. *Journal of Geophysical Research* **117**:F03024. DOI:10.1029/2012JF002428

Marsooli R and Wu W. 2014. 3-D finite-volume model of dam-break flow over uneven beds based on VOF method. *Advances in Water Resources* **70**:104-117. DOI:10.1016/j.advwatres.2014.04.020

Meyer-Peter E and Müller R. 1949. Formula for bed load transport. Proc 2nd Meeting IAHR 6.

Paasche O and Storen EWN. 2014. How does climate impact floods? Closing the knowledge gap. *Eos Transactions American Geophysical Union* **95**(28):253-254.

Sun J, Lin B, Yang H. 2015. Development and application of a braided river model with non-uniform sediment transport. *Advances in Water Resources* **81**:62-72. DOI:10.1016/j.advwatres.2014.12.012

van Rijn. 1984. Sediment transport part I: bed load transport. Journal of Hydraulic Engineering **110**(10):1431-1456.

Xenopoulos MA, Lodge DM, Alcamo J, Marker M, Schulze K, and Van Vuuren PD. 2005. *Scenarios of freshwater fish extinctions from climate change and water withdrawl* 11(10):1557-1564.

Yalin MS. 1963. An expression for bed load transport. *Journal of Hydraulics Division* **89**(3):221-250.

Yalin MS. 1985. On the determination of ripple geometry. *Journal of Hydraulic Engineering* **111**(8):1148-1155.

Yalin MS and da Silva AMF. 2001. Fluvial Processes. IAHR Monograph. IAHR. Delft, The Netherlands, 197 pages.

Chapter 5

5 Quantification of stream bed morphological response to variation in hydrograph shape

5.1 Introduction

Stream bed morphology develops and subsequently adjusts with the natural hydraulic regime. The projected global mean temperature change is suspected to produce unprecedented changes in global hydrologic regimes (Intergovernmental Panel on Climate Change, 2014) and, depending on region, may cause an increase in flooding (Hirabayashi et al., 2013). These climatic changes have resulted in alterations to the annual maximum and mean daily flow patterns in Canadian rivers (Whitfield and Cannon, 2000; Lemmen et al., 2008). Recent efforts to establish a relationship between the variables of climate, hydrology and hydraulics have been made (i.e., Burn and Elnur, 2002; Yue et al., 2003; Boyer et al., 2010; Burn and Whitfield, 2015), however, exact trends of these complex variables have not yet been produced. Considerable evidence shows a shift in the timing of the peak flow events with spring peak flow occurring earlier (Brooks et al., 2001; IPCC, 2014). These changes result in unsteady flow events in rivers and streams, and as a result, can alter the morphodynamic conditions in rivers.

River management and engineering measures are required in order to protect infrastructure and manage flows in response to changing climatic conditions (Ritcher and Thomas, 2007). As discussed previously in this thesis, these practices use predictive equations based on steady, two-dimensional flow in a straight channel to determine the sediment transport rates. Over the last few decades, there has been an increase in the number of studies seeking to establish a relationship between sediment transport rates and bed morphology in reponse to unsteady flow events. Several studies (De Sutter et al., 2001; Lee et al., 2004; Ahanger et al., 2008; Bombar et al., 2011; Nelson et al. 2011; Martin and Jerolmack, 2013) have simulated unsteady flow events in a laboratory setting using a variety of shaped hydrographs over sand beds. These researchers have manipulated the shape of the hydrograph (e..g., trapezoidal, triangular, etc) in order to simulate varying climatic influences on the discharge. General conclusions from these studies suggest that changes in the sediment transport rates and bed forms have a lag-in-time (hysteresis) in relation to the unsteady flow event hydrograph.

To date, no systematic effort has been made to quantify of the effect the hydrograph shape of the unsteady flow event on the sediment transport rates and bed morphological adjustments. Building

upon the recommendations and strategic opportunities outlined in Chapter 3 and the experimental research presented in Chapter 4, this Chapter investigates the relationship between hydrograph shape (i.e., time to the peak flow of the hydrograph) on stream bed morphodynamics. A series of experimental laboratory runs with systematically-designed stepped hydrographs that vary the time-to-peak flow are conducted. Results will quantify the geometric changes of bed forms and the hysteretic behaviour of the sediment transport rates in response to these stepped hydrographs.

5.2 Experimental set-up and hydraulic conditions of the runs

5.2.1 Laboratory set-up

The laboratory set-up for these experimental runs is as described in Section 4.1.1.

5.2.2 Experimental procedure

In order to satisfy the goal of this Chapter and build on the results from Chapter 4 where the effect of the magnitude and duration of unsteady flow event hydrographs was investigated, a new series of experimental runs (Series C), was designed. The experimental runs of Series C contained three step-change flood hydrographs, with each including five different stages: antecedent conditions (base-flow), unsteady event (b) (flood stage), unsteady event (c) (flood stage), unsteady event (d) (flood stage), and post-flood conditions (return to antecedent conditions). Each of the three flood stages ((b), (c) and (d)) lasted 5 min. The three flood stages were varied in magnitude in order to create systematic changes in the time-to-peak (skewness) of the unsteady flow events hydrographs. A schematic of the structure of the unsteady flow event hydrographs for these runs is seen in Fig. 21. The remaining details of the experimental procedure was nearly identical to that described in Section 4.1.2 and 4.2.2. However, in Series C bed elevation data was collected at the end of antecedent conditions, each of the three flood stages and the post-flood stage. Similar to Chapter 4, each experimental run was repeated three times and the reported specific volumetric bed load transport rates are averaged values. The standard deviation for the reported specific volumetric bed load transport rates for each experimental time step in each run of Series C can be seen in Appendix L.

a)

20 min	5 min	5 min	5min	30 min
BF	1.50 x *BF*	1.25 x *BF*	1.25 x *BF*	*BF*
antecedent	flood b	flood c	flood d	post-flood

b)

20 min	5 min	5 min	5 min	30 min
BF	1.25 x *BF*	1.50 x *BF*	1.25 x *BF*	*BF*
antecedent	flood b	flood c	flood d	post-flood

c)

20 min	5 min	5 min	5 min	30 min
BF	1.25 x *BF*	1.25 x *BF*	1.50 x *BF*	*BF*
antecedent	flood b	flood c	flood d	post-flood

Figure 20: Schematic of unsteady flow event hydrograph structure of Series C experimental runs: a) Run C1; b) Run C2; and c) Run C3

5.2.3 Hydraulic conditions of runs

The hydraulic conditions of the experimental runs of Series C are seen in Table 11. This table describes the experimental stage, discharge (Q), average flow depth (h_{av}), longitudinal bed slope (S), channel-averaged flow velocity (u_{av}), shear velocity (v_*), width-to-depth ratio $\left(\frac{B}{h_{av}}\right)$, relative depth $\left(\frac{h_{av}}{D}\right)$, channel-averaged Chézy resistance factor $\left(c_f\right)_{av}$, Reynolds number (R), Froude number (Fr), roughness Reynolds number (R_*), relative flow intensity (η_*), sediment mobility number (Y), critical mobility number (Y_{cr}), average specific volumetric bed-load rate $\left(q_{sb,\exp}\right)_{avg}$, and duration of each experimental stage (see Section 2.1 to 2.3 for a definition of these quantities). Hydraulic conditions

were selected so as to ensure that only bed load occurs during each stage of every experimental run. The flow is considered to be in the transitional regime of turbulent flow. The critical mobility number (Y_{cr}) associated with the D_{50} is 0.0365. During all experimental runs, the value of the mobility number (Y) varied from approximately 0.085 to 0.1123 and the η_*-value varied from 2.33 to 3.08. The average discharge of the antecedent stage of all three experimental runs was 0.006 m^3/s. The average discharge of the post-flood stage of all experimental runs was 0.006 m^3/s. The average flow depth (h_{av}) during the antecedent stage and post-flood stage of all runs was 5.08 cm (+/- 6%) and 5.43 cm ($^{+}/_{-}$ 4%), respectively.

Both the average discharge and flow depth of the flood stages varied from run to run in order to investigate the effect of variation in hydrograph shape of unsteady flow events (e.g., time-to-peak flow) on bed morphology and sediment transport rates. The average values for these quantities are displayed in Table 11. The time-to-peak flow (t_r) for the experimental runs of Series C were 22.5, 27.5 and 32.5 min for Runs C1, C2 and C3, respectively. As previously mentioned, the flood stages in Series C contained three steps made up of peak and intermediate stages. In each run the peak discharge stage had a magnitude of 1.50 times greater than base-flow conditions and the intermediate stages had a discharge of 1.25 times greater than base-flow conditions.

Table 11: Hydraulic conditions of experimental runs in Series C

Run	Phase	Q [m^3/s]	h_{av} [cm]	S	u_{av} [m/s]	v^* [m/s]	B/h_{av}	h_{av}/D_{50}	$(cf)_{av}$	R	Fr	R^*	η^* (= Y/Y_{cr})	$(q_{sb,exp})_{avg}$ [m^2/s]	Duration [min]
C1	*i*	-	-	0.001	-	-	-	-	-	-	-	-	-	-	-
	a	0.006	4.73	0.001	0.3883	0.0215	6.6	131.3	18.0	18347	0.57	15.5	2.33	5.390E-06	20
	b	0.009	6.22	0.001	0.4415	0.0247	5.0	172.8	17.9	27462	0.57	17.8	2.87	1.424E-05	5
	c	0.007	5.89	0.001	0.3950	0.0240	5.3	163.5	16.4	23247	0.52	17.3	2.71	7.101E-06	5
	d	0.007	5.71	0.001	0.4069	0.0237	5.4	158.6	17.2	23237	0.54	17.0	2.63	7.591E-06	5
	pf	0.006	5.63	0.001	0.3129	0.0235	5.5	156.3	13.3	17608	0.42	16.9	2.59	4.163E-06	30
C2	*i*	-	-	0.001	-	-	-	-	-	-	-	-	-	-	-
	a	0.006	5.34	0.001	0.3551	0.0229	5.8	148.3	15.5	18952	0.49	16.5	2.46	9.098E-06	20
	b	0.007	6.15	0.001	0.3904	0.0246	5.0	170.8	15.9	24011	0.50	17.7	2.83	6.450E-06	5
	c	0.009	6.62	0.001	0.4568	0.0255	4.7	183.8	17.9	30215	0.57	18.3	3.05	9.920E-06	5
	d	0.007	6.08	0.001	0.3885	0.0244	5.1	168.9	15.9	23624	0.50	17.6	2.80	5.054E-06	5
	pf	0.006	5.14	0.001	0.3550	0.0225	6.0	142.7	15.8	18240	0.50	16.2	2.36	4.506E-06	30
C3	*i*	-	-	0.001	-	-	-	-	-	-	-	-	-	-	-
	a	0.006	5.16	0.001	0.3663	0.0225	6.0	143.4	16.3	18911	0.51	16.2	2.38	6.657E-06	20
	b	0.007	5.80	0.001	0.3930	0.0239	5.3	161.1	16.5	22796	0.52	17.2	2.67	6.383E-06	5
	c	0.007	5.90	0.001	0.3856	0.0240	5.3	163.8	16.0	22731	0.51	17.3	2.72	4.282E-06	5
	d	0.010	6.68	0.001	0.4753	0.0256	4.6	185.6	18.6	31753	0.59	18.4	3.08	10.310E-06	5
	pf	0.006	5.52	0.001	0.3391	0.0233	5.6	153.2	14.6	18699	0.46	16.7	2.54	5.666E-06	30

5.3 Experimental observations and results

5.3.1 General

This section presents and discusses the results from the experimental runs. The antecedent conditions (which were similar in all runs) are first discussed. The results of the experimental runs of Series C are first discussed separately and then together in order to discuss observed trends in this series of runs.

As presented in Chapter 4, this section will present observations of experimental results for Series C in the form of bed elevation contour-plots, sediment transport profiles and plots of the variation of D_{50} of the transported sediment in response to the unsteady flow event hydrographs. Refer to Section 4.3.1 for complete details of the bed load sediment transport and bed form geometry equations. The calculated specific volumetric bed load transport rates for each experimental time step can be seen in Appendix M.

5.3.2 Antecedent conditions

The antecedent stage for all three experimental runs contained a base-flow discharge of approximately 0.006 m^3/s for a duration of 20 min. This stage included measurement time-steps every 5 min to allow for collection of the bed load transport data. The antecedent conditions in Runs C1, C2 and C3 all demonstrated similar trends in the sediment transport rates, variation of D_{50} of the sediment in transport, and bed form development. Similar to the experimental runs of Series A and B (presented in Chapter 4), antecedent hydraulic conditions during all three experimental runs of Series C were selected to ensure equilibrium sediment transport rates $q_{sb,\exp}$ (experimental specific volumetric bed load rate) and bed form geometry were established. Sediment transport rates during the antecedent stage were relatively variable but generally, $q_{sb,\exp}$ showed a decreasing trend during the 20 min period. $q_{sb,\exp}$ was relatively large at the earlier time-steps due to the initial displacement of sediment as the bed adjusts from its flat initial state. By the end of the 20 min antecedent period, $q_{sb,\exp}$ approached the predicted $q_{sb,calc}$-value (calculated specific volumetric bed load rate). During the antecedent stage of all three experimental runs in Series C $\left(q_{sb,\exp}\right)_{avg}$ was 7.05×10^{-6} m^2/s.

Equilibrium conditions were also observed in the D_{50}-value of the sediment in transport. The D_{50} of the sediment in transport fluctuated between 0.35 and 0.36 mm. By the end of the 20 min antecedent period, the D_{50}-value reached 0.36 mm. Fig.17 shows that during a steady flow preliminary experimental run with a duration of 70 min the D_{50} of the sediment in transport constantly fluctuates between 0.35 and 0.36 mm. Based on this, after the 20 min antecedent stage during the experimental runs of Series C, the D_{50} of the sediment in transport reached an approximate equilibrium with the base-flow conditions.

Partially formed ripples developed in the bed in all experimental runs within the first 5 min of the antecedent stage. Over the remaining 15 min, the ripples merged into dunes as newer ripples superimposed themselves on top of the larger bed forms. By the end of the 20 min antecedent stage, the bed forms reached equilibrium conditions as the bed became dominated by dunes of relatively consistent and stable geometry (i.e., stable bed form height $\Delta_{avg,\exp}$). Generally, the average bed form height $\Delta_{avg,\exp}$ reached the predicted calculated values by the end of the 20 min antecedent period. The average bed form height $\Delta_{avg,\exp}$ during the antecedent stage of all three experimental runs in Series C was 0.73 cm.

5.3.3 Series C results

This Section describes the trends and response of $q_{sb,\exp}$, $\Delta_{avg,\exp}$ and D_{50} of the sediment transport rate for the three experimental runs of Series C. These values will be compared to the predicted $q_{sb,calc}$- and $\Delta_{avg,calc}$-values calculated using traditional equations assuming steady flow conditions. Consistent with the discussion in Chapter 4, the bed-load transport equation of Meyer-Peter and Müller (1949) was used to determine $q_{sb,calc}$ (see Section 4.3.1 for a discussion of this). Due to the presence of bed forms, $q_{sb,calc}$-values were modified by considering the additional resistance to flow resulting from the bed forms. The equations take into account the resistance to flow due to the presence of bed forms are described in Chapter 2.

The average bed form heights ($\Delta_{avg,\exp}$) were calculated using expressions due to Yalin (1972; 1985) for ripples and dunes assuming steady flow conditions. These equations are summarized

in Section 2.2. The results of $\Delta_{avg,calc}$ for ripples and dunes were averaged to give an approximate size of possible bed forms present during the prescribed hydraulic conditions. The process of averaging the results give an accurate estimate of the size of bed forms throughout each experimental time-step. For example, during the antecedent condition, $\Delta_{avg,\exp}$-values reported were an average of bed form geometry over the entire stage, meaning that both the initial ripple formations that occurred within the first 5 min of experimentation and the dunes that were fully developed by the end of the 20 min stage are considered. Similarly, measurements of $\Delta_{avg,\exp}$ for all the flood stage time-steps were averaged over this stage to give an accurate representation of the bed form degradation or aggradation that occurred throughout the duration of the unsteady stage.

5.3.3.1 Run C1

Run C1 contained a total flood stage of 15 min in duration. The flood stage was composed of three flood stages ((b), (c) and (d)). Flood stage (b) lasted for 5 min and had a discharge magnitude 1.50 times greater than the antecedent conditions while flood stages (c) and (d) each lasted had a discharge magnitude 1.25 times greater than the antecedent conditions (see Fig. 20). This unsteady flow event represents an asymmetrical hydrograph. The hydrograph time-to-peak (t_r) occurred within the first flood stage (b) at 22.5 min Fig. 21 shows the bed elevation contour-plots for Run C1. This figure shows the bed morphology at the end of the antecedent stage (a), the end of the first flood stage (b), the end of the second flood stage (c), the end of the third flood stage (d), and the end of the post-flood stage (pf). The antecedent stage shows approximately uniform bed forms that have reached equilibrium with the steady hydraulic conditions. Flood stage (b) displays much fewer and more spread out bed forms. Flood stages (c) and (d) show slightly more bed forms than flood stage (b) and a few regions of aggradation. During the post-flood stage, the bed forms are slightly larger in comparison to the antecedent stage, but there is a similar spacing of bed forms to the antecedent stage.

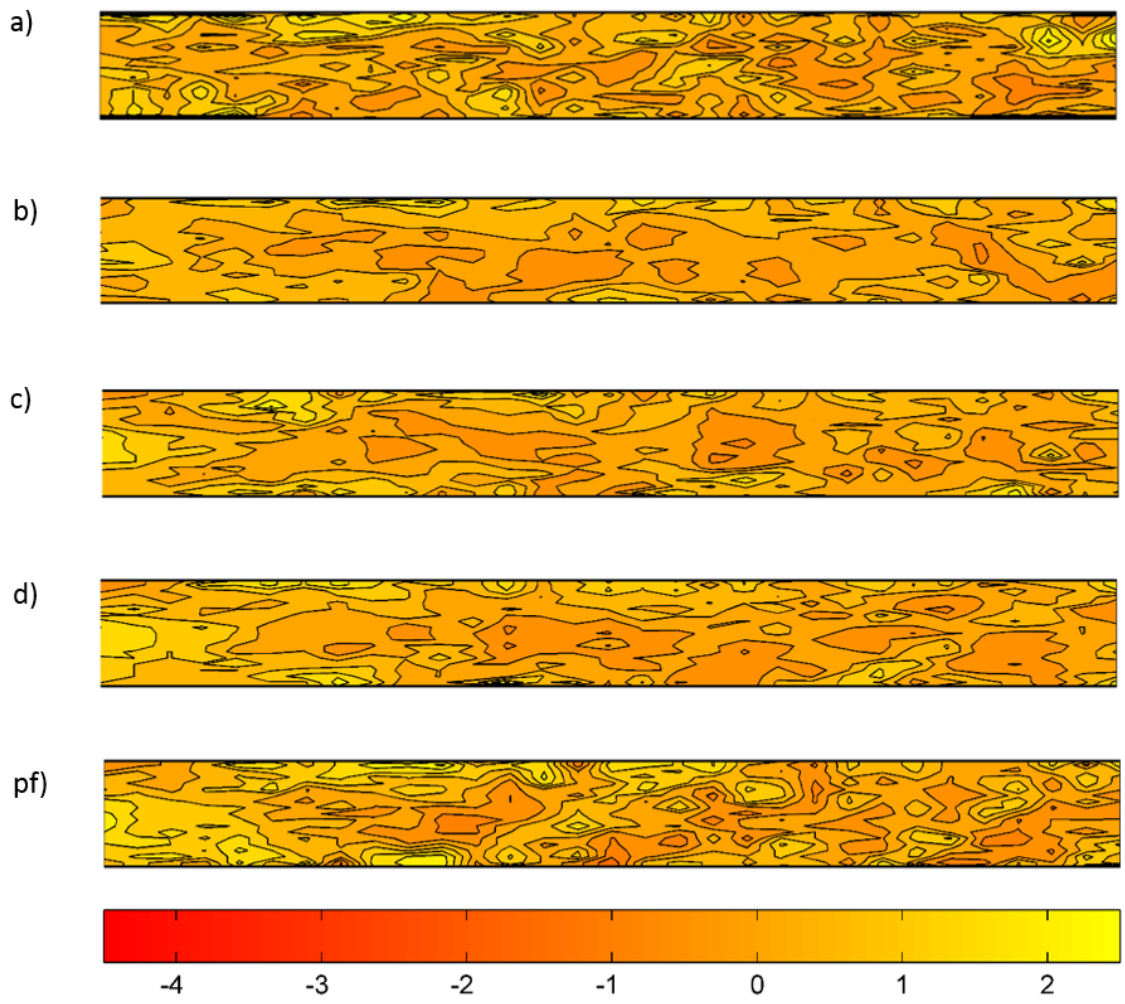

Figure 21: Bed elevation contour-plots for Run C1 (showing change in bed elevation from initial flat-bed conditions): antecedent (a); flood b (b); flood c (c); flood d (d); and post-flood (pf) stages [all values in cm]

Fig. 22a presents the sediment transport and discharge profiles for the entire duration of Run C1. While t_r occurred within the first flood stage at 22.5 min, the sediment time-to-peak (t_s) occurred at 21 min. t_s peaking before t_r suggests that clockwise hysteresis occurred in the sediment transport rates. After t_s occurred at 21 min, $q_{sb,\exp}$ gradually decreased until 25 min. A significant decrease in $q_{sb,\exp}$ occurred at 26 min. Between 27 and 35 min (the rest of the two flood stages c and d), $q_{sb,\exp}$ was observed to fluctuate slightly. During the post-flood stage $q_{sb,\exp}$ remained relatively stable. $\left(q_{sb,\exp}\right)_{avg}$ was 1.42x10^{-5} m^2/s, 7.10x10^{-6} m^2/s and 7.59x10^{-6}

m^2/s for flood stages (b), (c) and (d), respectively. The post-flood $\left(q_{sb,\exp}\right)_{avg}$ was $4.16x10^{-6}$ m^2/s. The antecedent stage value of $q_{sb,\exp}$ approached the predicted $q_{sb,calc}$-value by the end of the 20 min antecedent period. During flood stage (b), $q_{sb,calc}$ was 1.32 times greater than the corresponding predicted value for antecedent conditions while $q_{sb,\exp}$ was 3.27 times greater than the corresponding measured value for antecedent conditions. During flood stage (c), $q_{sb,calc}$ was 1.42 times greater than the corresponding predicted value for antecedent conditions while $q_{sb,\exp}$ was 1.66 times greater than the corresponding measured value for antecedent conditions. In the final flood stage (d), $q_{sb,calc}$ was 1.36 times greater than the corresponding predicted value for antecedent conditions and $q_{sb,\exp}$ was 1.63 times greater than the corresponding measured value for antecedent conditions.

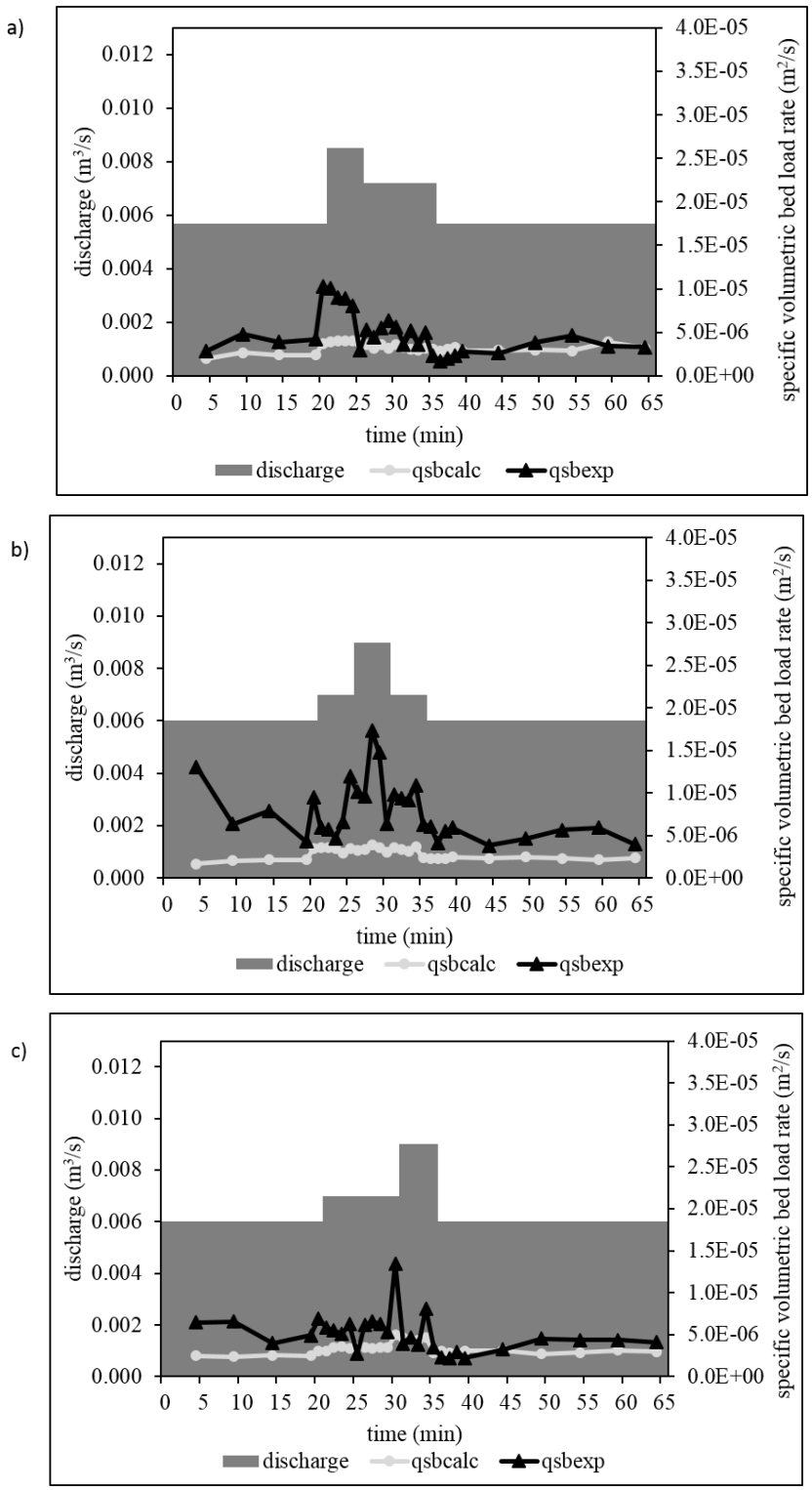

Figure 22: Sediment transport and discharge profiles for experimental runs in Series C: a) Run C1; b) Run C2; and c) Run C3

The measured average bed form height $\Delta_{avg,\exp}$ for each experimental stage and the percent change in average bed form height between each experimental stage are displayed in Table 13. The calculated (predicted) $\Delta_{avg,calc}$-value for each stage and the percent change in average bed form height between each experimental stage are displayed in Table 14. At the end of antecedent conditions $\Delta_{avg,\exp}$ was measured to be 0.82 cm. During the first flood stage (b), there was a 12% decrease in average bed form height as $\Delta_{avg,\exp}$ decreased to 0.72 cm by the end of the first flood stage. As the magnitude of the flood event decreased, $\Delta_{avg,\exp}$ increased by 18% as $\Delta_{avg,\exp}$ grew to 0.85 cm by the end of the second flood stage (c). During the final flood stage (d), the discharge was identical to that in second flood stage (c), but $\Delta_{avg,\exp}$ decreased by 27% to give a $\Delta_{avg,\exp}$-value of 0.62 cm at the end of this stage. During the post-flood stage, $\Delta_{avg,\exp}$ increased by 32% to reach 0.82 cm in height. There was no net change of $\Delta_{avg,\exp}$ from the end of antecedent to the end of the post-flood stages. The predicted value of $\Delta_{avg,calc}$ during the antecedent stage was slightly larger than $\Delta_{avg,\exp}$ ($\Delta_{avg,calc}$ = 0.94 cm). During the first flood stage (b) when the discharge was increased by 1.50 times antecedent conditions $\Delta_{avg,calc}$ increased by 71% to give $\Delta_{avg,calc}$ = 1.61 cm. $\Delta_{avg,calc}$ decreased by 11% by the end of the second flood stage (c) to give $\Delta_{avg,calc}$ = 1.43 cm. During the third flood stage (d) the average bed form height decreased by 7% to give $\Delta_{avg,calc}$ = 1.33 cm. The post-flood stage bed forms decreased by 17% to give $\Delta_{avg,calc}$ = 1.13 cm. Overall, there was a predicted increase in average bed form height of 17% from the end of the antecedent stage to the end of the post-flood stage, which was in contrast to what was observed experimentally.

Table 12: Measured average bed form height (cm) for each hydrograph stage and percent change in average bed form height between hydrograph stages for the experimental runs of Series C

	Average bed form height (cm)					Change in average bed form height (%)				
Run	**a**	**b**	**c**	**d**	**pf**	**a to b**	**b to c**	**c to d**	**d to pf**	**a to pf**
C1	0.82	0.72	0.85	0.62	0.82	-12	+18	-27	+32	0
C2	0.68	0.73	0.62	0.77	0.56	+7	-15	+24	-37	-18
C3	0.69	0.78	0.75	0.76	0.79	+13	-4	+1	+4	+14

Table 13: Calculated average bed form height (cm) for each hydrograph stage and percent change in average bed form height between hydrograph stages for the experimental runs of Series C

	Average bed form height (cm)					Change in average bed form height (%)				
Run	**a**	**b**	**c**	**d**	**pf**	**a to b**	**b to c**	**c to d**	**d to pf**	**a to pf**
C1	0.94	1.61	1.43	1.33	1.13	+71	-11	-7	+17	+17
C2	1.14	1.61	1.86	1.52	1.04	+41	+16	-18	-32	-9
C3	1.13	1.42	1.43	1.86	1.23	+26	+1	+30	-34	-8

A sieve analysis of the sediment in transport collected during each experimental time-step was performed to examine changes in the grain size composition of the sediment in transport during the run. The variation with time of the D_{50}-value of the sediment in transport over the entire duration of Run C1 is seen in Fig. 23a. A minimum D_{50} of 0.34 mm was reached at 21 and 22 min. The D_{50} of the sediment in transport returned to 0.36 mm by t = 25 min where it remained until t = 30 min. At 31 min the D_{50} of the sediment in transport decreased to 0.35 mm but returned to 0.36 mm from 32 to 33 min. Again, the D_{50} of the sediment in transport decreased to 0.35 mm at 34 and 35 min. This means that within the first flood stage (b), the D_{50} of the sediment in transport exhibited counter-clockwise hysteresis. The same type of hysteresis, but less pronounced, was demonstrated during the third flood stage (d). The D_{50} of the sediment in transport fluctuated between 0.35 and 0.36 mm during the post-flood stage.

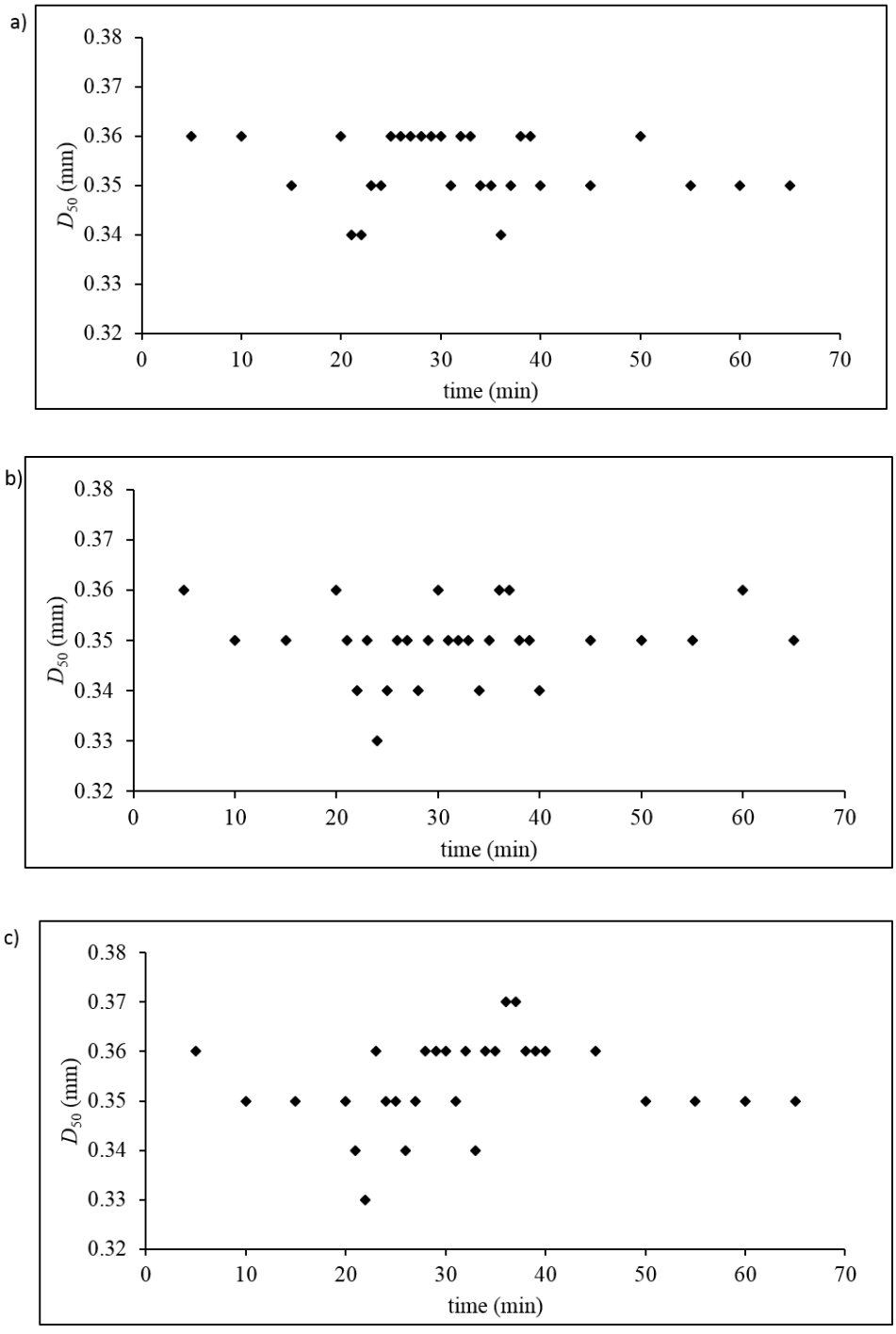

Figure 23: D_{50}-value versus time for the sediment in transport during: a) Run C1; b) Run C2; and c) Run C3

5.3.3.2 Run C2

Run C2 contained a total flood stage of 15 min in duration. The flood stage lasted for a total of 15 min and was composed of three flood stages ((b), (c) and (d)). As shown in Fig. 20, flood stage (b) and (d) each lasted for 5 min and had discharge magnitudes of 1.25 times greater than the antecedent stage. Flood stage (c) lasted for 5 min and had a discharge magnitude of 1.50 times greater than the antecedent stage. Hence this unsteady flow event represents a symmetrical hydrograph. Considering this, the hydrograph time-to-peak flow (t_r) occurred at 27.5 min (during flood stage (c)). Fig. 24 shows the bed elevation contour-plots for Run C2. Generally, at the end of the antecedent stage (a), the contour-plots show approximately uniform bed forms that have reached equilibrium with the hydraulic conditions. During flood stage (b), the bed forms appeared to be more sparsely distributed along the length of the flume, but were slightly larger in size in comparison to the antecedent stage. Flood stage (c) showed a similar distribution of bed forms to flood stage (b), but the bed form heights decreased slightly. In flood stage (d), the bed form heights increased substantially. During the post-flood stage, the bed forms developed more evenly across the bed, and the bed form heights were smaller in comparison to the flood stages.

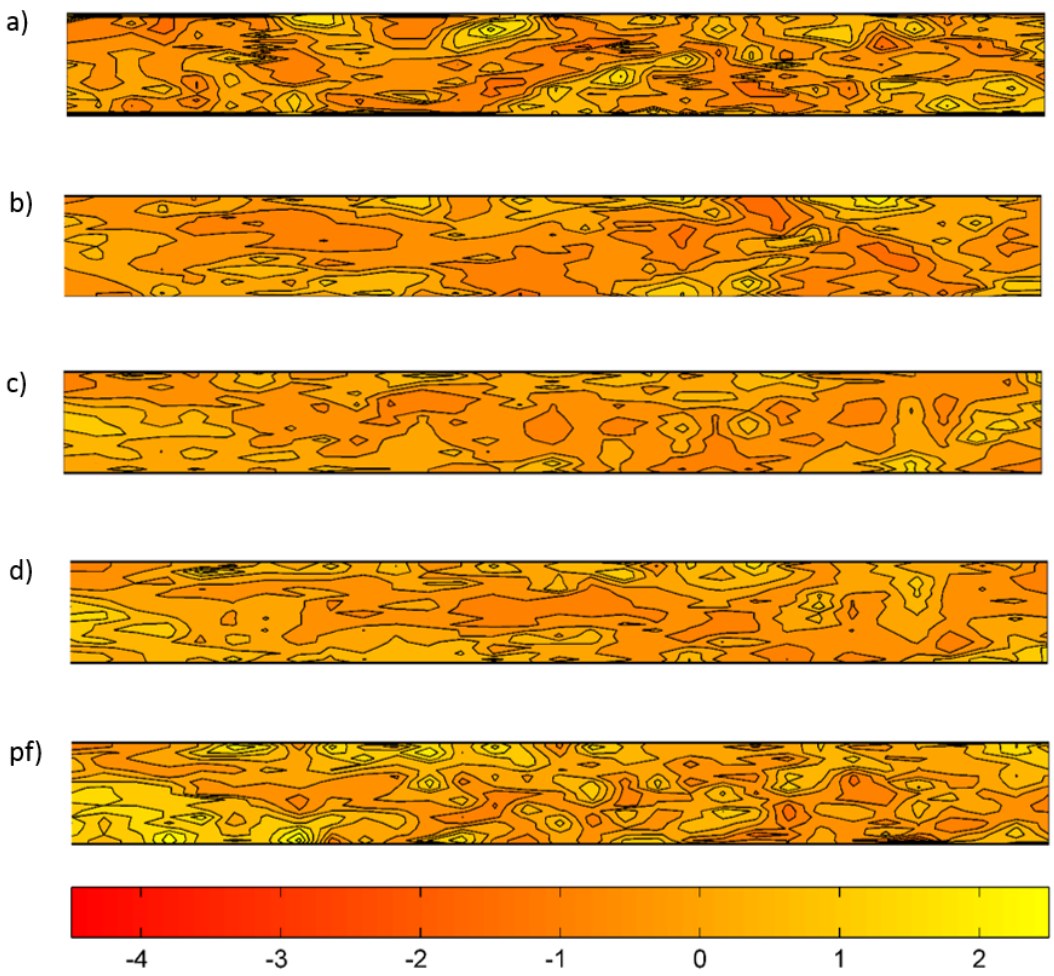

Figure 24: Bed elevation contour-plots for Run C2 (showing change in bed elevation from initial flat-bed conditions): antecedent (a); flood b (b); flood c (c); flood d (d); and post-flood (pf) stages [all values in cm].

Fig. 22b presents the sediment transport and discharge profiles for the entire duration of Run C2. While t_r occurred at 27.5 min (during flood stage (c)), t_s occurred at 29 min (during flood stage (d)). This represented counter-clockwise hysteresis since t_s occurred after t_r. Two $q_{sb,\exp}$ peaks at t = 21 and 26 min occurred prior to t_s being reached. After t_s was reached, $q_{sb,\exp}$ peaked considerably again at 35 min. During the post-flood stage $q_{sb,\exp}$ was relatively stable with the exception of an observed decrease which occurred at 45 min. $\left(q_{sb,\exp}\right)_{avg}$ was $6.450\text{x}10^{-6}$ m^2/s, $9.920\text{x}10^{-06}$ m^2/s and $5.050\text{x}10^{-6}$ m^2/s for flood stages (b), (c) and (d), respectively. $\left(q_{sb,\exp}\right)_{avg}$ for the post-flood stage was $4.510\text{x}10^{-6}$ m^2/s. The antecedent value of

$q_{sb,\exp}$ approached the predicted $q_{sb,calc}$-value at the end of the 20 min antecedent stage. $q_{sb,\exp}$ in flood stage (b) was 1.65 times greater than the corresponding $q_{sb,\exp}$-value in the antecedent stage; $q_{sb,\exp}$ in flood stage (c) was found to be 3.13 times greater than the corresponding $q_{sb,\exp}$ -value in the antecedent stage; and $q_{sb,\exp}$ in flood stage (d) was 2.01 times greater than the corresponding $q_{sb,\exp}$-value in the antecedent stage. The predicted $q_{sb,calc}$-values in flood stages (b), (c) and (d) were predicted to be 1.53, 1.67 and 1.56 times greater than the antecedent stage value, respectively.

The measured average bed form height $\Delta_{avg,\exp}$ for each experimental stage of Run C2 and the percent change in average bed form height between each experimental stage are seen in Table 12. The predicted $\Delta_{avg,calc}$-values for each stage and the percent change between each stage are seen in Table 13. By the end of the 20 min antecedent period, $\Delta_{avg,\exp}$ was 0.68 cm. There was a 7% increase in average bed form height by the end of flood stage (b) to give $\Delta_{avg,\exp}$ = 0.73 cm. There was a decrease in average bed form height of 15% to give a $\Delta_{avg,\exp}$ = 0.62 cm at the end of flood stage (c). From flood stage (c) to flood stage (d) there was a 24% increase in $\Delta_{avg,\exp}$ to give a $\Delta_{avg,\exp}$-value of 0.77 cm by the end of flood stage (d). At the end of the post-flood stage there was a 37% decrease in average bed form height to give $\Delta_{avg,\exp}$ = 0.56 cm by the end of the run. Overall, from the end of the antecedent stage to the end of the post-flood stage there was a net decrease in $\Delta_{avg,\exp}$ of 18%. The predicted $\Delta_{avg,calc}$-value was found to be larger than the measured $\Delta_{avg,\exp}$-values at the end of the antecedent stage ($\Delta_{avg,calc}$ = 1.14 cm). $\Delta_{avg,calc}$ increased by 41% by the end of flood stage (b) to give $\Delta_{avg,calc}$ = 1.61 cm, a similar increasing trend to what was observed experimentally. From flood stage (b) to flood stage (c) there was a 16% increase in average bed form height to produce $\Delta_{avg,calc}$ = 1.86 cm. This growth in bed forms was opposite to what was observed experimentally. By the end of flood stage (d) $\Delta_{avg,calc}$ decreased to 1.52 cm, representing an 18% decrease between flood stages (c) and (d). Again, this trend of decreasing bed form height was the opposite to what was observed experimentally between these stages. By the end of the post-flood stage $\Delta_{avg,calc}$ was predicted to be 1.04 cm, meaning a 32% decrease in average bed form height from flood stage (d) was

predicted. Overall, there was a net decrease in average bed form height of 9% predicted from the end of the antecedent stage to the end of the post-flood stage. This predicted net degradation of the bed geometry was also measured during the run, however, degradation that occurred during the run was twice as large as the predicted values.

The variation with time of the D_{50}-value of the sediment in transport over the entire duration of Run C2 is seen in Fig. 23b. A minimum D_{50} of 0.34 mm was reached at 24 and 34 min. The maximum D_{50} (0.36 mm) observed in all three flood stages occurred at 30 min. This represents counter-clockwise hysteresis in the D_{50}-value of the sediment in transport.

5.3.3.3 Run C3

Run C3 contained a total flood stage of 15 min in duration. As shown in Fig. 20, the flood stage and was composed of three 5 min flood stages ((b), (c) and (d)). Flood stage (b) and (c) had discharge magnitudes of 1.25 times greater than the antecedent stage. Flood stage (d) had a discharge magnitude of 1.50 times greater than the antecedent stage. Thus, this represented an asymmetrical experimental hydrograph. Considering this, the hydrograph time-to-peak flow (t_r) occurred at 32.5 min (during flood stage (d)). Fig. 25 shows the bed elevation contour-plots for Run C3. The antecedent stage contour-plot shows the bed morphology at approximate equilibrium with the hydraulic conditions. During flood stage (b), the bed forms appear slightly more spread out and larger compared to those observed in the antecedent stage. By flood stage (c), the bed forms appear slightly smaller compared to flood stage (b). By flood stage (d), the bed forms are approximately the same as those observed in flood stage (c). The end of the post-flood stage contour-plot shows bed forms larger and situated slightly closer together than in the previous four stages.

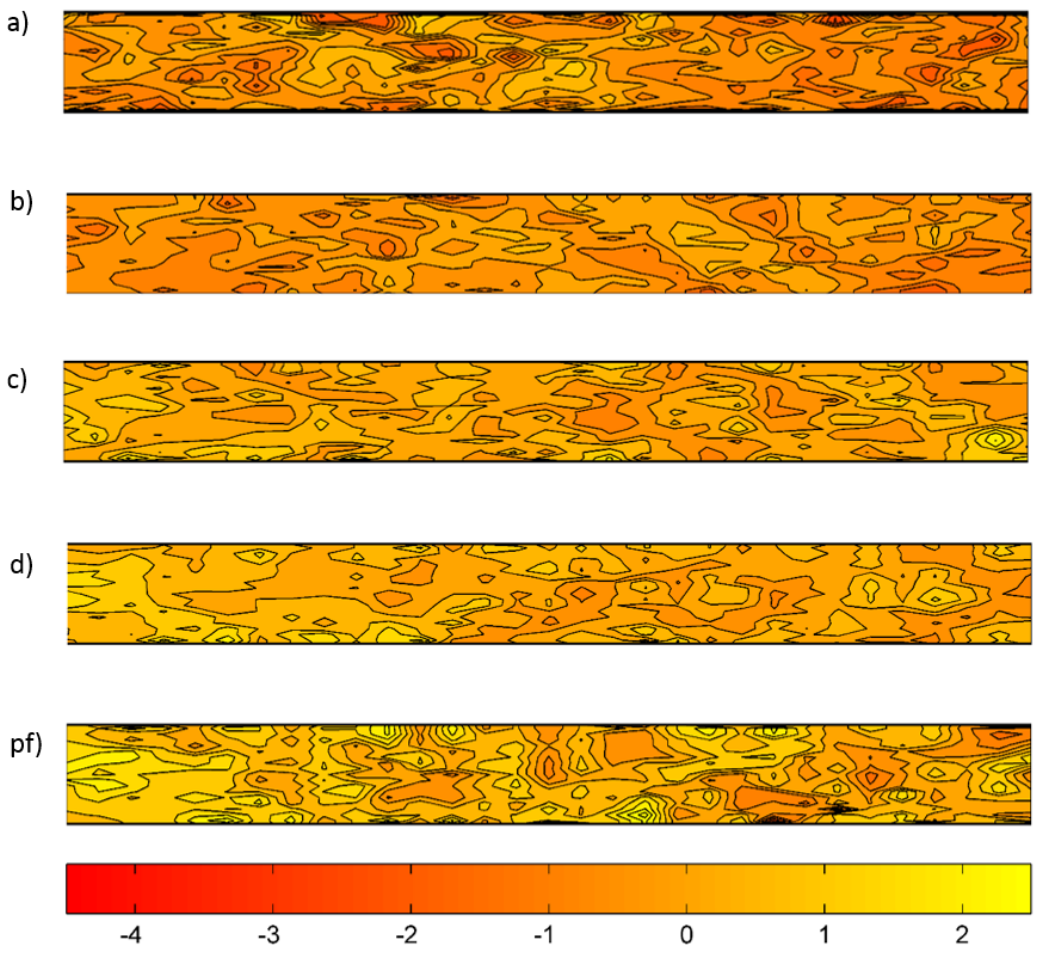

Figure 25: Bed elevation contour-plots for Run C3 (showing change in bed elevation from initial flat-bed conditions): antecedent (a); flood b (b); flood c (c); flood d (d); and post-flood (pf) stages [all values in cm].

Fig. 22c presents the sediment transport and discharge profiles for the entire duration of Run C3. While t_r occurred at 32.5 min, t_s occurred at 31 min (i.e., at the beginning of the flood stage (d)). This represents clockwise hysteresis of the sediment transport rates since t_s occurred prior to t_r. Prior to t_s being reached during flood stages (b) and (c), $q_{sb,\exp}$ fluctuated at a greater rate than that observed during the antecedent stage. Despite this finding, there was a considerable decrease in $q_{sb,\exp}$ which occurred at 26 min. After t_s was reached, $q_{sb,\exp}$ decreased until it peaked again at 35 min (end of the final flood stage). During the post-flood stage $q_{sb,\exp}$ remained relatively stable with a slight observed increase at t = 50 min. $\left(q_{sb,\exp}\right)_{avg}$ was $6.38\text{x}10^{-6}$ m^2/s, $4.28\text{x}10^{-6}$ m^2/s and $10.31\text{x}10^{-6}$ m^2/s for flood stages (b), (c) and (d),

respectively. During the post-flood stage $\left(q_{sb,\exp}\right)_{avg}$ was 5.67x10^{-6} m^2/s. The antecedent $q_{sb,\exp}$ approached the predicted $q_{sb,calc}$-value by the end of the 20 min antecedent stage. During flood stage (b), $q_{sb,calc}$ was predicted to be 1.33 times greater than the corresponding antecedent value of $q_{sb,calc}$; during flood stage (c), $q_{sb,calc}$ was predicted to be 1.38 times greater than the corresponding antecedent stage value and during flood stage (d) $q_{sb,calc}$ was predicted to be 1.84 times greater than the corresponding antecedent stage value. $q_{sb,\exp}$ during flood stage (b) was 1.52 times greater than $q_{sb,\exp}$ of the antecedent stage. While flood stage (c) had the same discharge magnitude as flood stage (b) , $q_{sb,\exp}$ was found to be only 1.16 times greater than $q_{sb,\exp}$ of the antecedent stage. This change in $q_{sb,\exp}$ is less than that observed with the predicted $q_{sb,calc}$-values. During the final flood stage (d) when the discharge magnitude was increased to be 1.50 times greater than the antecedent stage $q_{sb,\exp}$ was found to increase to 2.17 times greater than the measured $q_{sb,\exp}$-value of the antecedent stage.

The measured average bed form height $\Delta_{avg,\exp}$ for each experimental stage of Run C3 and the percent change in average bed form height between each experimental stage are seen in Table 12. The predicted $\Delta_{avg,calc}$-values for each stage and the percent change in average bed form height between each stage are seen in Table 13. By the end of the 20 min antecedent stage, $\Delta_{avg,\exp}$ was measured to be 0.69 cm. A 13% increase in average bed form height was observed by the end of flood stage (b) where $\Delta_{avg,\exp}$ grew to 0.78 cm. The average bed form height decreased by 4% by the end of flood stage (c) as $\Delta_{avg,\exp}$ decreased to 0.75 cm. When the discharge magnitude was increased from flood stage (c) to flood stage (d), there was a 1% increase in average bed form height as $\Delta_{avg,\exp}$ = 0.76 cm. The post-flood conditions allowed the average bed form height to increase by 4% as $\Delta_{avg,\exp}$ = 0.79 cm at the end of the post-flood stage. From the end of antecedent to the end of post-flood stages, there was an overall net increase in average bed form height of 15%. The predicted $\Delta_{avg,calc}$-values for the antecedent stage was 1.13 cm, which was substantially greater than what was observed during this stage of the run. As the discharge magnitude was increased to be 1.25 times greater than the

antecedent stage, there was a 26% predicted increase in average bed form height to give $\Delta_{avg,calc}$ = 1.42 cm by the end of flood stage (b). By the end of the flood stage (c), the average bed form height increased by 1% due to a slight increase in h_{av} to give $\Delta_{avg,calc}$ = 1.43 cm. As the discharge increased between flood stages (c) and (d), there was a 30% increase in average bed form height to give $\Delta_{avg,calc}$ = 1.86 cm. There was a 34% decrease in average bed form height from the end of flood stage (d) to the end of the post-flood stage when $\Delta_{avg,calc}$ = 1.23 cm. This substantial decrease in $\Delta_{avg,calc}$ was in contrast to what was observed during the run. Overall, there was a predicted net increase in average bed form height of 9% from the end of the antecedent stage to the end of the post-flood stage. This decreasing trend in $\Delta_{avg,calc}$-values was opposite to what is experimentally measured.

The variation with time of the D_{50}-value of the sediment in transport over the entire duration of Run C3 is seen in Fig.23c. A minimum D_{50}-value of the sediment in transport (0.34 mm) was measured at 21, 26 and 33 min during flood stages (b), (c) and (d), respectively. The maximum observed D_{50}-value (0.37 mm) occurred at the beginning of the post-flood stage of the run (i.e., at times t = 36 and 37 min). This lag-in-time of the D_{50}-value of the sediment in transport represents counter-clockwise hysteresis.

5.3.3.4 Summary of Series C

The experimental runs of Series C investigated the effect of hydrograph shape (i.e., time-to-peak flow) on the sediment transport rate and bed morphology. Each experimental run had a 20 min antecedent stage (base-flow conditions), three flood stages of varying magnitude ((b), (c) and (d)), and a 30 min post-flood (return to antecedent conditions) stage. The hydrograph shape of the three flood stages was manipulated by varying the discharge to create systematic changes of the unsteady event time-to-peak flow. The unsteady events in all three runs lasted 15 min, but t_r was altered from run to run. The unsteady event in Run C1 was asymmetrical with a t_r occurring at 22.5 min (skewed left). The unsteady event in Run C2 was symmetrical and had a t_r occurring at 27.5 min while the unsteady event in Run C3 was asymmetrical with a t_r occurring at 32.5 min (skewed right).

Table 14 presents a summary of the magnitude of the predicted ($q_{sb,calc}$) and experimental ($q_{sb,\exp}$) sediment transport rates greater than the antecedent conditions for the three flood stages of the experimental runs of Series C. Generally, it can be seen in Fig. 26 that $q_{sb,\exp}$ decreases linearly as t_r increases. In Run C1, flood stage (b) (which had the greatest discharge) had the greatest value of $q_{sb,\exp}$ that was 3.27 times greater than the antecedent conditions which decreased to 1.66 and 1.63 times base-flow in flood stages (c) and (d), respectively. In Run C2 (where flood stage c had the greatest discharge), flood stages (b), (c) and (d) had $q_{sb,\exp}$ magnitudes 1.65, 3.13 and 2.01 times greater than the antecedent conditions, respectively. In Run C3 (where flood stage d had the greatest discharge), $q_{sb,\exp}$ was 1.52, 1.16 and 2.17 times greater than antecedent conditions in flood stages (b), (c) and (d), respectively. Run C1 had the greatest magnitude of peak $q_{sb,\exp}$ values, followed by Runs C3 and C2. The peak $q_{sb,\exp}$ occurred in the asymmetrical (or skewed) hydrograph with an earlier times-to-peak (Run C1), while the lower values of $q_{sb,\exp}$ occurred in the runs with later time-to-peak flow (both asymmetrical (or skewed) and symmetrical unsteady flow hydrographs). Runs C1 and C3 exhibited clockwise hysteresis in the sediment transport rates, while Run C2 exhibited counter-clockwise hysteresis.

Table 14: Magnitude of predicted and experimental specific volumetric bed load transport rates above antecedent stages for the flood stages in the experimental runs of Series C

Run	Flood Stage	Description	$q_{sb,calc}$ flood magnitude above antecedent $q_{sb,calc}$	$q_{sb,exp}$ flood magnitude above antecedent $q_{sb,exp}$
C1	b	1.50 x base-flow	1.32	3.27
	c	1.25 x base-flow	1.42	1.66
	d	1.25 x base-flow	1.36	1.63
C2	b	1.25 x base-flow	1.53	1.65
	c	1.50 x base-flow	1.67	3.13
	d	1.25 x base-flow	1.56	2.01
C3	b	1.25 x base-flow	1.33	1.52
	c	1.25 x base-flow	1.38	1.16
	d	1.50 x base-flow	1.84	2.17

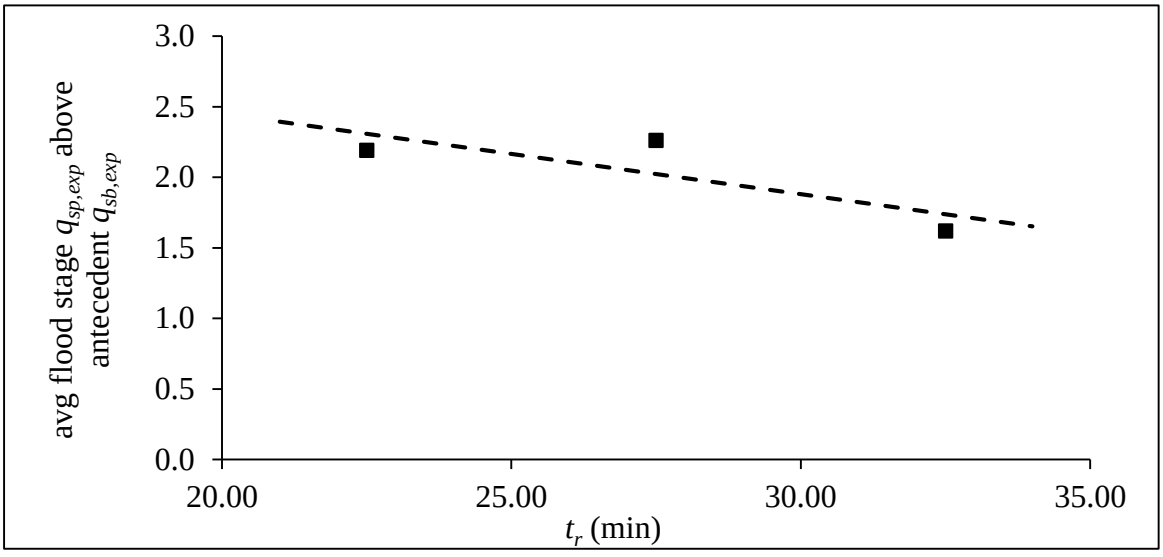

Figure 26: Relationship between t_r (min) and average $q_{sb,exp}$ during the flood stage for the experimental runs of Series C

As observed in Table 14, the magnitude of $q_{sb,calc}$ in Run C1 was 1.32, 1.42 and 1.36 times greater than the antecedent stage $q_{sb,calc}$-value in flood stages (b), (c) and (d), respectively; the magnitude of $q_{sb,calc}$ in Run C2 was 1.53, 1.67 and 1.56 times greater than the antecedent stage

$q_{sb,calc}$-value in flood stages (b), (c) and (d), respectively; and the magnitude of $q_{sb,calc}$ in Run C3 was 1.33, 1.38 and 1.84 times greater than the antecedent stage $q_{sb,calc}$-value in flood stages (b), (c) and (d), respectively. The predicted $q_{sb,calc}$-values of the flood stages varied much less than the observed $q_{sb,\exp}$-values due to the fixed discharge (1.25 and 1.50 times base-flow) and low variations in h_{av}. The predicted values did not take into account hysteresis of the sediment transport rates or bed morphology that would cause a lag in the $q_{sb,\exp}$ time-to-peak or change in the bed form geometry. Generally, in all experimental runs $q_{sb,\exp}$ of the post-flood stage fluctuates around the predicted $q_{sb,calc}$-value with a slight decrease initially around the 40 min time-step. Overall, $q_{sb,calc}$ under-estimates $q_{sb,\exp}$ during all stages of all runs, with the exceptions of Run C1 (during flood stage (d)) and Run C3 (during flood stage (c)) which were likely due to changes in bed morphology during these stages (such as sediment deposition on the lee side of bed forms) that resulted in increases in overall geometry of the bed forms instead of increased sediment transport volumes out of the flume.

Typically, the average bed form height ($\Delta_{avg,\exp}$) decreased at the end of the flood stage containing the peak discharge, but then increased during the following stage. For example, Runs C1, C2 and C3 all observed an increase in average bed form height of 18%, 24% and 4%, respectively, in the stage immediately following the peak flood stage. However, the opposite trend was observed in the predicted $\Delta_{avg,calc}$-values. The $\Delta_{avg,calc}$-values all predicted a decrease in average bed form height following the peak flood stage. For example, in Runs C1, C2 and C3 there was a predicted decrease of 11%, 18% and 34%, respectively, for the stage immediately following the flood stage containing the peak discharge. The $\Delta_{avg,\exp}$-values do not match the $\Delta_{avg,calc}$-values because the predicted values do not take into account the unsteadiness of the flow that results in hysteresis of the sediment transport rates (which is also observed in the bed morphological response). Fig. 27 shows the relationship between t_r and the observed percent change in the average bed form height. As t_r of the experimental run increases, the percent change in average bed form height changes from decreasing in height to increasing in height between the antecedent stage and t_r of each run. Between t_r and the post-flood stage the percent change in average bed form height decreases as t_r increases (but still

displays a percent increase in average bed form height for the largest value of t_r). Overall, the net change in average bed form height from the end of the antecedent stage to the end of the post-flood stage displays a slightly positive parabolic trend as t_r increases (see Fig. 27). Overall, the asymmetrical (skewed) hydrographs (Runs C1 and C3) show either no change or an increase in average bed form height, while the symmetrical hydrograph (Run C2) shows an overall decrease in average bed form height.

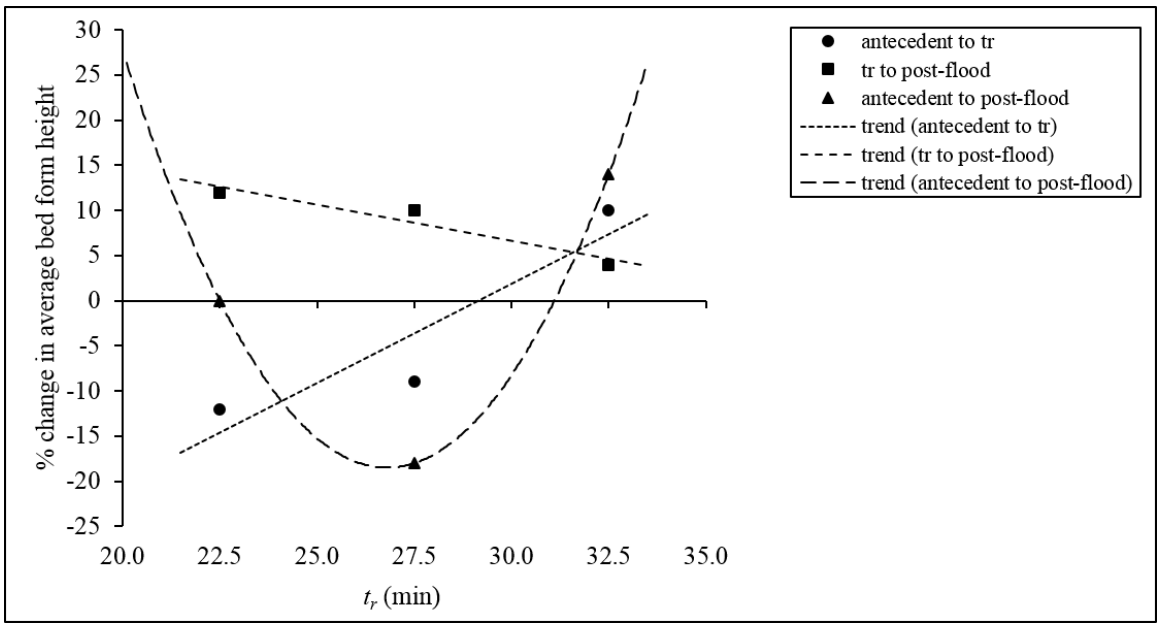

Figure 27: Relationship between the percent change in average bed form height and the time-to-peak flow of the unsteady flow event hydrograph between the various stages in the experimental runs of Series C

General trends from the grain size composition of the sediment in transport in the experimental runs of Series C are also observed. There was very little variation in the D_{50} of the sediment in transport throughout the experimental runs. All three runs in Series C demonstrated counter-clockwise hysteresis in the D_{50} of the sediment in transport (meaning there was a larger average grain size of the sediment in transport during the falling limb of the unsteady flow event hydrograph compared to the rising limb). The D_{50} of the sediment in transport reached a minimum and returned to the antecedent (original) D_{50}-value (0.36 mm) twice during the three flood stages. The D_{50} of the sediment in transport decreased as the bed adjusted to the flood stage and increased towards the end of the flood stage or during the post-flood stage as bed

forms that developed during the flood stage degraded and are were transported out of the flume. All experimental runs saw a minimum D_{50}-value of the sediment in transport occur within the initial time-steps of the three flood stages. However, this decrease of the D_{50} occurred later into the experimental run for runs with larger t_r-values. For example, the minimum D_{50} of the sediment in transport occurred at 21, 24 and 26 min in Runs C1, C2 and C3, respectively.

5.4 Discussion

In this Section, further discussion of the experimental results observed in Series C are made. Efforts to establish a relationship between the hysteresis of the sediment transport rate $q_{sb,\exp}$ and the variation in hydrograph shape (i.e., time-to-peak flow) are made. Table 15 shows the values of t_s, t_r and t_{lag} for all three experimental runs of Series C (the parameter t_{lag} is defined in Section 4.4). While the duration of the three flood stages combined remained constant at 15 min, t_r varied between the experimental runs according to where the peak flow occurred in the flood stage hydrograph. t_r was 22.5, 27.5 and 32.5 min for Runs C1, C2 and C3, respectively, and t_s was 21, 29 and 31 min for Runs C1, C2 and C3, respectively. Based on the relationship between t_s and t_r, hysteresis for Runs C1, C2 and C3 was determined to be clockwise, counter-clockwise and clockwise, respectively. In general, t_s occurred during later flood stages for greater values of t_r. Despite the time at which t_r and t_s occur, both values occur within the same 5 min flood stage in each experimental run (i.e., the flood stage with the greatest discharge magnitude). For example, in Run C1 both values occurred in flood stage (b), in Run C2 both values occurred in flood stage (c) and in Run C3 both values occurred in flood stage (d). Clockwise hysteresis of the sediment transport rates occurred for the runs with t_s-values occurring early and later in the flood stage (Runs C1 and C3) whereas the experimental run with an "intermediate" value of t_s produced counter-clockwise hysteresis. The relationship between the parameter manipulated in Series C (t_r) and t_{lag} form a positive parabolic relationship (see trend line displayed in Fig. 28). Based on these results for the present series of experimental runs, asymmetrical hydrographs produced clockwise hysteresis (positive t_{lag}-values) of the sediment transport rates and symmetrical hydrographs produced counter-clockwise hysteresis (negative t_{lag}-value) of the sediment transport rates.

Table 15: Summary of Series C values of t_s, t_r and t_{lag}

Run	Relative magnitude of flood stage above antecedent	Duration of flood stage (min)	t_s (min)	t_r (min)	t_{lag} (min)
C1	1.50	15	21	22.5	1.5
C2	1.50	15	29	27.5	-1.5
C3	1.50	15	31	32.5	1.5

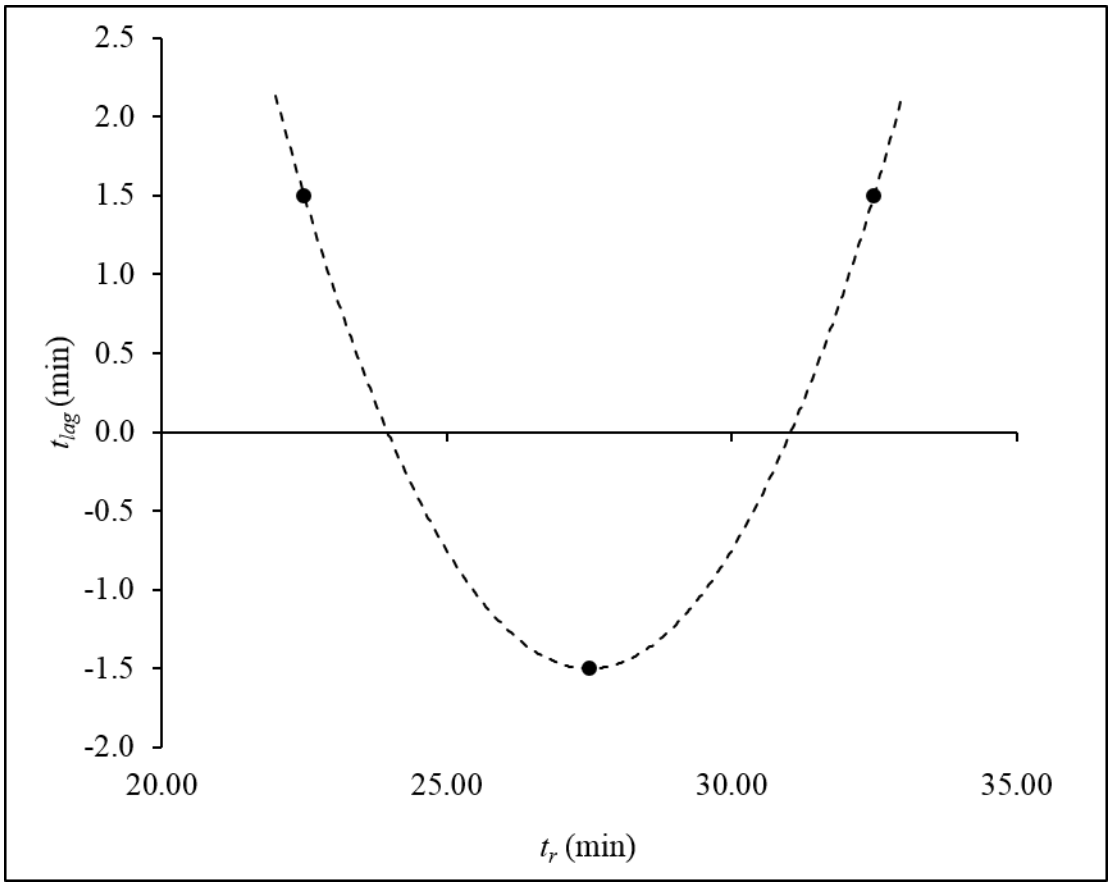

Figure 28: Relationship between t_{lag} (min) and t_r (min) for the experimental runs in Series C

A dimensionless representation combining the results of the experimental runs of Series A, B and C was created to further investigate the relationship between t_{lag} and the relative

magnitude and duration of unsteady flow events (see Fig. 29). t_{lag}-values were made dimensionless by dividing t_{lag} of each experimental run by the duration of the respective unsteady flow event. Based on the data, a parabolic trend (represented by the dashed line in Fig. 29), based on the results from the experimental runs in Series A (which had varying magnitude discharge and the duration of the event remained constant) is suggested. The data from the experimental runs of Series B (which had varying unsteady flow event durations and constant relative discharge) forms a vertical line that passes through the parabolic function of Series A. The data from the experimental runs of Series C follows a similar linear trend to that of Series B. If additional experimental runs were completed, it could be suggested that the results of Series B and C would also form parabolic functions similar to the trend shown for Series A. Fig. 29 can be used to predict possible t_{lag}-values (and corresponding hysteretic behaviour) for unsteady flow events of different magnitudes and durations that were not tested in the present series of experimental runs. If t_r and the magnitude and duration of the unsteady flow event hydrograph are known, then t_{lag} and t_s can be estimated using Fig. 29 and Eq. 40, respectively, and the type of hysteresis can thus be inferred. Clearly, extension of Fig. 29 in this manner is only valid within the conditions tested in the present runs (i.e., at relative discharge magnitudes less than 2.00 times the base-flow conditions) as further experimental testing of unsteady flow event hydrographs with greater discharges required.

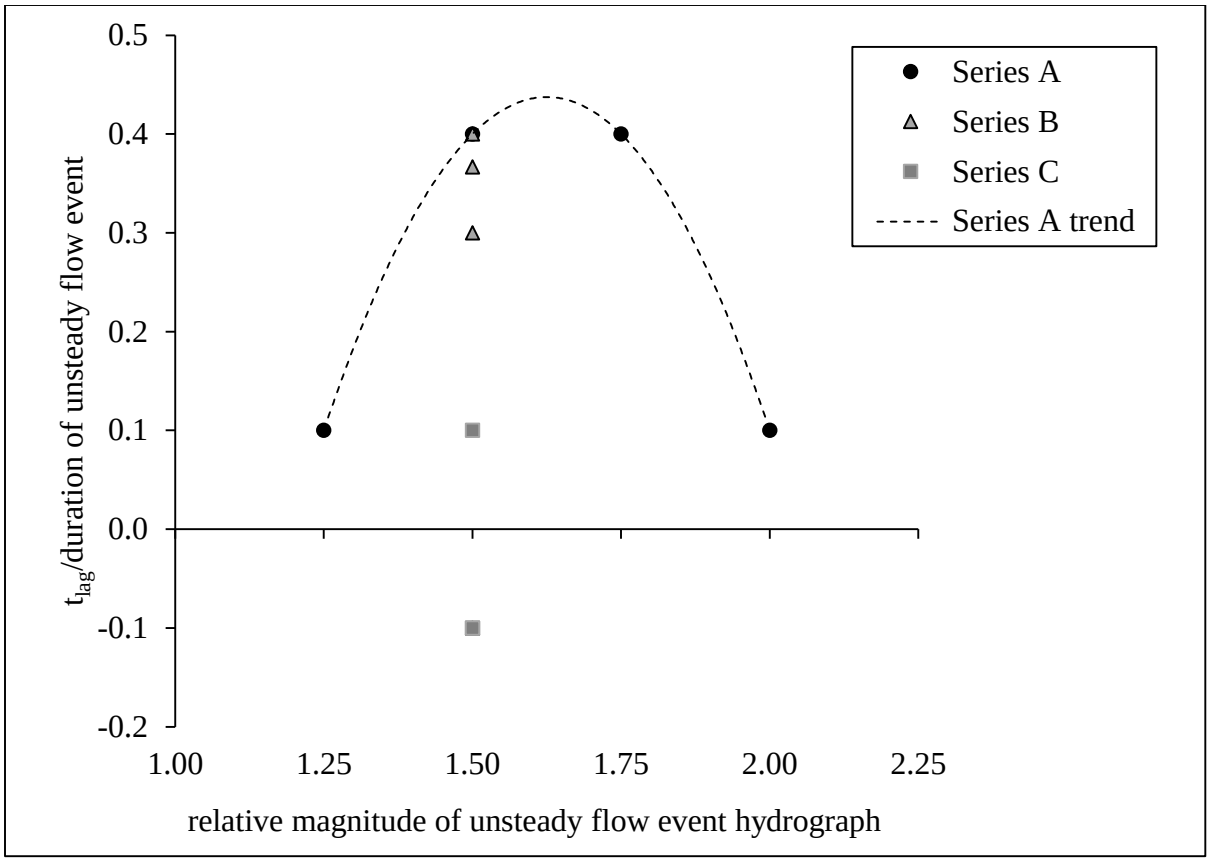

Figure 29: General relationship between the dimensionless t_{lag}/duration and the relative discharge magnitude change of the unsteady flow event hydrograph

The trend line in Fig. 29 is represented by the following formula:

$$y = -2.40(x - 1.63)^2 + 0.44, \qquad (42)$$

where y is the dimensionless t_{lag}/duration and x is the relative magnitude of the unsteady flow event hydrograph. This formula can be used to predict possible values of t_{lag} (y term) if the duration and relative magnitude of the unsteady flow event hydrograph (x term) are known. However, it should be made clear that this formula is only valid for experimental conditions investigated in this thesis. For unsteady flow events of varying magnitude at a duration other than 10 min (as used in Series A), the vertex of the parabolic function (h, k) would adjust vertically. More specifically, the k term represents the vertical adjustment of the vertex, and in turn, the influence of the magnitude for varying unsteady flow event hydrograph durations.

The use of Eq. 42 will predict possible t_{lag} values and the corresponding hysteretic behaviour for unsteady flow events below 2.00 times greater than the base-flow conditions.

5.5 Concluding remarks

The main findings of this Chapter are as follows:

1. On average, traditional predictive specific volumetric bed load transport rate equations assuming steady flow conditions equal the experimentally observed rates during steady flow stages. However, the calculated rates drastically under-estimate experimental specific volumetric bed load transport rates during unsteady flow conditions.

2. The magnitude of experimental specific bed load transport rates during the flood stage of unsteady flow event hydrographs decreases as the hydrograph time-to-peak flow increases.

3. Generally, sediment transport rate time-to-peak occurs at a later time-step as the hydrograph time-to-peak flow increases.

4. Clockwise hysteresis of the sediment transport rates occurs for asymmetrical hydrographs (positive t_{lag}, meaning the maximum sediment transport rate was reached prior to the hydrograph time-to-peak) while counter-clockwise hysteresis of the sediment transport rates occurs for symmetrical hydrographs (negative t_{lag}, meaning the sediment transport rate reached the maximum rate after the hydrograph time-to-peak).

5. In all experimental runs, the bed morphology experienced a lag-in-time before the bed form geometry adjusted to the unsteady flow event. During the peak flow stage, the bed geometry decreased during the maximum discharge flood stage and increased during the subsequent time-step.

6. The average grain size of the sediment in transport exhibited a counter-clockwise lag-in-time that occured at a later time-step as hydrograph time-to-peak flow event increased.

7. Eq. 42 can be used to estimate the specific volumetric bed load transport rate time-to-peak for unsteady flow event magnitudes in the range of hydraulic conditions tested in the present runs (up to 2.00 times greater than base-flow conditions). Based on the present experimental runs, the proposed relationship between the duration and magnitude of an unsteady flow event hydrograph (and corresponding hysteretic behaviour of the sediment transport rate response) is seen in Fig. 29.

5.6 References

Ahanger MA, Asawa GL, Lone MA. 2008. Experimental study of sediment transport hysteresis. *Journal of Hydraulic Research* **46**(5):628-635. DOI:10.3826/jhr.2008.3185

Allen JRL. 1976. Time-lag of dunes in unsteady flows: an analysis of Nasner's data from River Weser, Germany. *Sedimentary Geology* **15**:309-321.

Ashley GM. 1990. Classification of large-scale subaqueous bedforms – a new look at an old problem – bedforms and bedding structures. *Journal of Sediment Petrology* **60**:160-172.

Bagnold RA. 1968. An approach to the sediment transport problem from general physics. Geologic Survey Professional Paper 422(I).

Bombar G, Elci S, Tayfur G, Guney SM and Bor A. 2011. Experimental and numerical investigation of bed-load transport under unsteady flows. *Journal of Hydraulic Engineering* **137**:1276-1282. DOI: 10.1061/(ASCE)HY.1943-7900.0000412

Boyer C, Chaumont D, Chartier I and Roy AG. 2010. Impact of climate change on the hydrology of St. Lawrence tributaries. *Journal of Hydrology* **384**(1):65-83.

Brooks GR, Evans SG and Clague JJ. 2001. Flooding. A Synthesis of Natural Geological Hazards in Canada. Ottawa: *Geological Survey of Canada Bulletin* **548**:101-143.

Burn DH and Elnur MAH. 2002. Detection of hydrologic trends and variability. *Journal of Hydrology* **225**:107-122.

Burn DH and Whitfield PH. 2015. Changes in floods and flood regimes in Canada. *Canadian Water Resources Journal* **(ahead of print):**1-12.

De Sutter R, Verhoeven R, Krein A. 2001. Simulation of sediment transport during flood events: laboratory work and field experiments. *Hydrological Sciences Journal* **46**(4):599-610. DOI:10.1080/02626660109492853

Fredsoe J. 1982. Shape and dimensions of stationary dunes in rivers. *Journal of the Hydraulics Division* **108**(8):932-947.

Hirabayashi Y, Mahendran R, Koirala S, Konoshima L, Yamazaki D, Watanabe S, Kanae S. 2013. Global flood risk under climate change. *Nature Climate Change* **3**(9):816–821. DOI:10.1038/nclimate1911.

Intergovernmental Panel on Climate Change. 2014. Climate change 2014: impacts, adaptation, and vulnerability. Cambridge University Press, Cambridge, United Kingdom and New York, NY, USA, 1-32.

Lee KT, Liu YL, and Cheng KH. 2004. Experimental investigation of bedload transport processes under unsteady flow conditions. *Hydrological Processes* **18**(13):2439-2454. DOI: 10.1002/hyp.1473

Lemmen DS, Warren FJ, Lacroix J, and Bush E, editors 2008. From Impacts to Adaptation: Canada in a Changing Climate 2007; Government of Canada, Ottawa, ON, 448.

Martin RL and Jerolmack DJ. 2013. Origin of hysteresis in bed form response to unsteady flows. *Water Resources Research* **49**(3):1314-1333. DOI:10.1002/wrcr.20093

Meyer-Peter E and Müller R. 1949. Formula for bed load transport. Proc 2nd Meeting IAHR 6.

Nelson JM, Logan BL, Kinzel PJ, Shimizu Y, Giri S, Shreve RL and McLean SR. 2011. Bedform response to flow variability. *Earth Surface Processes and Landforms* **36**(14):1938-1947. DOI: 10.1002/esp.2212

Richter BD and Thomas GA. 2007. Restoring environmental flows by modifying dam operations. *Ecology and Society* **12**(1): 12.

van Rijn. 1984. Sediment transport part I: bed load transport. Journal of Hydraulic Engineering **110**(10):1431-1456.

Whitfield PH and Cannon AJ. 2000. Recent variations in climate and hydrology in Canada. *Canadian Water Resources Journal* **25**(1):19-65.

Yalin MS. 1963. An expression for bed load transport. *Journal of Hydraulics Division* **89**(3):221-250.

Yalin MS. 1972. On the formation of dunes and meanders. *Hydraulic Research and Its Impact on the Environment*.

Yalin MS. 1985. On the determination of ripple geometry. *Journal of Hydraulic Engineering* **111**(8):1148-1155.

Yue S and Hashino M. 2003. Long term trends of annual and monthly precipitation in Japan. *Journal of American Water Resources Association* **39**(3):587-596.

Chapter 6

6 Conclusions and recommendations

In this Chapter, a summary of main conclusions from the thesis, engineering implications and recommendations for future research are made. The summary of conclusions from this thesis are reported in three sub-sections according to Chapters 3 through 5. Engineering implications connect the results from this thesis to current engineering challenges. Lastly, recommendations for future research in this area are made.

6.1 Summary of conclusions

6.1.1 Recent literature review

Over the last few decades, efforts to further the understanding of sediment transport and bed morphological behaviour during unsteady flow events have been made. Researchers have taken a variety of approaches to investigate the problem with the use of numerical models, field research and laboratory experimentation. The focus of this thesis was on the effect of unsteady flow events on bed morphological response. Efforts to identify the causes responsible for the hysteresis occurring the sediment transport rates in response to unsteady flow events were made in Chapter 3. Despite a detailed review of the literature, there is still not complete agreement on the factors influencing or causing this lag-in-time of both the sediment transport rate and bed morphological response. Based on this review of the literature, the main factors affecting this hysteretic behaviour include: sediment composition, hydrograph shape, sediment supply, and bed morphological development. It is difficult to assess the influence of these factors individually as they can have counteracting effects. Based on the findings of the recent literature summarized in Chapter 3, the following three recommendations to further the knowledge of morphological response to unsteady flow events were reported:

1. Determine a hierarchical outline of the factors responsible for the hysteresis of sediment transport rates and bed morphological adjustments in response to unsteady flow events. Efforts to determine the degree that each factor influences the effect of hysteresis and their inter-dependency is recommended.

2. Establish the influence of the duration and magnitude of unsteady flow events and the shape of the hydrograph on bed morphological adjustments. Subsequently, develop a predictive method to more accurately assess the morphological adjustments in response to unsteady flow events of varying hydrograph characteristics. This will allow for the development of more accurate predictive numerical modeling tools that can be used to predict field-scale behaviour.

3. Investigate the effect of unsteady flow events on morphological response of non-uniform sediment beds.

6.1.2 Effect of unsteady flow event magnitude and duration on bed morphological response

Efforts to address the effect of the magnitude and duration of unsteady flow events on the bed morphological response were made in order to address the second recommendation from Chapter 3. Series A and B experimental runs investigated the effect of systematic changes in magnitude and duration of unsteady flow events, respectively. The effect of these two unsteady flow event hydrograph characteristics on the response of the sediment transport rates, bed morphological adjustments and change in the average grain size of the transported material were examined (see Chapter 4). The following five main conclusions were drawn:

1. The experimental flood stage specific volumetric bed load transport rate increases linearly with systematic increases in the magnitude and duration of the unsteady flow event. Increases in discharge magnitude had a greater effect on the sediment transport rate response than the changes in duration of the unsteady flow event.

2. The specific bed load transport rate during all eight experimental runs of Series A and B demonstrated hysteretic behaviour. Clockwise hysteresis occurs when the maximum sediment transport rate occurred before the hydrograph time to peak and counter-clockwise hysteresis occurs when the opposite occurred. Results indicated that unsteady flow events of greater magnitude and longer duration exhibit clockwise hysteresis while shorter duration events demonstrate counter-clockwise hysteresis of the sediment transport rates.

3. Generally, sediment transport rates calculated with steady flow expressions drastically under-predict the flood stage sediment transport rates. The factor by which calculated specific volumetric bed load transport rate (assuming steady flow conditions) under-predicts the experimental specific volumetric bed load transport rate (during unsteady flow conditions) increases as the relative discharge magnitude of the unsteady flow event increases. For a constant discharge magnitude, the factor by which the calculated specific volumetric bed load transport rate under-predicts the experimental specific volumetric bed load transport rate remains relatively constant as the duration of the event increases.

4. Generally, the average bed form height increases in response to an unsteady flow event (increases both with increase in discharge magnitude and duration of event). Smaller magnitude unsteady flow events increased the height of the bed forms during the flood stage and decreased the height of the bed forms during the post-flood stage, exhibiting counter-clockwise hysteresis of the sediment transport rates. Larger magnitude unsteady flow events decreased the height of the bed forms during the flood stage and increased the height of the bed forms during the post-flood stage, exhibiting clockwise hysteresis of the sediment transport rates.

5. The average grain size of the sediment in transport during the flood stage exhibited counter-clockwise hysteresis regardless of the changes in magnitude or duration of the unsteady flow event. Larger magnitude unsteady flow events emphasize the effect of the hysteresis in the average grain size of the sediment in transport while alterations in the duration of the event maintain a relatively constant average grain size of the sediment in transport.

6.1.3 Effect of unsteady flow event hydrograph shape on bed morphological response

The effect of the shape of the hydrograph (i.e., time-to-peak flow) of unsteady flow events on the bed morphological response was also investigated to address the second recommendation from Chapter 3. Series C experimental runs investigated systematic changes in the hydrograph time-to-peak flow on the response of sediment transport rates and bed morphology. Similar to Chapter 4, the effect of altering the unsteady flow event hydrograph shape on experimental

and predicted sediment transport rates, bed morphological adjustments, and the change in the average grain size of the transported material were examined (see Chapter 5). The following six main conclusion were drawn from this work:

1. The predicted sediment transport rates generally underestimate the experimental sediment transport rates during unsteady flow event hydrographs of varying time-to-peak flow (or skewness).

2. As the hydrograph time-to-peak flow increases, the magnitude of the experimental sediment transport rate in response to the unsteady flow event decreases but the time-to-peak sediment transport increases.

3. Asymmetrical (skewed) hydrographs produce clockwise hysteresis (sediment transport rate time-to-peak occurs prior to the hydrograph time-to-peak) while counter-clockwise hysteresis (hydrograph time-to-peak occurs prior to the sediment transport rate time-to-peak) is observed for symmetrical hydrographs.

4. Bed form geometry exhibits a lag-in-time (hysteresis) effect before it adjusts to the hydrograph time-to-peak. In all hydrographs shapes (asymmetrical and symmetrical skewness) the bed form geometry decreases during the maximum discharge period of the unsteady flow event, and then increases during the next time-step.

5. The average grain size of the sediment in transport exhibited a counter-clockwise lag-in-time that occurs at a later time step as the time-to-peak flow of the hydrograph increased.

6. The dimensionless relationship between t_{lag}/duration and the relative discharge magnitude of the unsteady flow event hydrograph were used to establish the proposed trend and function that can be used to estimate the time that the maximum specific volumetric bed load rate occurs at for unsteady flow event magnitudes below 2.00 times greater than base-flow conditions.

6.2 Engineering implications

This thesis has made considerable contributions towards evaluating the effect of various unsteady flow event hydrograph characteristics (i.e., magnitude, duration and time-to-peak flow) on sediment transport and bed morphological response. As discussed in Chapter 1, riverine flooding is a global issue that affects both infrastructure and society. Due to the increase in the frequency and duration of flooding events, an increase in river management, engineering and restoration efforts are required in order to mitigate adverse effects.

Engineered structures such as dams are designed to mitigate riverine flooding. However, due to the occurrence of a greater number of extreme rainfall events in some areas of the world, reservoirs are filling at a faster rate. This requires more frequent reservoir flushing operations which can result in an increase in the frequency of downstream changes in discharge. Determining the lag-in-time for a pre-determined magnitude will allow engineers to design flushing events with a sufficient duration to deposit a specific volume of sediment at an exact location downstream. Present river and dam management guidelines will need to adjust in order to minimize adverse impacts of downstream riverine flooding as a result of these unsteady flow events. In order to do so, a comprehensive understanding of sediment transport and bed morphological changes in response to unsteady flow events must is required to develop more reliable predictive models that will guide river and dam management strategies.

Similarly, results from this thesis can also be applied to river channel design projects in order to design rivers to be able to withstand the projected changes in discharge. Traditional channel design methods of channelization have been, for the most part, abandoned. New and innovative channel design philosophies aim to consider the behaviour of sediment transport rates and bed morphological changes during unsteady flow events in order to design effective riverine systems that are able to withstand the adverse effects of floods of varying magnitude, duration and time-to-peak flows.

Finally, the results of this thesis can also be applied to improve numerical modeling capabilities and accuracy. Experimental results and the equation proposed for unsteady flow events of varying magnitude, duration and time-to-peak flows will allow for calibration and validation of numerical models to improve the capability of numerical modeling to predict this behaviour.

This will allow for more reliable application of numerical modeling tools in real world engineering projects.

6.3 Recommendations for future research

Future research on this topic is required in order to accurately quantify the effect of unsteady flow events on bed morphological response at a larger model or field-scale. The following recommendations for future research are suggested:

1. Assess the duration and shape (i.e., time-to-peak flow) of the unsteady flow event where counter-clockwise sediment transport rate hysteresis changes to clockwise hysteretic behaviour. Further, investigate whether this phenomenon occurs at other unsteady event discharge magnitudes.

2. Examine the effect of greater magnitude unsteady flow events that are more representative of field scale riverine floods. This will allow for more accurate scaling of laboratory results to real-world conditions.

3. Quantify bed morphological and sediment transport rate adjustments during unsteady flow events in a compound channel to determine the effect of the floodplain hydraulics during unsteady flow events. This will investigate the response to an unsteady flow event that overtops the main channel banks and inundates the floodplains.

4. Investigate the effect of unsteady flow events on meandering river morphological adjustments. This will contribute to developing more resilient channel design efforts that focus on re-meandering previously channelized river systems.

5. Validate the proposed predictive function for the magnitudes of unsteady flow conditions greater than 2.00 times greater than base-flow conditions in laboratory, numerical and field-scale models.

6.4 References

Bombar G, Elci S, Tayfur G, Guney SM and Bor A. 2011. Experimental and numerical investigation of bed-load transport under unsteady flows. *Journal of Hydraulic Engineering* **137**:1276-1282. DOI: 10.1061/(ASCE)HY.1943-7900.0000412

De Costa C and Coleman S. 2013. Temporal and spatial changes in bed-form due to change in flow in a flume environment. *International Conference on Sustainable Built Environments* **13**:111-116.

De Sutter R, Verhoeven R, Krein A. 2001. Simulation of sediment transport during flood events: laboratory work and field experiments. *Hydrological Sciences Journal* **46**(4):599-610. DOI:10.1080/02626660109492853

Lee KT, Liu YL, and Cheng KH. 2004. Experimental investigation of bedload transport processes under unsteady flow conditions. *Hydrological Processes* **18**(13):2439-2454. DOI: 10.1002/hyp.1473

Nelson JM, Logan BL, Kinzel PJ, Shimizu Y, Giri S, Shreve RL and McLean SR. 2011. Bedform response to flow variability. *Earth Surface Processes and Landforms* **36**(14):1938-1947. DOI: 10.1002/esp.2212

Reesink AJH and Bridge JS. 2007. Influence of superimposed bedforms and flow unsteadiness on formation of cross strata in dunes and unit bars. *Sedimentary Geology* **202**(1):281-296. DOI:10.1016/j.sedgeo.2007.02.005

Reesink AJH and Bridge JS. 2009. Influence of superimposed bedforms and flow unsteadiness on formation of cross strata in dunes and unit bars – Part 2, further experiments. *Sedimentary Geology* **222**(3):274-300. DOI:10.1016/j.sedgeo.2009.09.014

Appendices

Appendix A: Schematic definition of hysteresis

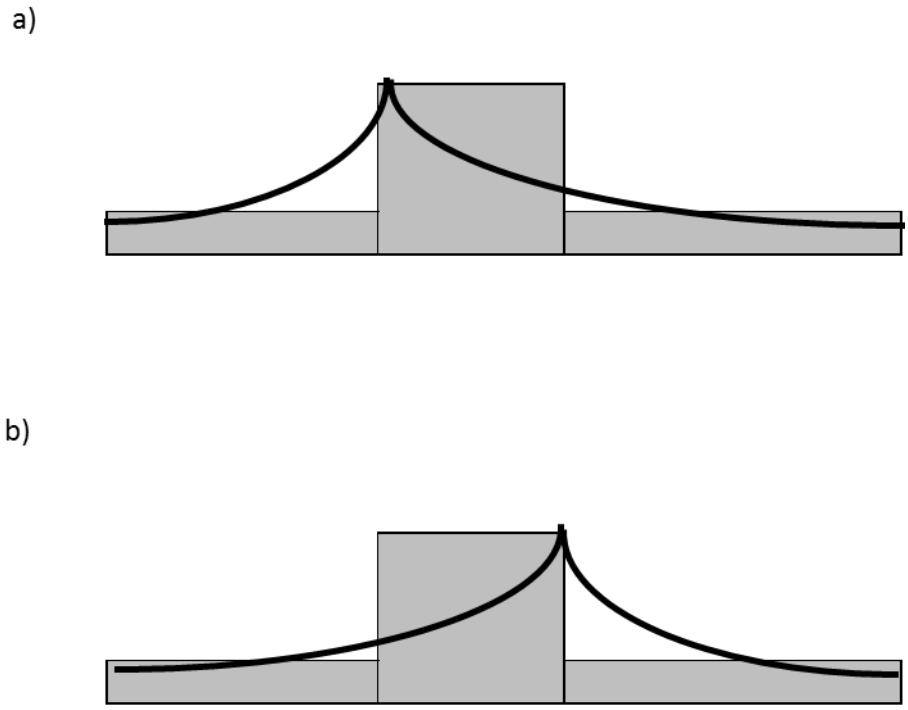

Figure 30: Schematic of a) clockwise and b) counter-clockwise hysteresis of sediment transport rates during unsteady flow events

Appendix B: Laboratory facility

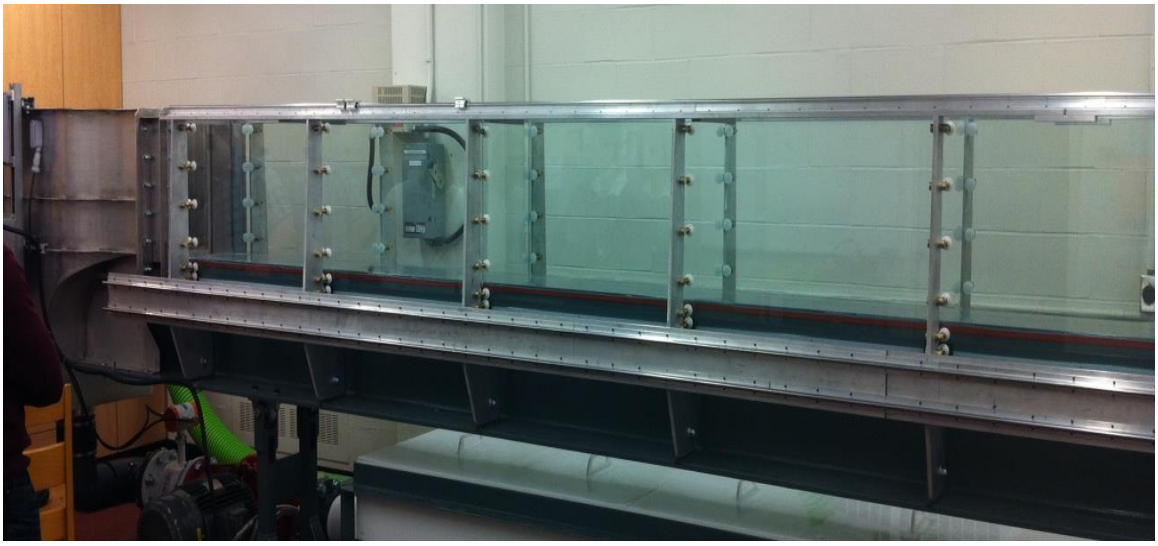

Figure 31: Sediment transport flume at the University of Western Ontario in London, Ontario, Canada

Appendix C: Schematic of the sediment transport flume

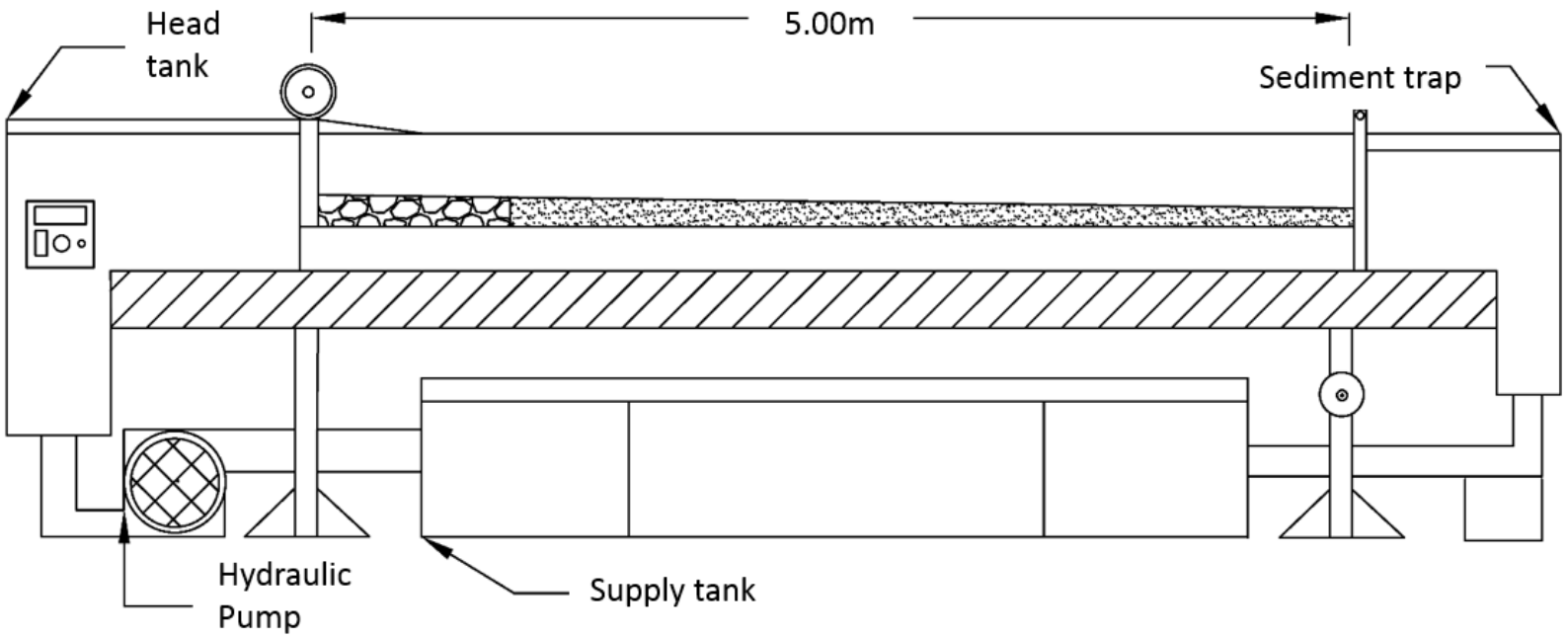

Figure 32: Schematic of the sediment transport flume at the University of Western Ontario in London, Ontario, Canada

Appendix D: Grain size analysis

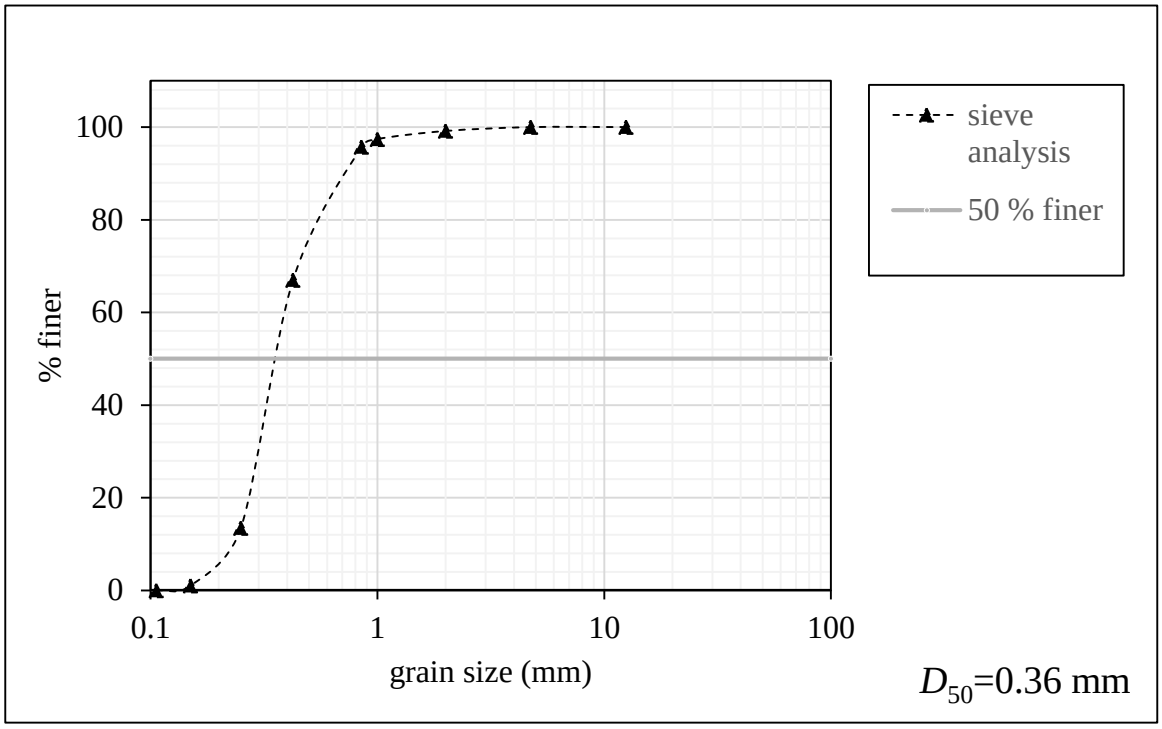

Figure 33: Grain size analysis of present material (well-sorted, medium sand with D_{50} of 0.36 mm)

Appendix E: Standard deviation of reported experimental specific volumetric bed load transport rates based on all repetitions of the experimental runs in Series A

Table 16: Specific volumetric bed load transport rates and standard deviation from the reported mean values for each experimental time step in all runs of Series A

time	Run A1					Run A2					Run A3					Run A4				
[s]	i	ii	iii	Reported	σ	i	ii	iii	Reported	σ	i	ii	iii	Reported	σ	i	ii	iii	Reported	σ
	$q_{sb,exp}$ [m^2/s]	qsb,exp [m^2/s]	$q_{sb,exp}$ [m^2/s]	$q_{sb,exp}$ [m^2/s]	[m^2/s]	$q_{sb,exp}$ [m^2/s]	$q_{sb,exp}$ [m^2/s]	$q_{sb,exp}$ [m^2/s]	$q_{sb,exp}$ [m^2/s]	[m^2/s]	$q_{sb,exp}$ [m^2/s]	$q_{sb,exp}$ [m^2/s]	$q_{sb,exp}$ [m^2/s]	$q_{sb,exp}$ [m^2/s]	[m^2/s]	$q_{sb,exp}$ [m^2/s]	$q_{sb,exp}$ [m^2/s]	$q_{sb,exp}$ [m^2/s]	$q_{sb,exp}$ [m^2/s]	[m^2/s]
5	1.412E-05	6.558E-06	6.444E-07	7.108E-06	6.756E-06	1.423E-05	9.357E-06	1.322E-06	7.222E-06	6.518E-06	4.249E-06	1.550E-06	4.249E-06	2.900E-06	1.558E-06	1.278E-05	4.276E-06	3.920E-06	8.528E-06	5.016E-06
10	6.591E-06	5.725E-06	1.289E-06	4.535E-06	2.323E-06	1.101E-05	5.537E-06	1.510E-06	5.744E-06	4.771E-06	5.094E-06	1.383E-06	5.094E-06	3.239E-06	2.143E-06	6.108E-06	6.719E-06	5.974E-06	6.413E-06	3.971E-07
15	1.013E-05	5.390E-06	1.671E-06	5.730E-06	3.461E-06	1.042E-05	5.940E-06	4.370E-06	5.888E-06	3.142E-06	3.564E-06	2.074E-06	3.564E-06	2.819E-06	8.603E-07	6.128E-06	2.155E-06	2.994E-06	4.141E-06	2.094E-06
20	4.202E-06	4.571E-06	3.047E-06	3.940E-06	6.490E-07	1.342E-06	3.812E-06	3.027E-06	3.314E-06	1.262E-06	7.155E-06	1.470E-06	7.155E-06	4.312E-06	3.282E-06	5.826E-06	6.571E-06	2.108E-06	6.199E-06	2.391E-06
21	9.632E-06	1.081E-05	4.967E-06	8.468E-06	2.522E-06	1.171E-05	9.229E-06	1.980E-05	1.288E-05	5.528E-06	2.410E-05	1.641E-05	2.410E-05	2.025E-05	4.437E-06	3.786E-05	2.202E-05	1.168E-05	2.994E-05	1.318E-05
22	7.551E-06	8.189E-06	5.303E-06	7.014E-06	1.238E-06	1.540E-05	5.537E-06	1.168E-05	9.917E-06	4.982E-06	1.889E-05	1.148E-05	1.889E-05	1.519E-05	4.282E-06	4.021E-05	1.252E-05	1.423E-05	2.636E-05	1.551E-05
23	6.981E-06	1.175E-05	9.867E-06	9.531E-06	1.960E-06	1.245E-05	6.611E-06	8.424E-06	8.751E-06	2.989E-06	2.178E-05	7.484E-06	2.178E-05	1.463E-05	8.254E-06	3.470E-05	2.302E-05	1.755E-05	2.886E-05	8.760E-06
24	9.732E-06	1.997E-05	5.135E-06	1.161E-05	6.200E-06	8.659E-06	9.430E-06	7.853E-06	7.794E-06	7.887E-07	1.628E-05	9.195E-06	1.628E-05	1.274E-05	4.088E-06	4.021E-05	2.903E-05	1.722E-05	3.462E-05	1.150E-05
25	1.205E-05	6.376E-06	2.316E-06	6.913E-06	3.991E-06	7.752E-06	6.746E-06	8.356E-06	6.997E-06	8.138E-07	2.453E-05	6.376E-06	2.453E-05	1.545E-05	1.048E-05	3.561E-05	2.061E-05	2.010E-05	2.811E-05	8.810E-06
30	9.732E-06	1.010E-05	4.578E-06	8.137E-06	2.522E-06	1.298E-05	8.122E-06	1.093E-05	9.541E-06	2.439E-06	1.297E-05	9.068E-06	1.297E-05	1.102E-05	2.255E-06	2.717E-05	1.794E-05	1.747E-05	2.256E-05	5.469E-06
31	4.967E-06	3.356E-07	3.759E-06	3.020E-06	1.961E-06	5.135E-06	2.383E-06	2.282E-06	3.222E-06	1.619E-06	3.356E-06	1.812E-06	3.356E-06	2.584E-06	8.913E-07	5.739E-06	3.155E-06	1.644E-06	4.447E-06	2.071E-06
32	4.430E-06	3.759E-07	3.826E-06	2.877E-06	1.786E-06	4.665E-06	5.470E-06	1.242E-06	3.750E-06	2.245E-06	5.000E-06	1.175E-06	5.000E-06	3.088E-06	2.209E-06	4.564E-06	1.678E-06	1.477E-06	3.121E-06	1.727E-06
33	4.531E-06	4.161E-07	2.685E-06	2.544E-06	1.683E-06	4.833E-06	8.759E-06	9.732E-07	4.875E-06	3.893E-06	4.967E-06	6.712E-07	4.967E-06	2.819E-06	2.480E-06	5.638E-06	1.175E-06	1.242E-06	3.406E-06	2.558E-06
34	5.806E-06	4.161E-07	3.625E-06	3.282E-06	2.214E-06	4.598E-06	6.712E-06	2.148E-06	4.153E-06	2.284E-06	6.242E-06	6.041E-07	6.242E-06	3.423E-06	3.255E-06	7.249E-06	8.054E-07	1.309E-06	4.027E-06	3.584E-06
35	7.987E-07	4.430E-07	2.181E-06	1.141E-06	7.498E-07	2.853E-06	3.121E-06	1.678E-06	2.685E-06	7.675E-07	2.886E-06	6.041E-07	2.886E-06	1.745E-06	1.318E-06	1.094E-06	2.416E-06	1.812E-06	1.755E-06	6.620E-07
40	2.705E-06	3.007E-06	2.651E-06	2.788E-06	1.566E-07	3.953E-06	3.121E-06	2.282E-06	3.593E-06	8.357E-07	6.491E-06	9.397E-07	6.491E-06	3.715E-06	3.205E-06	3.906E-06	2.161E-06	3.940E-06	3.034E-06	1.017E-06
45	6.074E-06	2.275E-06	2.826E-06	3.725E-06	1.676E-06	5.269E-06	3.692E-06	2.698E-06	3.985E-06	1.296E-06	4.054E-06	1.691E-06	4.054E-06	2.873E-06	1.364E-06	4.665E-06	2.161E-06	4.148E-06	3.413E-06	1.322E-06
50	6.376E-06	8.256E-07	2.792E-06	3.331E-06	2.298E-06	4.658E-06	6.343E-06	2.202E-06	4.524E-06	2.083E-06	3.551E-06	2.759E-06	3.551E-06	3.155E-06	4.573E-07	4.873E-06	3.819E-06	5.504E-06	4.346E-06	8.512E-07
55	4.698E-06	3.611E-06	1.141E-06	3.150E-06	1.488E-06	5.806E-06	7.531E-06	2.369E-06	4.724E-06	2.628E-06	3.289E-06	1.134E-06	3.289E-06	2.212E-06	1.244E-06	5.276E-06	3.900E-06	2.202E-06	4.588E-06	1.540E-06
60	3.135E-06	1.832E-06	1.316E-06	2.094E-06	7.653E-07	6.296E-06	6.705E-06	3.698E-06	4.853E-06	1.631E-06	4.000E-06	1.047E-06	4.000E-06	2.524E-06	1.705E-06	5.276E-06	5.833E-06	2.202E-06	5.554E-06	1.956E-06

Appendix F:Standard deviation of reported experimental specific volumetric bed load transport rates based on all repetitions of the experimental runs in Series B

Table 17: Specific volumetric bed load transport rates and standard deviation from the reported mean values for each experimental time step in all runs of Series B

time	Run B1					time	Run B2					time	Run B3					time	Run B4				
[s]	i	ii	iii	Reported	σ	[s]	i	ii	iii	Reported	σ	[s]	i	ii	iii	Reported	σ	[s]	i	ii	iii	Reported	σ
	$q_{sb,exp}$ [m^2/s]	$q_{sb,exp}$ [m^2/s]	$q_{sb,exp}$ [m^2/s]	$q_{sb,exp}$ [m^2/s]	[m^2/s]		$q_{sb,exp}$ [m^2/s]	$q_{sb,exp}$ [m^2/s]	$q_{sb,exp}$ [m^2/s]	$q_{sb,exp}$ [m^2/s]	[m^2/s]		$q_{sb,exp}$ [m^2/s]	$q_{sb,exp}$ [m^2/s]	$q_{sb,exp}$ [m^2/s]	$q_{sb,exp}$ [m^2/s]	[m^2/s]		$q_{sb,exp}$ [m^2/s]	$q_{sb,exp}$ [m^2/s]	$q_{sb,exp}$ [m^2/s]	$q_{sb,exp}$ [m^2/s]	[m^2/s]
5	9.840E-06	1.306E-05	2.396E-06	8.433E-06	4.466E-06	5	1.423E-05	9.357E-06	1.322E-06	7.222E-06	6.518E-06	5	1.612E-05	5.235E-07	1.612E-05	8.320E-06	9.002E-06	5	8.5847E-06	3.08754E-06	8.5847E-06	5.83612E-06	3.174E-06
10	4.544E-06	1.299E-05	4.799E-06	7.446E-06	3.925E-06	10	1.101E-05	5.537E-06	1.510E-06	5.744E-06	4.771E-06	10	8.578E-06	2.416E-07	8.578E-06	4.410E-06	4.813E-06	10	6.59122E-06	4.67829E-06	6.59122E-06	5.63476E-06	1.104E-06
15	2.752E-06	9.404E-06	3.779E-06	5.311E-06	2.924E-06	15	1.042E-05	5.940E-06	4.370E-06	5.888E-06	3.142E-06	15	5.470E-06	2.014E-07	5.470E-06	2.836E-06	3.042E-06	15	7.50406E-06	4.45679E-06	7.50406E-06	0.0000034	1.759E-06
20	3.282E-06	4.323E-06	3.141E-06	3.582E-06	5.268E-07	20	1.342E-06	3.812E-06	3.027E-06	3.314E-06	1.262E-06	20	3.302E-06	6.712E-07	3.302E-06	1.987E-06	1.519E-06	20	5.77235E-06	3.05398E-06	5.77235E-06	0.0000028	1.569E-06
21	9.195E-06	1.034E-05	6.276E-06	8.603E-06	1.710E-06	21	1.171E-05	9.229E-06	1.980E-05	1.288E-05	5.528E-06	21	8.759E-06	8.222E-06	8.759E-06	8.491E-06	3.100E-07	21	1.54377E-05	1.07393E-05	1.54377E-05	1.30885E-05	2.713E-06
22	6.947E-06	1.678E-05	7.618E-06	1.045E-05	4.486E-06	22	1.540E-05	5.537E-06	1.168E-05	9.917E-06	4.982E-06	22	1.517E-05	1.980E-06	1.517E-05	8.575E-06	7.615E-06	22	1.47665E-05	6.10796E-06	1.47665E-05	1.04372E-05	4.999E-06
23	8.692E-06	1.987E-05	1.272E-05	1.376E-05	4.621E-06	23	1.245E-05	6.611E-06	8.424E-06	8.751E-06	2.989E-06	23	1.275E-05	1.879E-06	1.275E-05	7.316E-06	6.278E-06	23	1.40953E-05	7.58461E-06	1.40953E-05	1.08399E-05	3.759E-06
24	1.094E-05	1.806E-05	7.182E-06	1.206E-05	4.509E-06	24	8.659E-06	9.430E-06	7.853E-06	7.794E-06	7.887E-07	24	1.104E-05	2.584E-06	1.104E-05	6.813E-06	4.883E-06	24	1.61425E-05	9.29618E-06	1.61425E-05	1.27193E-05	3.953E-06
25	7.954E-06	1.869E-05	1.171E-05	1.279E-05	4.450E-06	25	7.752E-06	6.746E-06	8.356E-06	6.997E-06	8.138E-07	25	1.222E-05	1.946E-06	1.222E-05	7.081E-06	5.929E-06	25	1.79883E-05	7.85309E-06	1.79883E-05	1.29207E-05	5.852E-06
26	7.115E-06	6.813E-06	2.785E-06	5.571E-06	1.973E-06	30	1.298E-05	8.122E-06	1.093E-05	9.541E-06	2.439E-06	30	1.173E-05	5.913E-06	1.173E-05	8.823E-06	3.360E-06	30	1.31422E-05	7.28928E-06	1.31422E-05	1.02157E-05	3.379E-06
27	5.839E-06	6.880E-06	3.524E-06	5.414E-06	1.403E-06	31	5.135E-06	2.383E-06	2.282E-06	3.222E-06	1.619E-06	35	1.238E-05	5.611E-06	1.238E-05	8.994E-06	3.906E-06	35	1.13568E-05	6.84628E-06	1.13568E-05	9.10153E-06	2.604E-06
28	5.470E-06	5.873E-06	2.785E-06	4.710E-06	1.370E-06	32	4.665E-06	5.470E-06	1.242E-06	3.750E-06	2.245E-06	36	8.189E-06	2.953E-06	8.189E-06	5.571E-06	3.023E-06	40	1.62029E-05	1.03433E-05	1.62029E-05	1.32731E-05	3.383E-06
29	5.571E-06	8.659E-06	2.483E-06	5.571E-06	2.521E-06	33	4.833E-06	8.759E-06	9.732E-07	4.875E-06	3.893E-06	37	6.947E-06	1.040E-06	6.947E-06	3.994E-06	3.410E-06	41	4.63131E-06	6.41E-06	4.63131E-06	5.52065E-06	1.027E-06
30	5.705E-06	6.376E-06	2.685E-06	4.922E-06	1.606E-06	34	4.598E-06	6.712E-06	2.148E-06	4.153E-06	2.284E-06	38	1.262E-05	7.048E-07	1.262E-05	6.662E-06	6.878E-06	42	6.7456E-06	3.38958E-06	6.7456E-06	5.06759E-06	1.938E-06
35	4.819E-06	5.115E-06	3.906E-06	4.613E-06	5.143E-07	35	2.853E-06	3.121E-06	1.678E-06	2.685E-06	7.675E-07	39	6.544E-06	8.726E-07	6.544E-06	3.708E-06	3.275E-06	43	4.32927E-06	3.35602E-06	4.32927E-06	3.84264E-06	5.619E-07
40	6.571E-06	8.377E-06	3.880E-06	6.276E-06	1.848E-06	40	3.953E-06	3.121E-06	2.282E-06	3.593E-06	8.357E-07	40	6.276E-06	1.477E-06	6.276E-06	3.876E-06	2.771E-06	44	4.89979E-06	2.9533E-06	4.89979E-06	3.92654E-06	1.124E-06
45	3.369E-06	5.551E-06	4.148E-06	4.356E-06	9.026E-07	45	5.269E-06	3.692E-06	2.698E-06	3.985E-06	1.296E-06	45	6.135E-06	2.389E-06	6.135E-06	4.262E-06	2.162E-06	45	2.44989E-06	1.51021E-06	2.44989E-06	1.98005E-06	5.425E-07
50	5.094E-06	6.101E-06	5.685E-06	5.627E-06	4.131E-07	50	4.658E-06	6.343E-06	2.202E-06	4.524E-06	2.083E-06	50	4.383E-06	2.564E-06	4.383E-06	3.473E-06	1.050E-06	50	5.71866E-06	2.89289E-06	5.71866E-06	4.30577E-06	1.631E-06
55	5.860E-06	2.792E-06	4.229E-06	4.293E-06	1.253E-06	55	5.806E-06	7.531E-06	2.369E-06	4.724E-06	2.628E-06	55	8.444E-06	2.987E-06	8.444E-06	5.715E-06	3.151E-06	55	2.10758E-06	4.1816E-06	2.10758E-06	3.14459E-06	1.197E-06
						60	6.296E-06	6.705E-06	3.698E-06	4.853E-06	1.631E-06	60	1.167E-05	2.524E-06	1.167E-05	7.095E-06	5.278E-06	60	3.91312E-06	3.77888E-06	3.91312E-06	3.846E-06	7.750E-08
												65	4.886E-06	1.685E-06	4.886E-06	3.286E-06	1.848E-06	65	3.28219E-06	5.18169E-06	3.28219E-06	4.23194E-06	1.097E-06
																		70	4.49035E-06	2.02032E-06	4.49035E-06	3.25534E-06	1.426E-06

Appendix G: Bed elevation measurement point gauge

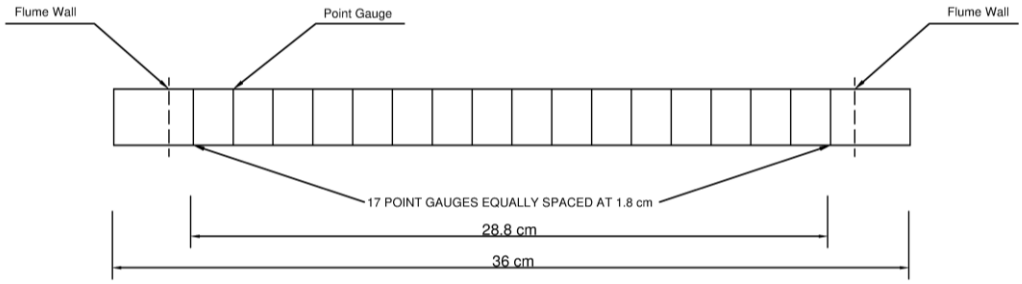

Figure 34: Schematic of bed elevation measurement point gauge

Appendix H: Sediment transport trap

Figure 35: Sediment transport trap installed at the exit of the flume

Appendix I: Bed elevation measurement cross-sections and zones

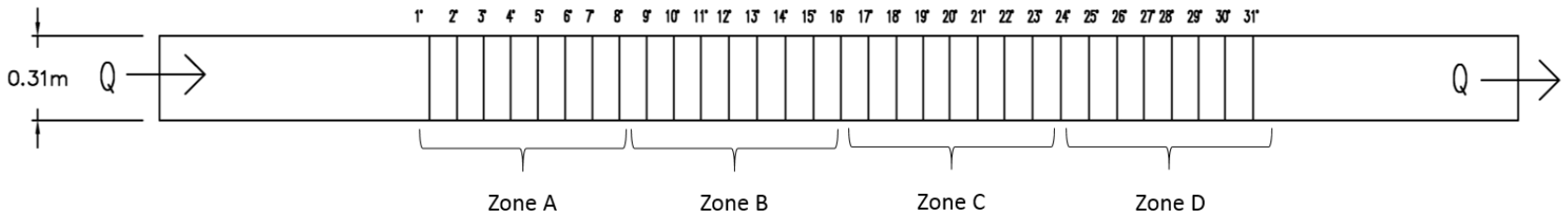

Figure 36: Planview of flume showing data collection zones A, B, C, and D

Appendix J: Calculated specific volumetric bed load transport rates for the experimental runs of Series A

Table 18: Summary of predictive sediment transport equations for experimental runs of Series A

	Run A1				Run A2				Run A3				Run A4			
time (min)	Meyer-Peter and Muller (1949)	Yalin (1963)	Bagnold (1968)	van Rijn (1984)	Meyer-Peter and Muller (1949)	Yalin (1963)	Bagnold (1968)	van Rijn (1984)	Meyer-Peter and Muller (1949)	Yalin (1963)	Bagnold (1968)	van Rijn (1984)	Meyer-Peter and Muller (1949)	Yalin (1963)	Bagnold (1968)	van Rijn (1984)
5	2.42E-06	1.16E-06	1.32E-06	1.41E-06	2.71E-06	1.36E-06	1.46E-06	1.64E-06	2.56E-06	1.26E-06	1.39E-06	1.57E-06	2.13E-06	9.75E-07	1.18E-06	1.22E-06
10	2.71E-06	1.36E-06	1.46E-06	1.66E-06	2.79E-06	1.42E-06	1.49E-06	1.71E-06	2.71E-06	1.36E-06	1.46E-06	1.69E-06	3.18E-06	1.70E-06	1.67E-06	2.12E-06
15	2.79E-06	1.42E-06	1.49E-06	1.71E-06	2.79E-06	1.42E-06	1.49E-06	1.73E-06	2.87E-06	1.47E-06	1.53E-06	1.78E-06	3.43E-06	1.88E-06	1.79E-06	2.34E-06
20	2.71E-06	1.36E-06	1.46E-06	1.69E-06	2.79E-06	1.42E-06	1.49E-06	1.73E-06	2.87E-06	1.47E-06	1.53E-06	1.78E-06	3.67E-06	2.07E-06	1.90E-06	2.55E-06
21	3.93E-06	2.27E-06	2.01E-06	2.83E-06	4.02E-06	2.34E-06	2.05E-06	2.86E-06	4.37E-06	2.63E-06	2.21E-06	3.25E-06	4.82E-06	3.00E-06	2.42E-06	3.78E-06
22	4.10E-06	2.41E-06	2.09E-06	2.99E-06	3.84E-06	2.20E-06	1.98E-06	2.73E-06	4.10E-06	2.41E-06	2.09E-06	3.02E-06	6.56E-06	4.57E-06	3.19E-06	5.77E-06
23	3.93E-06	2.27E-06	2.01E-06	2.79E-06	3.76E-06	2.14E-06	1.94E-06	2.64E-06	4.37E-06	2.63E-06	2.21E-06	3.25E-06	5.86E-06	3.92E-06	2.88E-06	4.97E-06
24	3.84E-06	2.20E-06	1.98E-06	2.70E-06	3.84E-06	2.20E-06	1.98E-06	2.73E-06	3.67E-06	2.07E-06	1.90E-06	2.58E-06	5.67E-06	3.75E-06	2.79E-06	4.68E-06
25	3.93E-06	2.27E-06	2.01E-06	2.79E-06	3.84E-06	2.20E-06	1.98E-06	2.73E-06	4.37E-06	2.63E-06	2.21E-06	3.29E-06	5.38E-06	3.49E-06	2.67E-06	4.40E-06
30	4.02E-06	2.34E-06	2.05E-06	2.92E-06	3.51E-06	1.94E-06	1.82E-06	2.37E-06	4.46E-06	2.70E-06	2.25E-06	3.32E-06	5.76E-06	3.83E-06	2.84E-06	4.84E-06
31	3.02E-06	1.58E-06	1.60E-06	1.94E-06	2.41E-06	1.16E-06	1.32E-06	2.09E-06	4.73E-06	2.93E-06	2.37E-06	3.64E-06	4.10E-06	2.41E-06	2.09E-06	2.95E-06
32	3.02E-06	1.58E-06	1.60E-06	1.96E-06	3.18E-06	1.70E-06	1.67E-06	1.86E-06	3.77E-06	2.14E-06	1.94E-06	2.64E-06	4.02E-06	2.34E-06	2.05E-06	2.89E-06
33	3.18E-06	1.70E-06	1.67E-06	2.07E-06	3.02E-06	1.58E-06	1.60E-06	1.94E-06	3.43E-06	1.88E-06	1.79E-06	2.34E-06	4.28E-06	2.55E-06	2.17E-06	3.15E-06
34	3.34E-06	1.82E-06	1.75E-06	2.26E-06	2.94E-06	1.53E-06	1.56E-06	1.83E-06	3.67E-06	2.07E-06	1.90E-06	2.52E-06	4.19E-06	2.48E-06	2.13E-06	3.05E-06
35	2.95E-06	1.53E-06	1.56E-06	1.86E-06	2.94E-06	1.53E-06	1.56E-06	1.88E-06	3.67E-06	2.07E-06	1.90E-06	2.52E-06	4.10E-06	2.41E-06	2.09E-06	2.99E-06
40	3.26E-06	1.76E-06	1.71E-06	2.12E-06	3.26E-06	1.76E-06	1.71E-06	2.15E-06	4.10E-06	2.41E-06	2.09E-06	3.02E-06	3.76E-06	2.14E-06	1.94E-06	2.64E-06
45	3.10E-06	1.64E-06	1.64E-06	1.99E-06	3.18E-06	1.70E-06	1.67E-06	2.09E-06	3.76E-06	2.14E-06	1.94E-06	2.64E-06	3.93E-06	2.27E-06	2.01E-06	2.79E-06
50	3.18E-06	1.70E-06	1.67E-06	2.09E-06	3.10E-06	1.64E-06	1.64E-06	1.99E-06	3.67E-06	2.07E-06	1.90E-06	2.55E-06	4.28E-06	2.55E-06	2.17E-06	3.12E-06
55	3.26E-06	1.76E-06	1.71E-06	2.18E-06	2.27E-06	1.07E-06	1.25E-06	1.32E-06	3.76E-06	2.14E-06	1.94E-06	2.64E-06	4.10E-06	2.41E-06	2.09E-06	2.99E-06
60	3.34E-06	1.82E-06	1.75E-06	2.26E-06	2.42E-06	1.16E-06	1.32E-06	1.39E-06	3.93E-06	2.27E-06	2.01E-06	2.83E-06	4.37E-06	2.63E-06	2.21E-06	3.22E-06

Appendix K: Calculated specific volumetric bed load transport rates for the experimental runs of Series B

Table 19: Summary of predictive sediment transport equations for experimental runs of Series B

Run B1					Run B2					Run B3					Run B4				
time (min)	Meyer-Peter and Muller (1949)	Yalin (1963)	Bagnold (1968)	van Rijn (1984)	time (min)	Meyer-Peter and Muller (1949)	Yalin (1963)	Bagnold (1968)	van Rijn (1984)	time (min)	Meyer-Peter and Muller (1949)	Yalin (1963)	Bagnold (1968)	van Rijn (1984)	time (min)	Meyer-Peter and Muller (1949)	Yalin (1963)	Bagnold (1968)	van Rijn (1984)
5	2.13E-06	9.75E-07	1.18E-06	1.16E-06	5	2.29E-06	1.36E-06	2.29E-06	1.64E-06	5	2.79E-06	1.42E-06	1.49E-06	1.71E-06	5	2.27E-06	1.07E-06	1.25E-06	1.28E-06
10	2.49E-06	1.21E-06	1.35E-06	1.45E-06	10	2.35E-06	1.42E-06	2.35E-06	1.71E-06	10	2.79E-06	1.42E-06	1.49E-06	1.73E-06	10	2.79E-06	1.42E-06	1.49E-06	1.71E-06
15	2.56E-06	1.26E-06	1.39E-06	1.52E-06	15	2.29E-06	1.42E-06	2.29E-06	1.73E-06	15	2.79E-06	1.42E-06	1.49E-06	1.73E-06	15	2.79E-06	1.42E-06	1.49E-06	1.73E-06
20	2.56E-06	1.26E-06	1.39E-06	1.54E-06	20	2.20E-06	1.42E-06	2.20E-06	1.73E-06	20	2.79E-06	1.42E-06	1.49E-06	1.76E-06	20	2.64E-06	1.31E-06	1.42E-06	1.64E-06
21	3.84E-06	2.20E-06	1.98E-06	2.67E-06	21	2.98E-06	2.34E-06	2.98E-06	2.86E-06	21	3.60E-06	2.01E-06	1.86E-06	2.46E-06	21	3.84E-06	2.20E-06	1.98E-06	2.70E-06
22	3.76E-06	2.14E-06	1.94E-06	2.55E-06	22	2.79E-06	6.36E-06	2.79E-06	2.73E-06	22	3.51E-06	1.94E-06	1.82E-06	2.37E-06	22	3.76E-06	2.14E-06	1.94E-06	2.67E-06
23	3.93E-06	2.27E-06	2.01E-06	2.64E-06	23	2.82E-06	6.36E-06	2.82E-06	2.64E-06	23	3.51E-06	1.94E-06	1.82E-06	2.37E-06	23	3.76E-06	2.14E-06	1.94E-06	2.64E-06
24	3.51E-06	1.94E-06	1.82E-06	2.46E-06	24	2.87E-06	6.36E-06	2.87E-06	2.73E-06	24	3.26E-06	1.76E-06	1.71E-06	2.15E-06	24	4.10E-06	2.41E-06	2.09E-06	2.95E-06
25	3.59E-06	2.01E-06	1.86E-06	2.49E-06	25	2.92E-06	6.36E-06	2.92E-06	2.73E-06	25	3.67E-06	2.07E-06	1.90E-06	2.55E-06	25	4.19E-06	2.48E-06	2.13E-06	3.12E-06
26	2.94E-06	1.53E-06	1.56E-06	1.88E-06	30	2.75E-06	4.30E-06	2.75E-06	2.37E-06	30	3.67E-06	2.07E-06	1.90E-06	2.58E-06	30	4.28E-06	2.55E-06	2.17E-06	3.18E-06
27	3.02E-06	1.58E-06	1.60E-06	1.91E-06	31	2.14E-06	1.70E-06	2.14E-06	2.09E-06	31	3.59E-06	2.01E-06	1.86E-06	2.46E-06	35	4.28E-06	2.55E-06	2.17E-06	3.12E-06
28	2.95E-06	1.53E-06	1.56E-06	1.86E-06	32	2.23E-06	1.70E-06	2.23E-06	2.12E-06	32	3.02E-06	1.58E-06	1.60E-06	1.96E-06	40	4.28E-06	2.55E-06	2.17E-06	3.15E-06
29	2.94E-06	1.53E-06	1.56E-06	1.88E-06	33	2.29E-06	1.58E-06	2.29E-06	1.94E-06	33	3.10E-06	1.64E-06	1.64E-06	1.99E-06	41	2.95E-06	1.53E-06	1.56E-06	1.86E-06
30	2.79E-06	1.42E-06	1.49E-06	1.71E-06	34	2.17E-06	1.53E-06	2.17E-06	1.83E-06	34	2.87E-06	1.47E-06	1.53E-06	1.78E-06	42	1.99E-06	8.88E-07	1.12E-06	1.69E-06
35	2.79E-06	1.42E-06	1.49E-06	1.76E-06	35	2.14E-06	1.53E-06	2.14E-06	1.88E-06	35	2.64E-06	1.31E-06	1.42E-06	1.59E-06	43	2.06E-06	9.31E-07	1.15E-06	1.71E-06
40	3.26E-06	1.76E-06	1.71E-06	5.86E-06	40	1.99E-06	1.76E-06	1.99E-06	2.15E-06	40	2.87E-06	1.47E-06	1.53E-06	1.78E-06	44	2.79E-06	1.42E-06	1.49E-06	1.71E-06
45	3.02E-06	1.58E-06	1.60E-06	1.96E-06	45	1.90E-06	1.70E-06	1.90E-06	2.09E-06	45	3.02E-06	1.58E-06	1.60E-06	1.94E-06	45	1.99E-06	8.88E-07	1.12E-06	1.71E-06
50	2.94E-06	1.53E-06	1.56E-06	1.88E-06	50	2.05E-06	1.64E-06	2.05E-06	1.99E-06	50	2.95E-06	1.53E-06	1.56E-06	1.88E-06	50	1.92E-06	8.46E-07	1.08E-06	1.66E-06
55	3.18E-06	1.70E-06	1.67E-06	2.07E-06	55	1.99E-06	1.07E-06	1.99E-06	1.32E-06	55	2.95E-06	1.53E-06	1.56E-06	1.83E-06	55	2.27E-06	1.07E-06	1.25E-06	1.83E-06
					60	2.23E-06	1.16E-06	2.23E-06	1.39E-06	60	2.87E-06	1.47E-06	1.53E-06	1.78E-06	60	2.87E-06	1.47E-06	1.53E-06	1.78E-06
										65	2.79E-06	1.42E-06	1.49E-06	2.09E-06	65	2.06E-06	9.31E-07	1.15E-06	1.73E-06
															70	2.41E-06	1.16E-06	1.32E-06	1.91E-06

Appendix L: Standard deviation of experimental specific volumetric bed load transport rates based on all repetitions of the experimental runs in Series C

Table 20: Specific volumetric bed load transport rates and standard deviation from the reported mean values for each experimental time step in all runs of Series C

time	Run C1					Run C2					Run C3				
[s]	i	ii	iii	Reported	σ	i	ii	iii	Reported	σ	i	ii	iii	Reported	σ
	$q_{sb,exp}$ [m^2/s]	$q_{sb,exp}$ [m^2/s]	$q_{sb,exp}$ [m^2/s]	$q_{sb,exp}$ [m^2/s]	[m^2/s]	$q_{sb,exp}$ [m^2/s]	$q_{sb,exp}$ [m^2/s]	$q_{sb,exp}$ [m^2/s]	$q_{sb,exp}$ [m^2/s]	[m^2/s]	$q_{sb,exp}$ [m^2/s]	$q_{sb,exp}$ [m^2/s]	$q_{sb,exp}$ [m^2/s]	$q_{sb,exp}$ [m^2/s]	[m^2/s]
5	1.980E-06	3.631E-06	1.980E-06	2.806E-06	9.533E-07	9.263E-06	1.685E-05	9.263E-06	1.306E-05	4.383E-06	1.006E-05	5.933E-06	3.383E-06	6.459E-06	3.370E-06
10	7.034E-06	2.524E-06	7.034E-06	4.779E-06	2.604E-06	5.900E-06	6.806E-06	5.900E-06	6.353E-06	5.232E-07	6.464E-06	5.853E-06	7.410E-06	6.576E-06	7.846E-07
15	5.880E-06	1.886E-06	5.880E-06	3.883E-06	2.306E-06	6.631E-06	9.209E-06	6.631E-06	7.920E-06	1.488E-06	4.853E-06	3.020E-06	4.041E-06	3.971E-06	9.182E-07
20	6.665E-06	1.752E-06	6.665E-06	4.208E-06	2.837E-06	5.074E-06	3.524E-06	5.074E-06	4.299E-06	8.952E-07	5.249E-06	5.215E-06	4.155E-06	4.873E-06	6.222E-07
21	1.426E-05	6.276E-06	1.426E-05	1.027E-05	4.611E-06	1.034E-05	8.625E-06	1.034E-05	9.481E-06	9.882E-07	6.913E-06	7.182E-06	6.746E-06	6.947E-06	2.201E-07
22	1.540E-05	4.631E-06	1.540E-05	1.002E-05	6.220E-06	5.303E-06	6.477E-06	5.303E-06	5.890E-06	6.782E-07	7.081E-06	5.000E-06	5.470E-06	5.851E-06	1.091E-06
23	1.480E-05	3.222E-06	1.480E-05	9.011E-06	6.685E-06	5.235E-06	6.142E-06	5.235E-06	5.688E-06	5.232E-07	5.571E-06	4.900E-06	6.074E-06	5.515E-06	5.893E-07
24	1.517E-05	2.517E-06	1.517E-05	8.843E-06	7.305E-06	5.202E-06	4.128E-06	5.202E-06	4.665E-06	6.200E-07	6.880E-06	5.000E-06	3.390E-06	5.090E-06	1.747E-06
25	1.154E-05	4.564E-06	1.154E-05	8.054E-06	4.030E-06	6.376E-06	6.880E-06	6.376E-06	6.628E-06	2.906E-07	5.470E-06	7.517E-06	5.739E-06	6.242E-06	1.113E-06
26	5.504E-06	3.423E-07	5.504E-06	2.923E-06	2.980E-06	1.295E-05	1.091E-05	1.295E-05	1.193E-05	1.182E-06	5.101E-06	1.550E-06	1.389E-06	2.680E-06	2.098E-06
27	8.659E-06	1.980E-06	8.659E-06	5.319E-06	3.856E-06	1.064E-05	9.699E-06	1.064E-05	1.017E-05	5.425E-07	5.806E-06	6.276E-06	6.444E-06	6.175E-06	3.305E-07
28	6.611E-06	2.215E-06	6.611E-06	4.413E-06	2.538E-06	1.232E-05	6.813E-06	1.232E-05	9.565E-06	3.178E-06	4.866E-06	6.242E-06	8.591E-06	6.567E-06	1.884E-06
29	7.618E-06	3.390E-06	7.618E-06	5.504E-06	2.441E-06	2.228E-05	1.245E-05	2.228E-05	1.737E-05	5.677E-06	2.148E-06	1.044E-05	6.276E-06	6.287E-06	4.145E-06
30	7.115E-06	5.638E-06	7.115E-06	6.376E-06	8.525E-07	2.004E-05	9.430E-06	2.004E-05	1.473E-05	6.123E-06	3.490E-06	6.276E-06	6.041E-06	5.269E-06	1.545E-06
31	6.007E-06	5.101E-06	6.007E-06	5.554E-06	5.232E-07	8.021E-06	4.698E-06	8.021E-06	6.360E-06	1.918E-06	6.678E-06	1.910E-05	1.460E-05	1.346E-05	6.287E-06
32	6.444E-06	7.920E-07	6.444E-06	3.618E-06	3.263E-06	1.520E-05	4.430E-06	1.520E-05	9.816E-06	6.220E-06	6.578E-06	2.014E-06	3.182E-06	3.924E-06	2.371E-06
33	9.498E-06	7.585E-07	9.498E-06	5.128E-06	5.046E-06	1.480E-05	4.027E-06	1.480E-05	9.414E-06	6.220E-06	1.024E-05	1.691E-06	2.161E-06	4.696E-06	4.803E-06
34	6.544E-06	6.108E-07	6.544E-06	3.578E-06	3.426E-06	1.252E-05	5.839E-06	1.252E-05	9.179E-06	3.856E-06	7.820E-06	1.987E-06	1.524E-06	3.777E-06	3.509E-06
35	9.464E-06	4.497E-07	9.464E-06	4.957E-06	5.204E-06	1.557E-05	6.276E-06	1.557E-05	1.092E-05	5.367E-06	2.024E-05	1.933E-06	2.195E-06	8.122E-06	1.049E-05
36	4.195E-06	3.960E-07	4.195E-06	2.296E-06	2.193E-06	8.356E-06	4.229E-06	8.356E-06	6.293E-06	2.383E-06	8.994E-06	7.182E-07	6.108E-07	3.441E-06	4.809E-06
37	2.920E-06	4.766E-07	2.920E-06	1.698E-06	1.411E-06	8.390E-06	3.692E-06	8.390E-06	6.041E-06	2.713E-06	5.403E-06	8.122E-07	5.705E-07	2.262E-06	2.723E-06
38	3.289E-06	5.907E-07	3.289E-06	1.940E-06	1.558E-06	5.000E-06	3.289E-06	5.000E-06	4.145E-06	9.882E-07	5.235E-06	5.168E-07	6.913E-07	2.148E-06	2.675E-06
39	4.094E-06	4.497E-07	4.094E-06	2.272E-06	2.104E-06	5.403E-06	5.537E-06	5.403E-06	5.470E-06	7.750E-08	7.618E-06	4.833E-07	7.249E-07	2.942E-06	4.051E-06
40	5.235E-06	4.296E-07	5.235E-06	2.832E-06	2.775E-06	6.578E-06	5.235E-06	6.578E-06	5.907E-06	7.750E-07	5.437E-06	4.564E-07	8.122E-07	2.235E-06	2.778E-06
45	3.651E-06	1.517E-06	3.651E-06	2.584E-06	1.232E-06	4.396E-06	3.255E-06	4.396E-06	3.826E-06	6.588E-07	3.725E-06	3.188E-06	2.718E-06	3.211E-06	5.038E-07
50	4.370E-06	3.242E-06	4.370E-06	3.806E-06	6.510E-07	4.329E-06	4.860E-06	4.329E-06	4.594E-06	3.061E-07	5.960E-06	4.980E-06	2.604E-06	4.515E-06	1.726E-06
55	6.578E-06	2.705E-06	6.578E-06	4.641E-06	2.236E-06	5.578E-06	5.665E-06	5.578E-06	5.621E-06	5.038E-08	4.618E-06	5.041E-06	3.470E-06	4.376E-06	8.127E-07
60	4.544E-06	2.235E-06	4.544E-06	3.390E-06	1.333E-06	5.752E-06	6.061E-06	5.752E-06	5.907E-06	1.783E-07	5.913E-06	3.685E-06	3.531E-06	4.376E-06	1.333E-06
65	2.759E-06	3.853E-06	2.759E-06	3.306E-06	6.317E-07	4.678E-06	3.235E-06	4.678E-06	3.957E-06	8.332E-07	3.759E-06	4.531E-06	4.054E-06	4.114E-06	3.895E-07

Appendix M: Calculated specific volumetric bed load transport rates for the experimental runs of Series C

Table 21: Summary of predictive sediment transport equations for experimental runs of Series C

	Run C1				Run C2				Run C3			
time (min)	Meyer-Peter and Muller (1949)	Yalin (1963)	Bagnold (1968)	van Rijn (1984)	Meyer-Peter and Muller (1949)	Yalin (1963)	Bagnold (1968)	van Rijn (1984)	Meyer-Peter and Muller (1949)	Yalin (1963)	Bagnold (1968)	van Rijn (1984)
5	1.99E-06	8.88E-07	1.12E-06	1.06E-06	2.13E-06	9.75E-07	1.18E-06	1.22E-06	2.56E-06	1.26E-06	1.39E-06	1.52E-06
10	2.64E-06	1.31E-06	1.42E-06	1.61E-06	2.27E-06	1.07E-06	1.25E-06	1.30E-06	2.42E-06	1.16E-06	1.32E-06	1.41E-06
15	2.42E-06	1.16E-06	1.32E-06	1.41E-06	2.56E-06	1.26E-06	1.39E-06	1.52E-06	2.56E-06	1.26E-06	1.39E-06	1.52E-06
20	2.42E-06	1.16E-06	1.32E-06	1.41E-06	2.42E-06	1.16E-06	1.32E-06	1.41E-06	2.56E-06	1.26E-06	1.39E-06	1.52E-06
21	3.67E-06	2.07E-06	1.90E-06	2.58E-06	3.84E-06	2.20E-06	1.98E-06	2.76E-06	2.56E-06	1.26E-06	1.39E-06	1.96E-06
22	3.76E-06	2.14E-06	1.94E-06	2.76E-06	3.76E-06	2.14E-06	1.94E-06	2.61E-06	2.56E-06	1.26E-06	1.39E-06	1.96E-06
23	3.93E-06	2.27E-06	2.01E-06	2.83E-06	3.76E-06	2.14E-06	1.94E-06	2.61E-06	3.43E-06	1.88E-06	1.79E-06	2.34E-06
24	4.02E-06	2.34E-06	2.05E-06	2.89E-06	3.59E-06	2.01E-06	1.86E-06	2.46E-06	3.59E-06	2.01E-06	1.86E-06	2.46E-06
25	4.02E-06	2.34E-06	2.05E-06	2.86E-06	3.43E-06	1.88E-06	1.79E-06	2.34E-06	3.43E-06	1.88E-06	1.79E-06	2.34E-06
26	3.76E-06	2.14E-06	1.94E-06	2.61E-06	3.84E-06	2.20E-06	1.98E-06	2.76E-06	3.59E-06	2.01E-06	1.86E-06	2.46E-06
27	3.67E-06	2.07E-06	1.90E-06	2.52E-06	3.76E-06	2.14E-06	1.94E-06	2.61E-06	3.43E-06	1.88E-06	1.79E-06	2.34E-06
28	3.18E-06	1.70E-06	1.67E-06	2.09E-06	4.02E-06	2.34E-06	2.05E-06	2.89E-06	3.34E-06	1.82E-06	1.75E-06	2.20E-06
29	7.19E-06	5.18E-06	3.47E-06	2.73E-06	4.19E-06	2.48E-06	2.13E-06	3.05E-06	3.43E-06	1.88E-06	1.79E-06	2.34E-06
30	3.10E-06	1.64E-06	1.64E-06	2.01E-06	4.02E-06	2.34E-06	2.05E-06	2.89E-06	3.43E-06	1.88E-06	1.79E-06	2.34E-06
31	3.59E-06	2.01E-06	1.86E-06	2.46E-06	3.34E-06	1.82E-06	1.75E-06	2.20E-06	4.91E-06	3.08E-06	2.46E-06	3.86E-06
32	3.26E-06	1.76E-06	1.71E-06	2.18E-06	3.76E-06	2.14E-06	1.94E-06	2.61E-06	4.64E-06	2.85E-06	2.33E-06	3.53E-06
33	3.02E-06	1.58E-06	1.60E-06	1.94E-06	3.59E-06	2.01E-06	1.86E-06	2.46E-06	4.46E-06	2.70E-06	2.25E-06	3.36E-06
34	2.95E-06	1.53E-06	1.56E-06	1.83E-06	3.43E-06	1.88E-06	1.79E-06	2.34E-06	4.28E-06	2.55E-06	2.17E-06	3.18E-06
35	3.18E-06	1.70E-06	1.67E-06	2.09E-06	3.43E-06	1.88E-06	1.79E-06	2.34E-06	4.64E-06	2.85E-06	2.33E-06	3.53E-06
36	3.02E-06	1.58E-06	1.60E-06	1.94E-06	2.56E-06	1.26E-06	1.39E-06	1.52E-06	2.79E-06	1.42E-06	1.49E-06	1.73E-06
37	2.87E-06	1.47E-06	1.53E-06	1.78E-06	2.27E-06	1.07E-06	1.25E-06	1.30E-06	3.02E-06	1.58E-06	1.60E-06	1.96E-06
38	3.02E-06	1.58E-06	1.60E-06	1.96E-06	2.27E-06	1.07E-06	1.25E-06	1.30E-06	2.95E-06	1.53E-06	1.56E-06	1.83E-06
39	3.26E-06	1.76E-06	1.71E-06	2.18E-06	2.27E-06	1.07E-06	1.25E-06	1.30E-06	2.95E-06	1.53E-06	1.56E-06	1.83E-06
40	2.87E-06	1.47E-06	1.53E-06	1.81E-06	2.56E-06	1.26E-06	1.39E-06	1.52E-06	3.02E-06	1.58E-06	1.60E-06	1.96E-06
45	2.95E-06	1.53E-06	1.56E-06	1.83E-06	2.27E-06	1.07E-06	1.25E-06	1.30E-06	3.18E-06	1.70E-06	1.67E-06	2.09E-06
50	2.94E-06	1.53E-06	1.56E-06	1.91E-06	2.42E-06	1.16E-06	1.32E-06	1.41E-06	2.79E-06	1.42E-06	1.49E-06	1.73E-06
55	2.87E-06	1.47E-06	1.53E-06	1.78E-06	2.42E-06	1.16E-06	1.32E-06	1.41E-06	2.95E-06	1.53E-06	1.56E-06	1.83E-06
60	3.84E-06	2.20E-06	1.98E-06	2.76E-06	2.42E-06	1.16E-06	1.32E-06	1.41E-06	3.18E-06	1.70E-06	1.67E-06	2.09E-06
65	3.18E-06	1.70E-06	1.67E-06	2.09E-06	2.56E-06	1.26E-06	1.39E-06	1.52E-06	2.95E-06	1.53E-06	1.56E-06	2.09E-06

Curriculum Vitae

Name:	Etta Haley Gunsolus
Post-secondary Education and Degrees:	McMaster University Hamilton, Ontario, Canada 2009-2013 B.Sc. The University of Western Ontario London, Ontario, Canada 2013-Expected 2015 M.E.Sc.
Honours and Awards:	McMaster Entrance Scholarship 2009 David French Bursary 2009
Related Work Experience:	Junior Environmental Officer Ministry of Environment 2011 Resource Developer Imperial Oil Outreach Initiative 2013 Teaching Assistant The University of Western Ontario 2014-2015
Presentations:	Gunsolus EH, McKee JL, Brand J, and Binns AD. Water resources and hydraulic engineering: Mitigating impacts to surface water environments. Western Environment and Sustainability Showcase. 6 March, London, Canada, 2014. Gunsolus EH and Binns AD. Morphodynamic response of laboratory stream beds to unsteady flow events of varying magnitude and duration. 2014 American Geophysical Union Fall Meeting, 15-19 December, San Francisco, USA, 2014. Gunsolus EH and Binns AD. Variation in river bed morphology and sediment transport rates during flood events. Canadian Society for Civil Engineering (CSCE) 22nd Canadian Hydrotechnical Conference, 29 April-2 May, Montreal, Canada, 2015.

Gunsolus EH and Binns AD. River bed morphological adjustments in response to flood events of varying magnitude and duration. High North Program Workshop (Managing the Water Hazards in a Changing Climate in the High North through Collaborative Networks), 12-14 May, London, Canada, 2015.